UNIVERSITÀ DEGLI STUDI DELL'AQUILA

DIPARTIMENTO DI MEDICINA CLINICA, SANITÀ PUBBLICA, SCIENZE DELLA VITA E DELL'AMBIENTE

DOTTORATO DI RICERCA IN

MEDICINA CLINICA E SANITA' PUBBLICA

XXXII ciclo

Curriculum

Medicina Interna, Scienze dell'Invecchiamento e Nutraceutica

Titolo della tesi

Human glioblastoma stem cells and inflammatory tumor microenvironment: Involvement of nitric oxide synthase 2 (NOS2) expression and activity

SSD MED/06 – Oncologia medica

Dottorando

Dott. Ylli Alicka

_____

Coordinatore del corso

Chiar.mo Prof. Claudio Ferri

_____

Tutor

Chiar.mo Prof.ssa Maria Penco

_____

Chiar.mo Prof. Pietro Leocata

_____

A.A. 2018/2019

Al Prof. Pietro Leocata

Maestro,

desidero ringraziarTi per la pazienza, la fiducia in me e l'entusiasmo che sei riuscito a trasmettermi.

Tu hai stimolato il mio interesse per l'argomento di questa Tesi, mostrandomi aspetti che, senza di Te, avrei ignorato.

Maestro, forse non Te l'ho dimostrato abbastanza ma sono infinitamente grato per avere avuto la fortuna di averTi come Guida, Tutore, Relatore, Mentore, Amico…..

Sei stato un Maestro insostituibile e incredibile, fonte di ispirazione e di pensieri "buoni".

Ora….. non sei più qui, sei andato altrove……..ma l'eredità che mi hai lasciato sarà duratura; ho fatto e farò tesoro di tutti i Tuoi insegnamenti, che hanno influenzato e influenzeranno sempre i miei pensieri, il mio comportamento, il mio sguardo, la mia attenzione verso gli altri….

Maestro, Tu mi hai insegnato che cos'è la bontà e l'altruismo!

Maestro……mi mancherai infinitamente

Maestro mio……GRAZIE!

Ylli

L'insegnante mediocre parla.
Il buon insegnante spiega.
L'insegnante superiore dimostra.

Il grande Maestro ispira.

(William A. Ward)

Summary

1. OVERVIEW ON GLIOBLASTOMA (GBM)

Gliomas are classified by the World Health Organization (WHO) grade criteria (I to IV) into multiple specific histologic subtypes, based on cell type of origin and molecular characteristics [1]. Afterward, an increasing number of molecular biomarkers was discovered in these tumors, also including TERT (Telomerase Reverse Transcriptase) promoter mutation, EGFR (Epidermal Growth Factor Receptor) and P53 [2] Grade IV Glioblastoma (GBM) is one of the most lethal brain cancers worldwide since it is the most highly infiltrating and aggressive tumor of the central nervous system, characterized by a high degree of genetic and cellular heterogeneity. GBM accounts for 70–75% of all diffuse glioma diagnoses and has a median overall survival of 14–17 months [3]. The incidence rates of GBM increases with age, with a median age of 64 years at diagnosis and is ranged between 0.6 to 3.7 per 100,000 persons depending on reporting country/organization [4] and with geographic differences [5]. Glioblastoma (GBM) represents the most common and aggressive type of central nervous system primary tumors in adults representing about 15% of intracranial tumors, and about 65% of astrocytic neoplasms. It can occur at any age, can affect children, but the peak incidence is between 45 and 75 years (80% of patients are over 50 years old, while less than 1% is diagnosed before the age of 20 age). The most frequent localization of GBM is in the supratentorial region, which includes frontal, temporal-parietal, and occipital lobes, where the frontal lobe has the highest incidence among them. Unlike other aggressive malignancies, GBMs appear to develop exclusively and only in the brain microenvironment; thus, extracranial metastases remain rare. Over 90% of GBM has no previous identified lesions of minor histopathological grading, and have a brief clinical history (mainly less than 3 months). They are defined as primary glioblastomas, and typically develop in advanced age patients (mean age at diagnosis ~62 years). About 10% is represented by secondary glioblastomas, which develop from a previous lesion of minor grade (astrocytoma's of any category if not treated, can progress into a glioblastoma).

Despite the best available treatments, the survival of patients affected by GBM is very poor, and GBM early recurs. In this regard, there is an urgent need to improve the current therapeutic approaches to GBM treatment. In 2017 the European Association for Neuro.-Oncology (EANO) has released guidelines on the diagnosis and treatment of adult astrocytic and oligodendroglial gliomas [6]. The goals of surgery are to obtain a diagnosis, alleviate symptoms of increased intracranial pressure or compression, improve neurological function, increase survival, while limiting unnecessary treatments and costs. Adjuvant treatment options depend on the patient's performance status, age, and MGMT promoter methylation status. Nowadays, for the treatment of GBM, surgical resection is usually followed by radiotherapy or radiotherapy plus chemotherapy with temozolomide (TMZ) [7]. These therapeutic approaches have increased median patient survival of 15-23 months [8,9], but resistance to therapy limits its effectiveness and GBM cannot be effectively controlled being characterized by extremely wide set of genetic and epigenetic alterations and high rates of recurrences [9,10]. In addition, neuroinflammation also increases after treatment, making the development of alternative therapeutic approaches critically imperative. Indeed, the median patient survival of 15 months, where less than 5% of patients survive for more than 5 years after diagnosis [11]. Although the complex biomolecular framework underlying GBM aggressiveness is not yet fully defined, an increasing amount of studies aimed at identifying the mechanisms responsible for GBM progression, chemo/radiotherapy resistance and high recurrence rate led to the identification of glioma stem cell (GSC) as an election target for anti-GBM therapy [12,13].

Factors associated with GBM risk are prior radiation, decreased susceptibility to allergy, immune factors and immune genes, and some nucleotide polymorphisms detected by genome-wide association [14,15]. The lower risk of GBM in people with asthma and other allergic conditions is consistent with findings that have been confirmed by objective evidence from asthma and other allergies-related germline polymorphism in patients with GBM [16-18]. Genotypes that increase asthma risk are associated with decreased GBM risk. Nevertheless, both familial aggregation of glioma and the inverse association of allergies and immune-related conditions with glioma have been shown

consistently. Lower risk of gliomas is associated with allergy or atopic disease (e.g., asthma, eczema, psoriasis).

Other factors associated with GBM risk are high socioeconomic status and a person's height. Regarding lifestyle characteristics, there is no substantial evidence with GBM association, such as cigarette smoking, alcohol consumption, drug use, or dietary exposure to nitrous compounds [19,20]. Inconsistent and indefinite reports published regarding the association of GBM with the use of mobile phones [21,22]. Prognostic factors that affect the survival of GBM patients include tumor removal, its location, size, as well as advanced age, comorbidities, and the general condition of the patient [23]. There are no hereditary traits that are predisposing to GBM development; therefore, all characteristic genetic alterations are somatic and acquired aberrations [24].

Complex and "poor" diagnoses, inability to accurately predict susceptibility or resistance to chemotherapy treatments contribute to poor prognosis for patients with glioblastoma [25]. Therefore, understanding the aggressive behavior of its molecular mechanisms underlying can lead to better management, appropriate therapy, and better outcomes. Cancer development is influenced by somatic evolution, a process in which an accumulation of mutations causes the genome of a carcinogenic cell to change from that of a healthy cell. The development of GBM is remarkable, which in this way occurs through a complex network of different genetic and molecular aberrations, leading to significant changes in the main signal pathways. In recent years, validated data have emerged and demonstrated that tumors are composed of numerous populations of carcinogenic cells that contain specific genetic alterations in addition to classical genetic abnormalities found. This heterogeneity in tumors results from genetics characterized by instability and increased mutation levels that accompany all neoplasms, and from a Darwinian selection of the most capable clones through genetic and epigenetic modifications. GBMs are deadly as they spread widely throughout the brain, making total surgical resection impossible, also due to vascularization. Thus, the need for tumor-specific drugs and pharmacological agents to inhibit cell migration, proliferation, and angiogenesis, is in fact, infinite.

1.1 Classification

GBMs can be classified into primary and secondary GBMs [1]. Primary GBM occurs de novo without evidence of any malignant precursor, whereas secondary GBM develops from initially low-grade astrocytomas (WHO grade II-IIII). Up to 90% are primary GBMs, and patients' age tends to be higher than those with secondary GBM. Genetic alterations which are typically seen in primary GBM include EGFR overexpression, PTN mutation, and loss of chromosome 10, while IDH1 mutations, TP53 mutations, and 19q loss, mostly in secondary GBM. The presence of IDH1 mutation is associated with increased overall survival; thus, a better outcome. Studies show that IDH1 mutations are present in 80% of diffuse astrocytoma and anaplastic astrocytoma and less than 5% in primary GBM.

Based on aberrations and gene expression are distinguished in four related subtypes: proneural (PDGFRA/IDH1 expression), neural, classical (EGFR expression), and mesenchymal (NF1 expression). GBMs have significant genetic heterogeneity and tumor subtypes with genetic alterations, which carry prognostic significance. The classical subtype display frequently loss of chromosomal 10 and mutations in TP53 and IHD1. The mesenchymal subtype has gene expression patterns of astrocytes and microglial markers, while the proneural subtype with patterns of genes expressed in oligodendrocytes with characteristic alterations in TP53, platelet-derived growth receptor (PDGFR), and ILDH1. The neural subtype is the most similar to the astrocytic and oligodendrocytic markers.

Finally, according to 2016 WHO classification of CNS tumors [1], GBM is divided into the following groups:

- GBM, IDH-wild type, corresponding most frequently to the clinically defined primary GBM (**Table 1**).
- GBM, IDH-mutant (about 10% of cases) corresponding to the secondary GBM (**Table 1**).
- GBM, NOS, a diagnosis that is reserved for those tumors for which full IDH evaluation cannot be performed.

Table 1: The WHO 2016 GBM classification: IDH- wildtype *vs* IDH-mutant		
	IDH-wildtype glioblastoma	**IDH-mutant glioblastoma**
Synonym	Primary glioblastoma, IDH-wildtype	Secondary glioblastoma, IDH-mutant
Precursor lesion	Not identifiable; develops *de novo*	Diffuse astrocytoma Anaplastic astrocytoma
Proportion of glioblastoma	~90%	~10%
Median age at diagnosis	~62 years	~44 years
Man-to-female ratio	1.42:1	1.05:1
Mean lenght of clinical hystory	4 months	15 months
Median overall survival • **Surgery + radiotherapy** • **Surgery + radiotherapy + chemotherapy**	9.9 months 15 months	24 months 31 months
Location	Supratentorial	Preferentially frontal
Necrosis	Extensive	Limited
TERT promoter mutations	72%	26%
TP53 mutations	27%	81%
ATRX mutations	Exceptional	71%
EGFR amplification	35%	Exceptional
PTEN mutations	24%	Exceptional

1.2 Pathogenesis

The diagnose complexity, and the resistance to chemotherapy regimens produce a poor prognosis for patients with glioblastoma. Thus, we must understand the molecular mechanisms where lies its aggressive behavior to achieve better management, appropriate therapies, and better outcomes should be better understood. Cancer progression is prompted by somatic evolution, a process in which a collection of mutations engenders a cancer cell genome to diverge from that of a healthy cell. GBM progression occurs as a consequence of various genetic and molecular aberrations that lead to essential changes in main signaling pathways. In last years, proven data have demonstrated that tumors are build-up from multiple cancer cell populations that harbor specific genetic alterations in addition to the classic well-defined genetic abnormalities. Genetic instability and

increased rates of mutation that associate all neoplasms through genetic and epigenetic modifications are responsible for tumors heterogeneity.

- ***Oncogenic pathways***

Receptor tyrosine kinases (RTKs) are the most frequently altered pathway. In all types of CNS cells, the EGFR signaling roles are responsible for the proliferation, migration, differentiation, and survival of them [26]. The EGFR signaling can be activated by overexpression or mutation of receptors, EGFR locus amplification, or by ligands overexpression. It is important to note that any combination of these alterations may coexist within the same tumor. The EGFR oncogenic properties are linked with constitutive activation and uncontrolled phosphorylation activity increase. The most common mutation of the EGFR gene in primary GBMs is the EGFRvIII mutation, so making the receptor ligand-independent and constitutively active [27]. The EGFRvIII mutation is never seen in secondary GBMs or healthy tissues.

Another pathway altered in GBM is the PI3K/PTEN/Akt pathway [28]. Activation of growth factor receptor stimulates PI3K in the cell membrane, as a result, generates the PIP3 (phosphatidylinositol (3,4,5)-trisphosphate), a wll known secondary messenger. Akt is a PIP3 downstream effector that causes in cells inhibition of apoptosis, and stimulates cell proliferation, while PTEN, in general, terminates the PIP3 signal by acting as a negative regulator of PI3K. This tumor-suppressing function of PTEN is frequently inactivated in GBM.

One of the pathways that play a crucial role in the cell cycle is the retinoblastoma (RB) pathway. When cells are in a non-proliferative state or dormant, the hypo-phosphorylation of RB causes an active RB-E2F bond, which prevents the transcription of genes necessary for cell mitosis, and the cell cycle stays at the G1/S phase. The phosphorylation of RB by active CDK/cyclin complexes results in free E2F release, which induces the transcription of genes that promote the synthesis of DNA. Thus, cell proliferation occurs. While only 20% of GBMs are mutated at the Rb locus, inactivating mutations of the upstream regulator p16INK4a, or activating mutations in the downstream factors CDK4 or cyclin D result in dysregulated control of the E2F1 transcription factor are very common [29]. In addition, promoter methylation of the Rb

gene is 43% more prevelant in secondary GBM as compared to primary tumors. This is not, however, found in low grade or anaplastic astrocytomas, suggesting that it may be a late event in astrocytoma progression [30].

The functions of the TP53 pathway are related to cell cycle control, DNA repair (TP53 increases transcription of p21, as a result, constrain the cell to remain in the G1 phase of the cell cycle), differentiation, and cell death. If there is more damage than can be repaired quickly, TP53 will induce cell death to prevent the division of cells containing mutated or damaged DNA. The TP53 pathway has negative feedback loops. TP53 induces transcription of MDM2, a proto-oncogene, which leads to the degradation of TP53 and the prevention of DNA repair. To maintain TP53 activity, the CDKN2A-p14ARF inactivates MDM2 via degradation. MDM4, a regulator of TP53, can inactivate TP53 via binding of the transcriptional activation domain. In human gliomas, TP53 mutations are often missense mutations that target exons crucial for DNA binding [31].

Other alterations seen in GBMs are MDM2 amplification, MDM4 amplification, and CDKN2A-p14ARF deletion. MDM2 amplification appears to be specific to primary GBMs that lack the *p53* mutation [32,33]. In normal cells, WT *p53* induces the expression of MDM2, which in turn inhibits the function of WT *p53*. Furthermore, WT *p53* inhibits the function of *p14*ARF, which would normally inhibit the downregulation of p53 by MDM2. This autoregulatory loop is disrupted when any of the above is dysfunctional, adversely affecting cell-cycle control, DNA damage repair, cell proliferation/differentiation, and neovascularization [34].

Currently, there is no defined sequence of events that definitively lead to GBM development. Any number or combination of these pathways may contribute to GBM formation. Genetic alterations of the main altered pathways in GBM are schematized in **Figure 1.**

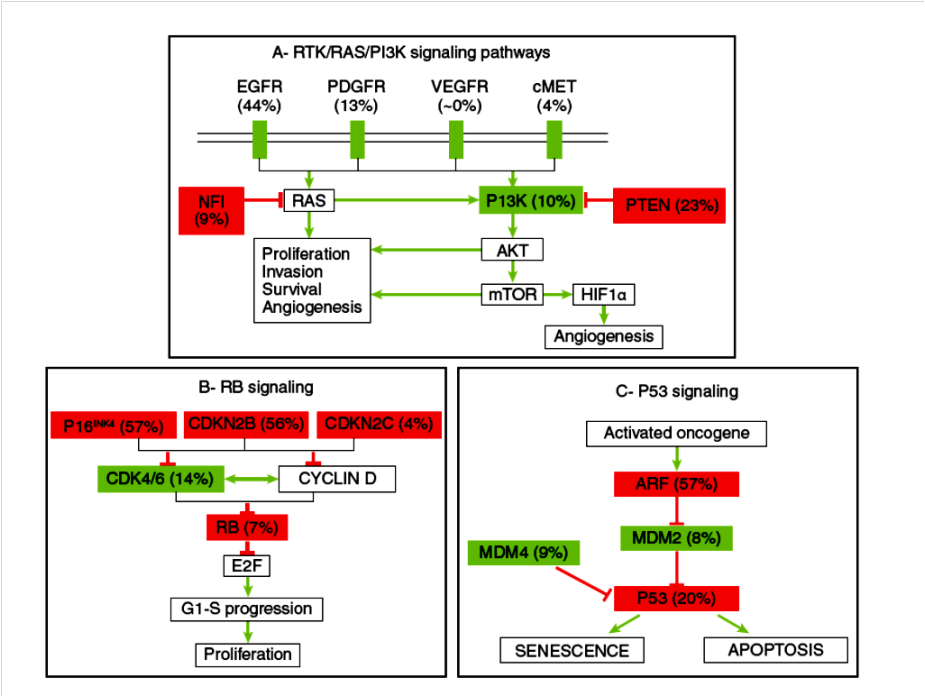

Figure 1. Genetic alteration in major key pathways altered in glioblastoma (*from Glioblastoma, De Vleeschouwer S, editor, Brisbane (AU): Codon Publications; 2017 Sep 27*)

- ***Intratumor heterogeneity***

The presence of diverse different cell subpopulations into a single tumor determines intratumor heterogeneity, which permits tumor to respond to selective pressures, thus contributes to its aggressiveness and growth, as well in treatment failure [35,36]. The cancer stem cells (CSC), with their ability to self-renew, differentiate into different tumor cell types and clonal evolution, which may enhance genetic diversity in affected tissues, currently are two proposed mechanisms for the development of intratumor heterogeneity. The central zone (core) of a GBM tumor is characterized by inflammation, high proliferation, and noted necrosis [37,38]. Between the tumor tissue and brain parenchyma lies a margin called interface. The density of tumor cells decreases as the distance from the core to interface increases. The outside area of GBM is known as the peripheral brain zone (PBZ). It consists mainly of brain parenchymal tissue with isolated infiltrates, which are dispersed throughout healthy brain tissues and may explain why total surgical resection can't be possible, and recurrence is almost inevitable. According to recent studies, the level of genomic alterations or gene expression is tumor

area dependent, biopsies taken from the core or margin zones had much higher levels of genomic alterations compared to biopsies taken from the PBZ. These results state that tumor fragments from the same patient can be classified into different molecular subtypes [38]. Tumor recurrence is still a significant challenge despite new therapies and interventions. This is related to astrocytic tumor diffusion and invasion properties that are linked to the migrating glioma stem cells [39].

- ***Epithelial to mesenchymal transition***

The epithelial to mesenchymal transition (EMT) is a scheduled event in which epithelial cells, through a genetic reprogramming or selection, acquire a mesenchymal phenotype. This process results from alterations in cell architecture and behaviors following cell-cell and cell-extracellular matrix interactions, leading to a clonal outgrowth of localized tumors to promote a mesenchymal phenotype, conferring an unusual property for the cell to colonize surrounding areas and activate angiogenesis [40,41]. Following studies, tumors with high EMT activation are associated with hyper-vascularization and worse outcomes. Aberrant activation of several signaling pathways and EMT regulators can lead to oncogenic EMT and cancer progression. Wnt, TGF-β, and NOTCH pathways, among other signaling pathways, have been shown to play significant roles in EMT [42]. They act via modulating several EMT key transcription factors such as Snai1, Slug, ZEB1, ZEB2, Twist1, and Twist2 [42]. Specifically, a positive correlation found between activation of NOTCH signaling pathway and the expression of EMT markers such as Snail in GBM specimens [43]. Further studies have revealed that NOTCH acts upstream of Snai1 to confer invasive ability and mesenchymal phenotype to glioma cells [43]. Moreover, recent transcriptomic studies have shown that among many cancer signature genes, mesenchymal genes are overexpressed at the expenditure of proneural genes in several GBM biopsies from patients with poor prognosis [44]. Specifically, C/EBPb and STAT3 have been shown to act as mesenchymal driving genes of prognostic value [44]. Patients with tumors that are double-positive for C/EBPb and STAT3 have shorter survival when compared to patients with tumors that are single- or double-negative [44]. This confirms that these two genes are global regulators of mesenchymal transformation in stem cells and that they are

necessary for the maintenance of the aggressive mesenchymal phenotype in glioma cells both in vitro and in vivo, and highlights potential cross-talk between glioblastoma stem cell (GSC) theory and the EMT process.

EMT can generate cancer cells with stem-like properties [45]. Indeed, upon acquisition of EMT phenotype, GSCs acquire both stemness and mesenchymal properties. Unlike tumors that metastasize, this double property may explain tumor invasion that is one of the hallmarks of recurrent GBM. The Slug (EMT marker) correlates with higher grade glioma and is associated with high levels of the GSC marker, CD44, which also has been reported to promote glioblastoma cell migration, invasion, and angiogenesis [46,47].

GBM tumors are extensively vascularized, resulting from overactivated angiogenesis, a process of forming new blood vessels, which is a critical step for supplying oxygen for tumor growth [48]. However, it is often an inefficient process, leading to tumors with areas of hypoxia, necrosis, and edema [49]. Mechanisms of new blood vessel formation include differentiation of GSC into vascular endothelium in addition to the generation of new vessels that involves the recruitment of endothelial progenitor cells [50]. In response to hypoxia, the hypoxia-inducible factor-1 (HIF-1α) is frequently activated in GBM and induces VEGF expression [51]. There is increasing evidence that GSCs are maintained with a vascular niche, which in turn is maintained with VEGF secreted by GSCs and acting through VEGFR-2/KDR [52]. This shows that the VEGF pathway might be the rate-limiting step of angiogenesis expansion. VEGFRs and PDGFRs are structurally, and functionally related growth factor receptors that function in the promotion of angiogenesis and are well-known targets of cancer cells. The angiogenesis transition is believed to be a balance between pro- and anti-angiogenesis factors [53]. Several other mediators have been shown to play roles in GBM angiogenesis, i.e., NOTCH, angiopoietins, PDGF, FGF, integrins, ephrins, and IL-8 [54-56]. Conversely, many endogenous inhibitors such as angiostatin, thrombospondins, endostatin, tumstatin, and interferons oppose the action of these mediators [53]. Many angiogenesis inhibitor drugs are used in recent clinical trials, most commonly targeting VEGF, VEGFR, PDGF, and PDGFR, the key players in the angiogenesis pathway.

1.3 Therapy resistance

Chemoresistance is one of the factors leading to poor survival in GBM patients [57] Therefore, finding out novel strategies to overcome chemoresistance are desperately needed for the treatment of human GBM. Multiple mechanisms, including overexpression of drug efflux transporter pumps such as P-glycoprotein, augmented DNA repair activities, cancer stem cells, and dysregulation of apoptosis, appear to be involved in the development of drug resistance in tumor cells. These properties of chemoresistance originate as a result of changes within the tumor cells, but there is now evidence that the tumor microenvironment also influences chemosensitivity. However, the involvement of brain-resident and infiltrating cells in the chemoresistance of GBM is poorly understood.

- ***Endothelial Cells***

In vivo studies revealed that tumors implanted in the brain display 50% higher blood vessel density than the same tumors implanted subcutaneously [58]. In addition, the endothelial cells (EC) of blood vessels in GBM are morphologically distinct from those in normal brain. GBM-associated ECs have characteristics like having a flat appearance, large nuclei, abundant cytoplasm, multiple nucleoli, and veil-like structures [58]. The ECs derived from GBM are not sensitive to chemotherapy. The enhanced survival properties of tumor ECs are consistent with complementary DNA microarray studies which show that in migrating glioma cell, the proapoptotic genes are down-regulated and anti-apoptotic genes are up-regulated. The abnormal centromeres in tumor ECs may be the intrinsic cause of chemoresistance. GBM-associated ECs also have characteristics like migrating faster, producing high levels of growth factors, having a lower proliferating rate. Understanding these is especially important in the treatment of tumor, because most current antiangiogenic drugs target rapidly proliferating cells, which is one of the factors attributing to their failure in the clinical use. ECs are critical for the assembly and limitation of the blood–brain barrier (BBB). Although the BBB protects the brain from injury and diseases, it also prevents anti-tumor agents from entering the brain tumors. Basically, there are two principle ways to deliver a drug to the target cells: systemic delivery and local administration. Systemic delivery relies on the existing

vessels to deliver anti-tumor drugs to the tumor, but it has to overcome the impediment of the BBB. Local delivery doesn't have this problem, but its transmission distance is too limited to reach distant infiltrating tumor cells.

In order to overcome poor drug transport across the BBB, many strategies have been designed, including chemical modification of drugs, high dose chemotherapy, inducing transient BBB disruption, strategies that use drug carriers (nanoparticle drug carriers), and peptide-based drug delivery for drug delivery to brain tumors. Although much progress has been achieved, most of these strategies fail to meet expectations due to their invasive capabilities, toxicity or instability

More and more compelling results demonstrate that most malignant cells in cancers are generated by CSCs, with characteristics of self-renewing, multipotent, and tumor-initiating cells. Because of their properties of high expression of anti-apoptotic protein, ATP-binding cassette (ABC) pump, and increased capacity of DNA damage repair, CSCs are relatively radio- and chemo-resistant (**Figure 2**).

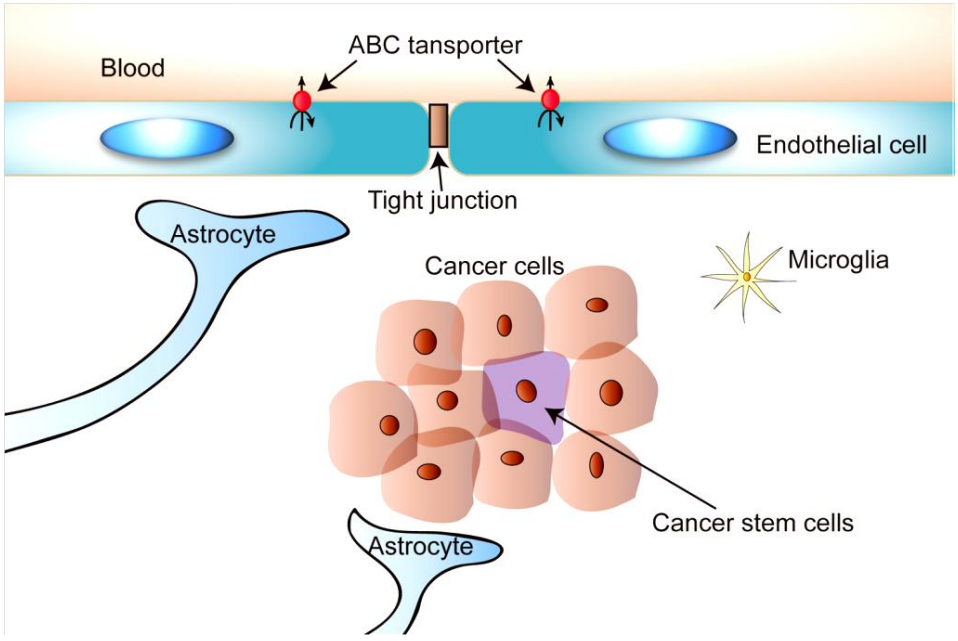

Figure 2. Microenvironment of glioblastoma. The microenvironment of GBM consists of diverse stromal cell types, including astrocytes, microglia, and endothelia cells [58].

CSCs also show high capacity of migration and invasion. The tumor microenvironment is involved in promoting the formation and maintenance of brain CSCs, which is supported by studies. CSCs in brain tumors secrete angiogenic factors

which enhance the formation of tumor blood vessels. This property explains why the most aggressive brain tumors are highly angiogenic. Further studies indicate that tumor microenvironment can promote cell survival in CSCs, which is also one of the factors leading to chemoresistance. For example, vascular endothelial growth factor (VEGF), one of the most potent growth factors to promote angiogenesis, has been shown to enhance the survival of neural stem cells. Thus, inhibitors targeting VEGF are thought to impact brain tumor growth by targeting both the vascular niche and the associated CSCs. Clinical trials investigating the combined treatment of bevacizumab, one VEGF inhibitor, and the chemotherapeutic drug CPT-11 already indicate that this combination is one of the most effective treatments for GBM. While angiogenesis inhibitors alone have been disappointing for GBM [58].

- ***Astrocytes***

Astrocytes are the most abundant and widely distributed glial cell population, accounting for about 50% of the volume of the human brain. It is reported that astrocytes are the first cell type in the brain to react to gliomas and encircle them. Astrocyte activation, also known as reactive gliosis, is characterized by cellular hypertrophy and changes in astrocyte gene expression patterns, such as the up-regulation of glial fibrillar acidic protein (GFAP) [59]. Reactive astrocytes have many similar biologic and morphologic features in common with tumor cells, including the expression of growth factor receptors, increased migration and proliferation capabilities. Moreover, the signaling pathways involved in astrocyte activation are the same in astrocytoma. A variety of basic studies have revealed that many factors, such as TGF-α, CXCL12, S1P and GDNF, secreted by astrocytes can promote the growth of brain tumor cells. By producing heparanase, astrocytes may also promote the invasiveness of brain cancer cells.

Normal astrocytes are reported to regain proliferative status after development, which has long been overlooked. For example, like high-grade gliomas, reactive astrocytes exhibit enhanced migratory and invasive phenotypes [60]. Furthermore, activated astrocyte may undergo cellular dedifferentiation, and this is characterized by upregulation of several important stem cell markers, such as nestin and SOX-2. Cellular activation also induces anchorage-independent growth in astrocytes, which is an

important characteristic of tumor-initiating cells from high-grade gliomas. Over-expression of Nanog in p53−/− astrocytes has been shown to increase oncogenic properties of these cells, including growth rate, foci formation, anchorage independent growth, and tumor formation. Increases in the growth factor sonic hedgehog (Shh) as well as other molecules in injured astrocytes synergistically induces dedifferentiation of GFAP-expressing astrocytes to Cancer Progenitor Cells (CPCs) or neural stem cells (NSCs). All together, these results indicate that astrocytes have the potential to be dedifferentiated into cancer stem cells.

- ***Microglia/Macrophages (MG/MP)***

Antiangiogenic therapy is one of the most important therapies in the treatment of many solid tumors. However, clinical trials failed to achieve the expected effect in GBM patients. Similar observations were made in human recurrent GBMs treated with anti-angiogenic therapy. Microglia/macrophages, which are involved in the development of the vasculature in the CNS, might contribute to the resistance of GBM to antiangiogenic therapy. Increased numbers of microglia/macrophages correlate with poor survival, further supporting the idea that microglia/macrophages may contribute to the escape of GBM from antiangiogenic therapy [59]. These cells therefore represent a potential biomarker of resistance as well as a logical therapeutic target for recurrent GBM treatment. Microglia/macrophages are also involved in the maintenance of GBM cancer stem cells, which further contributes to the chemoresistance.

- ***Noncellular factors***

1. Extracellular matrix

Factors such as the extra-cellular matrix (ECM), interstitial fluid pressure, the hypoxic core and the extracellular pH of tumors will act as a physical barrier to influence the intake and distribution of chemical drugs. These factors may even enhance the chemoresistance of tumors by promoting selection of tumor cells with greater potential to adapt to the changing microenvironment [59].

ECM consists of a mix of collagen and elastin fibers, proteoglycans and hyaluronic acid, which may create significant resistance to the diffusion of therapeutic particles. For

example, the extracellular matrix protein CCN1 has also been shown to limit efficacy of oncolytic viral therapy in glioma. Thus, release of the drug or therapy can occur too far from the tumor space decreasing its intended effect. While ECM has a powerful influence on the diffusion of anticancer drugs, it also participates in promoting tumor progression. C6 glioma-derived ECM activates microglia which promotes secretion of IL-18, and ultimately C6 migration. In addition, coating cell culture plates with purified ECM components, especially fibronectin and vitronectin, enhanced secretion of IL-18 by activated microglia.

Considering the various roles of ECM, it can be an attractive target in the treatment of GBM.

2. Hypoxia, pH and glucose

The oxygen concentration and extracellular pH decreases when it gets closer to the tumor space, which can be explained by the Warburg effect [61]. Data shows that the oxygen concentration in blood is about 10–12.5%, and in healthy normal tissue is about 3–6%. In contrast, solid tumors are typically hypoxic with the oxygen concentration at 1–2%. Hypoxia can be classified into two modes, cycling and chronic. Chronic hypoxia is recognized as an independent prognostic indicator for patients with cancer [85], while cycling hypoxia is still unclear. Hypoxia has many roles in the development of GBM. Hypoxia can induce a shift in phenotype and increases migration/invasion in GBM cells [62]. In hypoxic tumors, the expression of the chemokine ligand 28 (CCL28) is up-regulated, which suggests increased angiogenesis and evasion of immune cell detection. In addition, hypoxia promotes the formation and tumorigenic potential of glioma stem cells.

Studies show that acidic pH and low oxygen levels can increase the resistance to radiotherapy and chemotherapy [62]. The chemoresistance caused by chronic hypoxia may be attributed to a lack of oxygen that is necessary for anti-tumor drugs to act. Cycling hypoxia has recently been shown to induce chemoresistance in GBM by increasing the expression and function of ATP-binding cassette subfamily B member 1 (ABCB1).

Given that hypoxia can be used as an independent diagnostic marker, targeting hypoxia could thus improve the efficacy of chemotherapy or radiotherapy.

3. Signal transduction pathways

Irradiation and/or TMZ treatment can induce DNA strand breaks, which leads to activation of DNA-damage response signaling. In normal cells, DNA damage triggers multiple responses, including cell cycle arrest, DNA repair, angiogenesis, cell death, and metabolic changes, in a manner depending on the strength and duration of the DNA damage stimuli. During glioma treatment, DNA damage-induced cell death and cell cycle arrest are mostly expected as therapeutic effects; however, the existence of gene mutations, signaling molecules related to epigenetic regulation of DNA damage, or an unfavorable DNA damage response prevents better outcomes [63].

Exposing glioma cells to ionizing radiation or TMZ eventually induces DNA strand breaks and activates DNA damage-response pathways. Following the occurrence of a DNA double-strand break (DSB), repair occurs via homologous recombination (HR) if a homologous piece of DNA is present, or non-homologous end-joining (NHEJ) if homologous DNA is absent [64].

Activated p53 induces several cellular responses, and each response varies depending on the degree and duration of the DNA damage. If the DNA damage is mild, then DNA repair and cell cycle arrest are triggered, which results in cell survival, whereas cell death or senescence (permanent cell cycle arrest) is induced by severe DNA damage. In terms of altered molecular signaling related to DNA-damage responses in gliomas, mutation of the p53 gene is most frequently observed (˜30% of all cases) [65]. Most of these mutations are missense point mutations. Data deposited in the COSMIC database (https://cancer.sanger.ac.uk/cosmic) show that these mutations in glioma cases are localized not only in the DNA-binding domain (DBD), the representative hot spots in other cancer systems, but also in several other regions. The p53 mutations found in gliomas result in the loss of p53 function or hemizygous antagonism of wild-type p53 function, such that the normal effects of ionizing radiation or TMZ treatment (i.e., induction of cell cycle arrest or apoptosis) are blocked in glioma cells. Moreover, not only is the function of wild-type p53 lost, but mutant p53 facilitates the oncogenicity of

tumor cells by antagonizing wild-type p53 function or promoting the formation of a beta sheet-like cubic structure that escapes from proteolysis and interferes with the functions of other molecules, including tumor suppressors. Collectively, these findings indicate that p53 mutations confer tumorigenic ability, including refractoriness, and lost tumor-suppressive functions in glioma cells.

Replication stress due to DNA damage stimulated by ionizing radiation or TMZ activates the ataxia-telangiectasia- and RAD3-related (ATR) protein, followed by serine/threonine kinase checkpoint 1 (CHK1) activation. Activated CHK1 phosphorylates and inhibits the function of the cell cycle regulator, CDC25 A, resulting in cell cycle arrest and CHK2-mediated CDC25C inhibition. Regarding the replication stress-induced machinery, a moderate constitutive activation of the ATR–CHK1 pathway by continuous replication stress due to low-dose irradiation contributed to resistance against ionizing radiation in glioma cells, suggesting a potent therapeutic target for gliomas with radio-resistance [66]. Therefore, these reports suggest that replication stress-induced signaling could be an important machinery regulating glioma refractoriness.

As TMZ is an alkylating agent, it promotes the methylation of adenine or guanine residues in DNA (N7-guanine > N3-adenine > O6-guanine), which subsequently causes base-excision repair (BER) and mismatch repair (MMR) of DNA [67]. This response results in DSBs in DNA and activates DNA-damage responses that induce glioma cell growth arrest/death. Among these DNA modifications by TMZ, despite having the lowest frequency, the O6-modification is most toxic and is important for TMZ-induced cell death. TMZ-induced DNA modification of O6 can be reversed by O6-alkylguanine DNA alkyltransferase (MGMT), a DNA-repair enzyme that is encoded by the MGMT gene. Especially in glioma cases, MGMT protein expression is silenced by MGMT gene prompter methylation (compared with other systemic malignancies) and was inversely correlated with disease prognosis in studies of glioma cases treated with TMZ. Interestingly, MDM2–p53 signaling upregulates MGMT expression and confers TMZ resistance to glioma cells, suggesting a cytoprotective role of MDM2. DNA modification of O6-guanine by TMZ can induce pairing with cytosine or thymidine followed by activation of the MMR system. The MMR system removes only newly synthesized

strands, while the O6-modifide guanine remains intact, and this synthesis-strand-removal cycle is repeated. This futile DNA-repair system finally induces a stall at the DNA-replication folk and triggers a single-stranded break (SSB) followed by a DSB. In the MMR system, the MutS protein homolog 2 (MSH2)–MSH6 heterodimer complex first senses a mismatched base and recruits the MLH1–PMS2 heterodimer, which initiates excision of the mismatched base and incorporation of a new base. In gliomas, decreased expression or mutation of MSH6 has been discovered in TMZ-treated or recurrent glioma cases and (to a lesser degree) in pretreated cases. In addition, mutation of MSH6 was also reported to contribute to recurrence and resistance in gliomas treated with TMZ. These findings probably reflect escape from cell death and the accumulation of mutations induced by an impaired MMR system. Methylation of N7- by TMZ is usually repaired immediately by the DNA-repair enzyme poly (ADP-ribose) polymerase (PARP) in the BER pathway. If the BER pathway is suppressed by PARP activity inhibition, then N7-methylation triggers an SSB. In MMR-deficient TMZ-resistant glioma cells, PARP inhibition has been demonstrated to overcome resistance to TMZ treatment. In addition, the expression of the N7- and N3- repair enzyme alkylpurine-DNA-N-glycosylase (APNG) is also essential for resistance to TMZ-induced toxicity in glioma cells and can potentially serve as a prognostic marker of gliomas. These insights suggest the regulatory mechanism of TMZ-induced glioma cell death via N7- and N3- modification, as well as O6-modification.

Other than DSB-mediated signaling, ionizing radiation or TMZ triggers various molecular signaling pathways, even including cell-survival pathways. Intracellular reactive oxygen species (ROS) represent one of the key types of molecules involved. Ionizing radiation removes an electron from intracellular water and generates the highly reactive hydroxyl radical. In contrast, chemotherapeutic agents (including TMZ) produce intracellular ROS via peroxisomal, microsomal, and mitochondrial oxidation [68]. In addition, DSBs triggered by irradiation or chemotherapeutic drugs also generate secondary ROS. ROS affects multiple intracellular organs including DNA strand breaks and activates multiple stress-response signaling pathways, including cell death-signaling cascades. In glioma cells, nuclear factor erythroid 2-related factor 2 (NRF2) expression is

also induced upon TMZ treatment or combination treatment with TMZ and ionizing radiation, which leads to expression of the antioxidant, glutathione. Thus, glioma cells may have molecular machinery, which functions at the level of ROS production to protect against cell death induced by TMZ or irradiation. When irradiation or TMZ mediates cell death signaling, ROS initially activates c-JUN N-terminal kinase (JNK) and triggers p53 activation or activation of pro-apoptotic Bcl-2 family proteins. During this time, activated-p53 also transcriptionally upregulates expression of the pro-apoptotic Bcl-2 proteins and enhances JNK-mediated signaling. In addition, JNK activation can potently induce MGMT expression and paxillin activation in glioma cells, which promotes DNA repair and the invasion of glioma cells, suggesting that pro-survival and oncogenic signaling are also triggered in parallel with cell death-signal activation induced by ROS in glioma cells. Then, the ROS-activated pro-apoptotic Bcl-2 proteins can begin to accumulate on the outer mitochondrial membrane and form pores by homo- or hetero-multimerization with other pro-apoptotic Bcl-2 proteins, which drives the release of molecules localizing to the inter mitochondrial membrane space (such as cytochrome c [Cyt C]) into the cytosol. Released Cyt C triggers activation of the initiator caspase, Caspase-9, and activated-Caspase-9 subsequently activates cytosolic executioner caspases (e.g., Caspase-3). Activated executioner caspases cleave their substrates and finally induce a type of apoptosis known as mitochondria-dependent (intrinsic) apoptosis. Finally, apoptosis-mediated secondary ROS production further enhances pro-apoptotic signaling. Although genetic alteration of these signaling molecules is uncommon in gliomas, it is noteworthy that oncogenic activation of other signaling pathways caused by genetic alteration interferes with the ROS-mediated mitochondrial cell death mechanism in glioma cells. In this case, one of the key molecules in glioma cells is the X-linked inhibitor of apoptosis protein (XIAP), which interacts and blocks these caspases resulting in the inhibition of apoptosis. Augmented expression of XIAP in high-grade gliomas is reported, and inhibition of XIAP also resulted in the sensitization of glioma cells against TMZ or irradiation. The regulatory mechanism of XIAP expression in glioma cells is relatively complicated. MDM2 stabilizes mRNA of XIAP and enhances XIAP expression. In addition, as described above, MDM2 is overexpressed in gliomas. On the

other hand, activation of Akt is upregulated as a result of mutations of RTK signaling-related molecules in gliomas. Enhanced activation of Akt finally triggers augmented activation of nuclear factor kappa B (NF-κB), a transcription factor that induces transcriptional expression of XIAP. Furthermore, as mentioned above, Akt upregulates MDM2 expression. These finding suggests that elevated XIAP expression via complicated signaling crosstalk between Akt, MDM2, and NF-κB contributes to resistance against irradiation or TMZ treatment in gliomas. Collectively, these data indicate that in glioma cells, ionizing radiation or TMZ-induced mitochondrial apoptosis is attenuated by multiple mechanism, suggesting that these mechanisms contribute to refractoriness of gliomas.

Ionizing radiation- or TMZ-mediated ROS production can also potently induce endoplasmic reticulum (ER) stress responses in glioma cells [69]. ER stress is usually caused by the intracellular accumulation of misfolded proteins or disruption of intracellular calcium ion homeostasis, and induces various cellular responses including cell survival and cell death, which are referred to ER stress responses (ERSRs). Among the signaling activated by irradiation-mediated ROS-induced ERSRs in glioma cells, activating transcription factor 6 (ATF6), a transmembrane transcription factor that is activated upon ER stress, is reported to protect glioma cells from irradiation-induced cell death via upregulation of binding immunoglobulin protein (BiP, also known as GRP78) and Notch expression. Although the involvement of ROS production is unclear when treating glioma cells with TMZ, ERSR can be activated, and expression of BiP and activation of protein kinase R (PKR)-like endoplasmic reticulum kinase (PERK; an ER-resident kinase that initiates ERSR signaling) are subsequently triggered. PERK activation has also been demonstrated to contribute to the growth of glioma cells, suggesting that TMZ-mediated ERSRs can potentially drive not only induction of glioma cell death but also the refractoriness of gliomas. In addition, ER stress can potentially enhance the expression of the cell-surface death receptor 5 (DR5) in glioma cells, which binds to its specific death ligand TNF-related apoptosis-inducing ligand (TRAIL) and triggers extrinsic apoptosis pathway-mediated cell death. Importantly, DNA damage-induced p53 also upregulates DR5 expression in glioma cells, which suggests that DR5

and ROS-mediated crosstalk of ER stress-mediated signaling with p53-depndent signaling are important for understanding irradiation- or TMZ-induced cellular responses of glioma.

Ionizing radiation induces not only cell death signaling, but also survival/oncogenic signaling at the RTK level. Ionizing radiation induces activation of RTKs by triggering forced homo-or hetero-dimerization of each RTK. In glioma cells, irradiation mediated EGFR stabilization by interfering with ubiquitin ligase casitas B-lineage lymphoma B (CBL-B), resulting in EGFR activation and the induction of glioma cell invasion [69]. Gliomas are often reported to relapse with a more aggressive form after standard therapy, and acquisition of this enhanced malignant phenotype may be caused by these kinds of therapy-induced mechanisms.

1.4 Glioma stem cells

Solid tumors such as GBMs are characterized by a high degree of heterogeneity, which has been explained by two different theories. According to the first theory, the stochastic model, tumor cells share the same genetic mutations (homogeneous), and heterogeneity is the result of intrinsic as well as extrinsic factors. According to the second theory, the hierarchy model, cells are intrinsically different in terms of differentiation stage and only a small subset, the CSCs, can initiate tumor growth and progression. This subpopulation is increasingly referred to as the cause of tumor onset and recurrence as well as therapeutic resistance.

Similar to many solid tumors, GBM development leads to the formation of hypoxic areas. Uncontrolled proliferation of tumors, especially in the high cellular density pseudo-palisading region, leads to a decrease in O2 tension. In response to this stress, cancer cells stabilize the hypoxia-inducible factor 1 (HIF-1), which in turn induces overexpression of VEGF. The binding of this growth factor to its receptor on endothelial cells promotes neo-angiogenesis. This vascularization is characterized by abnormal, dysfunctional, and/or occluded vessels, which are unable to sustain normoxia, hence the formation of hypoxic regions. Although a hypoxic microenvironment could induce cell

death in normal conditions, it is also well known to maintain CSCs, especially in GBM [70].

While actively proliferating cells are more likely to be found close to the vessels, stem-like cells lie in the central parts of the tumor, the core region which contributes to a CSC niche. The core region is more likely to be radioresistant and chemo-resistant, and usually necrotic. These different distributions of cells illustrate the GBM heterogeneity. CSC population density and aggressiveness are inversely related to oxygen tension. In the context of vasculature and oxygen supply deficiency, several studies, including ours, demonstrated that autophagy is induced as a cytoprotective mechanism. This catabolic process, which is complementary to the ubiquitin–proteasome system, leads altered organelles and proteins to lysosomes where they are degraded. Besides basal physiological level, autophagy is upregulated when cells are subjected to various stresses such as nutrient starvation, oxygen deprivation, or therapy. In GBM, hypoxia-induced autophagy promotes cell survival and aggressiveness. This could be explained in part by the pro-survival effects of autophagy in response to antiangiogenic therapy, leading to hypoxia. Furthermore, it has been shown that antiangiogenic agents targeting the VEGF or its receptor induce expansion of CSCs in tumors implanted in animals, supporting the link between hypoxia-induced autophagy and stemness.

CSCs are known to display different properties which give them the ability to relapse and be more resistant to chemotherapy or radiation therapy [71]. These properties are currently being investigated in order to better characterize CSCs. The self-renewal of CSCs (which is one of the properties defining CSCs) can be determined with two different tests: the colony forming unit approach and the limiting dilution assay. Both tests are based on the ability of a single CSC to proliferate and create a new neurosphere in vitro. CSCs share common properties with normal stem cells such as their ability to differentiate into specific cell lineage. For GBM, the CSCs should be able to differentiate into neurons, astrocytes, and oligodendrocytes. Moreover, the most important feature of CSCs is their ability to resist treatment. In GBM, this property leads to tumor relapse and unfortunately to patient death. The most conventional approach includes the evaluation of the apoptotic impact of temozolomide and/or radiation on CSCs. A strong resistance to

these treatments is a characteristic of CSC. Finally, the capability of CSC to form a tumor has to be addressed by xenograft or orthotopic cell engraftment.

The classical cell sorting methods are based on the recognition of specific extracellular or intracellular antigens using fluorescent (FACS) or magnetic (MACS) probes. Other methods such as affinity chromatography, panning, and aptamers also use the immunological recognition principle. In GBM, some of the most useful markers are SOX-2, OCT4, NANOG, CD133, and ABCG2 [72]. However, no single marker can be considered a gold standard, and, therefore, a series of markers is mandatory to validate the stemness status.

SOX-2 is a gene located on chromosome 3q26.3-q27, a member of neural growth transcription factors family called SOX [sex determining region Y (SRY)-box], which controls several developmental processes and maintain stem cell activity in different tissues during embryogenesis and adult stages. Many studies have implicated SOX-2 expression with growth, tumorigenicity, metastasis, drug resistance, and prognosis of various cancers [73]. The expression of SOX-2 is up or downregulated by various mechanisms like transcriptional factors, signaling pathways, post-transcriptional, and post-translational regulators. Transcription factors such as Oct4, Nanog, and less Stat3 co-operate with SOX-2, and this collaboration promotes the expression of genes, hereupon the production of molecules, activation of metabolic processes, which guarantee the self-renewal and the maintenance of stem cell characteristics. AP-2, PROX1, PAX6, etc. are transcriptional factors that upregulate SOX-2 and are well-expressed in the early stages of neurodevelopment, E2F3a, E2F3b, and Cyclin-dependent kinase inhibitor P21 are involved in SOX-2 expression and so control the proliferation of NPCs. Another way that regulates the expression of SOX-2 is through SOX4, which in turn, mediated by the TGF-β signaling pathway forms a complex with OCT4 in SOX-2 promoter's sites. SOX-2 expression, also participate in Shh, Wnt, and FGFR signaling pathways. SOX-2 is one of the most important transcription factors that regulate cancer stem cell properties. SOX-2 could reprogram differentiated cells into pluripotent cells in concordance with other factors and is overexpressed in various cancers; it is a marker of

cancer stem-like cells (CSCs) in neurosphere cultures and is correlated with the proneural molecular subtype.

SOX-2 is expressed in all gliomas, and the proportion of SOX-2-positive cells – ranging from 6–80% of cells in the tumor – correlates with the malignancy grade [74]. In GBM, SOX-2 is intensely expressed in the most malignant component of the tumor and in highly proliferating cells of oligodendrogliomas. The gene encoding Sox-2 is also amplified in approximately 14.4 and 11.1% of GBM and anaplastic oligodendrogliomas, respectively, compared with EGFR amplification in 36–40% and loss of PTEN due to loss of heterozygosity in 60–80% of GBM cases. In malignant glioma samples, the intense positive staining for SOX-2 overlaps with Ki67/MIB.1-positive nuclei, which is a gold standard marker for proliferating cells. In addition, tumor regions showing intense SOX-2 staining also show frequent amplification of the *SOX-2* gene. In cultured neurospheres, the Sox-2 gene is often amplified, and therefore, the hypothesis that a genetic correlation exists between neurospheres and the most anaplastic regions in glioma is validated by the expression pattern of SOX-2.

The extent of SOX-2 expression is also concordant with the degree of heterogeneity observed in the cell population found in gliomas, which appear in various stages of differentiation. Gangemi et al. [75] demonstrated that suppression of SOX-2 expression in GBM tumor-initiating cells prevented their proliferation and reduced their tumorigenicity in long-term culture conditions and no obvious short-term effects on apoptosis, cell senescence or increased differentiation was detected. They also found that the downregulation of SOX-2 using siRNA targeting the 3′ UTR of *SOX-2* mRNA in GBM cell lines results in reduced Ki67 expression in these cells. This effect was independent of defects in progression through the cell cycle and more likely due to loss of the ability of GBM cells to divide indefinitely, hence their reduced stemness. Reduced proliferation of these cells eventually leads to their premature exit from the cell cycle and eventual disappearance from the culture. Annovazzi et al. [76] conducted a study in order to evaluate SOX-2 expression, distribution, and gene copy number status in normal nervous tissue, and in a number of neuroepithelial tumors and cell lines derived from primary GBM tumors by immunohistochemistry, western blotting, and other molecular

biology techniques. Consistent with other reports, they also observed a correlation between the expression of SOX-2, Ki 67/MIB.1, and NESTIN. In this regard, it is possible that SOX-2 creates a permissive environment for the induction of pluripotency and tumor development.

1.5 Inflammatory tumor microenvironment

Studies of inflammatory mediators have established the tumor micro-environment as a driver of oncogenesis [77]. This inflammatory milieu often precedes cancer, however recent data also point to the ability of oncogenic changes to induce inflammatory responses that are later harnessed by the tumor to survive and proliferate. The IDH1 mutation, present in the majority of low-grade gliomas, initiates an inflammatory cascade that is ultimately hijacked by the tumor. Glioma infiltrating macrophages and microglia are polarized to the M2 phenotype, subverting the host's adaptive immune response, and fostering a tumor milieu ripe for angiogenesis, migration, and metastasis [78]. As data continue to expand the role of inflammation in low-grade gliomas, new molecular pathways may emerge as therapeutic targets that offer a window of opportunity to intervene before the malignant transformation of low-grade glioma occurs.

DNA damage of varying origins can stimulate an inflammatory response thereby promoting tumorigenesis via active signaling pathways that upregulate the production of additional pro-inflammatory mediators [79]. One such example in the context of lowgrade gliomas is the genetic mutation encoding the enzyme isocitrate dehydrogenase 1 (IDH1). IDH1 is of particular interest due to its fairly well-established role in the earliest stages of gliomagenesis, even before 1p/19q codeletion or a TP53 mutations occurs [80]. IDH1 mutations sensitize gliomas to radiation and chemotherapy and have therefore been associated with greater overall survival [81]. However, numerous associations between IDH1mut and inflammation have also been suggested, implicating this oncogenic mutation as a potential initiator of the inflammatory cascade presented in this perspective review. It is of note that 88% of low-grade diffuse astrocytomas, 79% of oligodendrogliomas, and 94% of oligoastrocytomas harbor IDH1 mutations. The accumulation of 2HG in the brain has been repeatedly linked with an increased risk of developing brain tumors in patients with the metabolic disorder 2-hydroxyglutaric

aciduria [82]. 2HG, which is structurally similar to the excitatory neurotransmitter glutamate, drives tumorigenesis [83]. To protect tissue against excitotoxicity, extracellular glutamate concentration is tightly regulated to control both its release and uptake. However, 2HG – which is structurally similar to glutamate – mimics an extracellular increase in the neurotransmitter, leading to the over-excitation of NMDA receptors and an increase in mitochondrial production of ROS. IL-1β, a pro-inflammatory cytokine, invades brain tissue following NMDA-induced excitotoxicity, fueling a cascade that fosters a tumor-promoting microenvironment [84]. IL-1β, in addition to Tumor Necrosis Factor-alpha (TNF- α) and IL-6, is among a series of cytokines that initiates the inflammatory cycle, which ultimately fuels an immunosuppressive tumor niche [84]. These data suggest that the IDH1 mutation, so commonly found in tumors that progress toward higher stages of malignancy, may drive an inflammatory cascade that feeds this progression. Studies comparing the inflammatory microenvironment of LGGs that are IDH1mut compared to those that are not, are of considerable interest and necessity.

1.6 Nitric oxide synthase (NOS2) and GBM

Nitric oxide (NO) is a free radical gas transmitter that regulates various biological functions in the body. After it was identified in the 1980s as a small vasoactive molecule, the cardiovascular activities of NO were more notable mainly related to its vascular relaxation function, and to its anti-thrombotic and anti-inflammatory effects. Besides blood flow regulation, NO involvement is recognized in other physiological functions such as neurotransmission, immune-response facilitation, and antipathogenic response. The production of NO in cells under normal physiological conditions occurs from the conversion of L-arginine in L-citrulline by the enzyme nitric oxide synthase (NOS). There are three isoforms of NOS (**Figure 3**): neuronal NO synthase (nNOS, also known as NOS1), inducible NO synthase (iNOS or NOS2), and endothelial NO synthase (eNOS or NOS3).

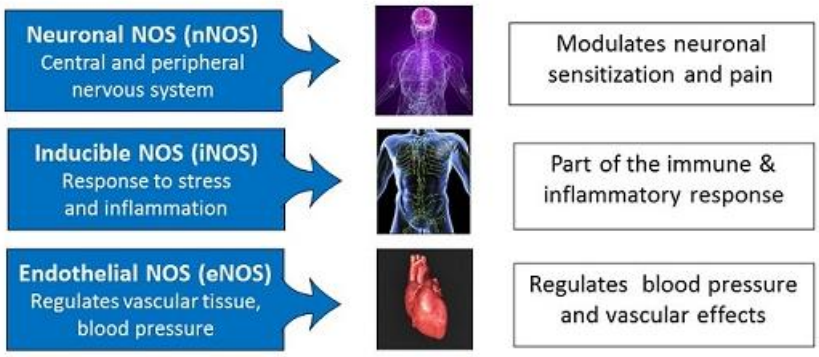

Figure 3. Isoforms of Nitric Oxide Synthase

The category called constitutive NOS (cNOS) includes both nNOS and eNOS and, when activated, only produce nanomolar concentrations of NO for seconds or minutes. However, NOS2, the inducible isoform, generates higher amounts of NO, in the micromolar range and for longer intervals such as for hours or days. Both cNOS members depend on increases in calcium ion concentrations for activity; hence, produce low amounts of NO for short durations, whereas NOS2 is calcium-independent. In general, the expression levels of NOS2 in tissues is also a measure of NO generated in that tissue or its surrounding environment.

Among the effects of NO in cancer, it is now evident that NO plays important roles in various stages of carcinogenesis such as DNA damage, oncogene activation, inhibition of DNA repair enzymes and tumor suppressor genes, and the modulation of apoptosis and metastasis [85,86]. Anti-tumor effects of NO produced by the immune-defense system were demonstrated to function against tumors of different human origins in animal models, while implications of pro-tumor effects of NO were made by association with expression of enzymes that produce NO in tumor cells in progressing tumors and metastasized tissue. Over the years, a dual role of NO in cancer has been acknowledged and studied with more momentum to dissect the mechanisms leading to these two activities with respect to tumorigenesis. During the past two decades or so much has been written about the dual nature of NO, which strongly suggests a concentration-dependent relationship between NO expression and biological response. The current thinking based on observations that NOS2 expression is high in a number of

tumors and that this correlates with poor survival has led to the conclusion that induction of this NOS isoform may somehow be related to tumor genesis or that its expression may be used as a marker for not so favourable outcomes. However, it appears that the dual role of NOS2 is well influenced by the cell situation and is environment-dependent, with either induction or inhibition of NOS2 possessing anti-cancer potential based on tumor and cell types.

Aberrant NOS2) expression and its enzymatic product NO, which play a crucial role in the pathophysiology of several inflammatory disorders, have been implicated in the development, growth and progression of several human malignant tumors, including glioma [87-89]. NOS2 has been reported highly expressed in grade III astrocytomas and glioblastomas, with a positive correlation between its expression and tumor grade [87]. As recently reviewed [90], an overexpressed NOS2/NO system in the tumor cell induces invasion, angiogenesis, immunosuppression, differentiation, and therapeutic resistance in gliomas. GSCs have been shown to express high NOS2 levels, which were correlated with a poorer glioma patient survival [86]. Furthermore, the silencing of NOS2 expression by RNA interference decreased in vitro brain glioma-initiating cells (GICs), highlighting the main role of NOS2 in GSC biology and maintenance [86]. NOS2 knockdown by RNA interference strategy or by specific inhibitors negatively affected the proliferation and invasiveness of GBM cells [87,91], and was able to reduce the progression of subcutaneous and intracranial human glioma xenografts in mice [86]. The increase or the significant inhibition of tumor cell migration were respectively recorded after treating a co-culture of U87-MG and C6 glioma cell lines with the NO-donor sodium nitroprusside (SNP), or the NOS inhibitor NAME (Nomega-nitro-l-arginine methyl ester) [92]. The key roles of NOS2 in tumor development and vessel maturation in the C6 rat glioma cell line were also published [93]. In a recent study, our group reported that NOS2 expression was highly and significantly upregulated in glioma cells that were kept in the specific medium for neurosphere generation [94]. Moreover, a high and significant correlation was observed among the expression of NOS2 and SOX-2 (Sex determining region Y-box 2), which is a stemness marker that is aberrantly upregulated in both human glioma cell lines and primary cultures. NOS2 pharmacological inhibition

might therefore have potential therapeutic value in the treatment of GBM. A major class of NOS2 inhibitors are amidine derivatives, such as L-NIL, the cyclic amidine ONO-1714, and the aromatic acetamidine 1400W [95] **(Figure 4).** This latter is considered to be one of the most potent and selective NOS2 inhibitors reported to date [95-97], although it has never been approved into clinical use. Pharmacokinetic studies showed that 1400W is an irreversible or an extremely slowly reversible inhibitor of NOS2, although it has been reported to be active for a few hours after administration [98,99]. In the continuous effort to develop even more selective and effective NOS2 inhibitors, different acetamidines structurally related to the 1400W leading scaffold have been published [95,100-103], thus confirming the growing interest in the pharmacologic potential of NOS2 activity inhibition in different diseases, including GBM.

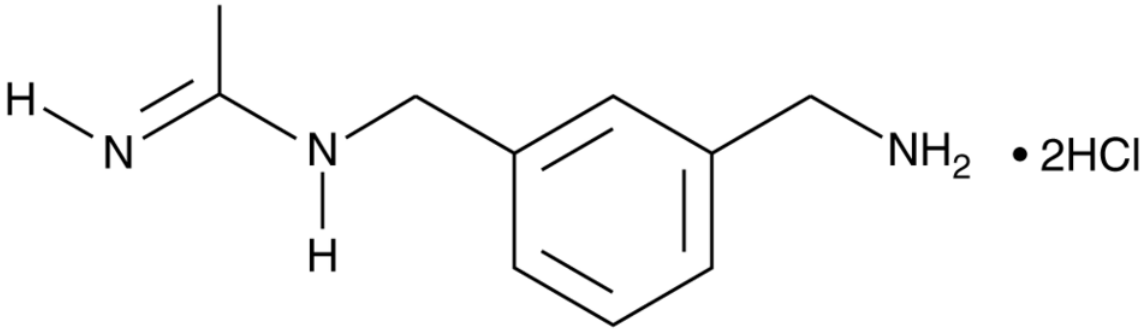

Figure 4. Structure of 1400W (hydrochloride)

1.7 Role of autophagy

The autophagy is an essential metabolic process in degrading and recycling cellular components. **(Figure 5)**

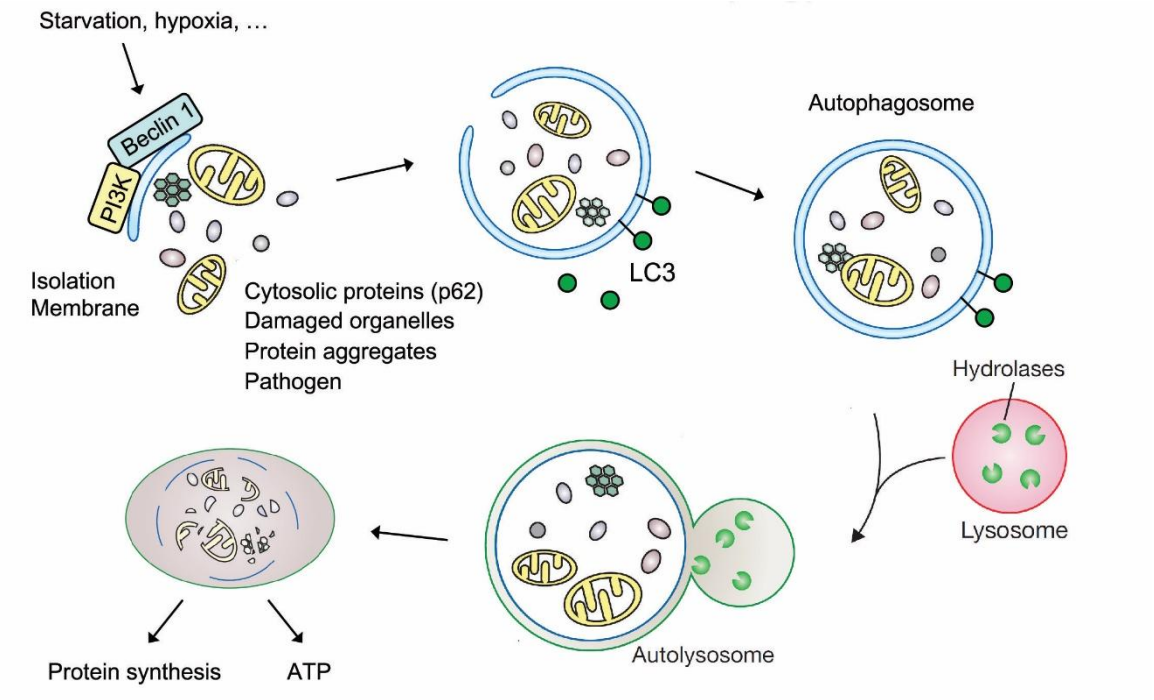

Figure 5. Schematic model of autophagy

According to GBM has been proposed therapies which activate or inhibit autophagy, suggesting a dual role of autophagy in GBM tumorigenesis, thus understanding the molecular pathways involved in autophagy targets is critical for GBM therapy.

Over the last decade, is evidenced autophagy with its dual roles in cytoprotection and cell death in several human diseases, including GBM [104]. Various studies debated that autophagy may have either GBM-suppressing or GBM-promoting effect [105-111]. On the one hand, autophagy can be tumor-promoting by recycling intracellular substrates to support metabolism and maintain mitochondrial functions. It could also suppress GBM by eliminating oncogenic protein substrates, damaged organelles, toxic unfolded proteins, and preventing chromosomal instability. The role of autophagy in tumorigenesis is tissue and genetic context-dependent, and it is crucial to understand its paradoxical role in GBM.

GBM has a lower expression or deletion of relevant genes for autophagy initiation and elongation like BECN1, UVRAG, ATG4, and ATG5 [106]. The mechanistic study

claimed that autophagy inhibits tumor progression by limiting inflammatory response, which favors necrosis-associated tumor growth [104,112]. supported by the EGFR antagonist, which could induce T98 G glioma cell death through autophagy-reduced inflammatory response. Secondly, autophagy induces glioma cell senescence. Treatment of adenovirus strains expressing shMet (hepatocyte growth factor receptor) on glioma cells U343 could activate autophagy through PI3K/AKT/mTOR pathway, resulting in cell senescence. Inhibition of autophagy by 3-MA could block TMZ-induced senescence and induce apoptosis, while activation of autophagy by inhibiting mTOR signaling could enhance TMZ-induced senescence in glioma cells. Thirdly, autophagy inhibits glioma invasion and cell motility [113]. Catalano et al. reported that the induction of autophagy might block the GBM cell migration and invasion [113].

Despite its role in limiting tumorigenesis, autophagy also has positive effects on glioma cell proliferation, chemoresistance, and decreasing cell apoptosis. Facing insufficient vascularization and a limited supply of oxygen and nutrients, GBM could be assisted by autophagy through the energy production of metabolic substrates [114]. The increase of reactive oxygen species (ROS) could also induce autophagy to increase tumor cells' survival by promoting glycolysis and increasing lactate, acetoacetate, and 3-hydroxy-butyrate. Oxidative stress might activate hypoxia-inducible factor-1α (HIF-1α) and NF-κB, which induce degradation of caveolin-1 (Cav-1), the tumor suppressor through autophagy. Under hypoxic conditions, increased levels of the BNIP3 (a HIF-1α downstream target protein) in U87 and T96 G cells could activate autophagy and promote cell survival. Besides, autophagy may also facilitate the metastasis of tumor cells. Autophagy may promote the detachment of cancer cells from the extracellular matrix [115]. Furthermore, autophagy inhibitors could enhance chemotherapy against GBM [116]. Co-treatment with chloroquine (CQ) and ZD6474, a small molecule that blocks the VEGF receptor on GBM cell lines, could significantly increase cell apoptosis [117]. The autophagy inhibitor 3-MA could enhance the antitumor effect of WP1066, an inhibitor of the signal transducer and activator of transcription-3 (STAT3) on U251 glioma cells [118].

Autophagy may be involved in stemness maintenance by promoting GSCs differentiation and the expression of stem cell markers through ROS generation, EGFR, TGF-βand NFκB signaling pathways [119]. Autophagy may promote differentiation of GSCs into cells with a neuronal, astrocytic, or oligodendroglial phenotype [120,121].

The metabolic homeostasis of GSCs could also be regulated by autophagy. High-energy metabolites (lactate and ketones) are revealed crucial to promote growth and metastasis of cancer stem cells. However, nutrient supply is usually insufficient in the microenvironment of GSCs due to rapid tumor growth, where autophagy is primarily activated to compensate for the metabolic deficiency [122].

A recent study revealed that the treatment of cannabidiol on GSCs could induce autophagy via the transient receptor potential vanilloid-2 (TRPV2) channel, which inhibits their capacities to metabolic self-renew and increase resistance to therapeutic agents [120].

Autophagy could also affect GSCs' motility [123]. Two small-molecule inhibitors of dopamine receptor 4 functions (L-741, 742, and PNU 96415E) are shown to impede autophagic flux through PDGFR-beta, ERK1/2 and mTOR signaling, resulting decrease of cell motility and differentiation in patient-derived GSCs comparing with normal neural stem cells [123]. Autophagy-related proteins are decreased in GSCs with chemoresistance to TMZ. GSCs could also be inhibited by chemotherapy agents through autophagic cell death [124].

In conclusion, autophagy is now considered as an alternative cell survival/death mechanism in tumorigenesis of GBM. Despite the arguments on the dual functions of autophagy on GBM, autophagy plays an crucial role in GBM tumorigenesis. The advances in our understanding of the autophagy process involved in GBM tumorigenesis may provide biological and therapeutic insights into the glioma research. Of note, the prognosis of GBM could be influenced by autophagy, either positively [106,107] or negatively [108-110, 125], as well as a defective autophagic pathway has been associated with GBM [126]. Autophagy may also limit the tumor-associated inflammation profile through the removal of inflammasomes as well as damaged mitochondria, which are considered to be crucial in supporting the inflammatory microenvironment determinant

for tumor progression and invasiveness [127]. Autophagy activation has also been associated with the impairment of GBM cell migration and invasion, which could conversely be stimulated by autophagy inhibition [113]. In this respect, it is noteworthy that the apoptotic pathway is often mutated in human tumors, including GBM [128,129]. Autophagy can then represent a valid alternative form of programmed cell death to prevent tumor growth and progression.

1.8 Role of extracellular vesicles

Extracellular vesicles (EVs) found in biofluids of GB patients make a novel approach for GBM diagnose. EVs are known to carry molecular loads such as nucleic acids, proteins, lipids; thus, GBM molecular patterns may be present in the EVs of GBM patients [130]. Like normal cells, GB cells are capable of communicating with neighboring cells through molecules. Based on recent studies, these molecules secreted by tumor cells frequently are encapsulated by lipid layer-based structures, denominated as extracellular vesicles. These EVs are involved in immune regulation, angiogenesis, tumor progression, and intercellular communication by exchanging proteins and RNA [131].

Based on their origin and/or size, EVs can be classified into three subclasses: apoptotic bodies, microvesicles, and exosomes [132] **(Figure 6).** During the process of programmed cell death, cells release apoptotic bodies as blebs, with a size range between 1000 and 5000 nm. Microvesicles, with size ranging from 100 to 1000 nm, also known as ectosomes, are produced in the plasma membrane by the process of external budding. The EVs with size ranging from 30 to 100 nm are known as exosomes (the smallest) and are created inside the cell through internal budding of vesicles in the lumen of early endosome.

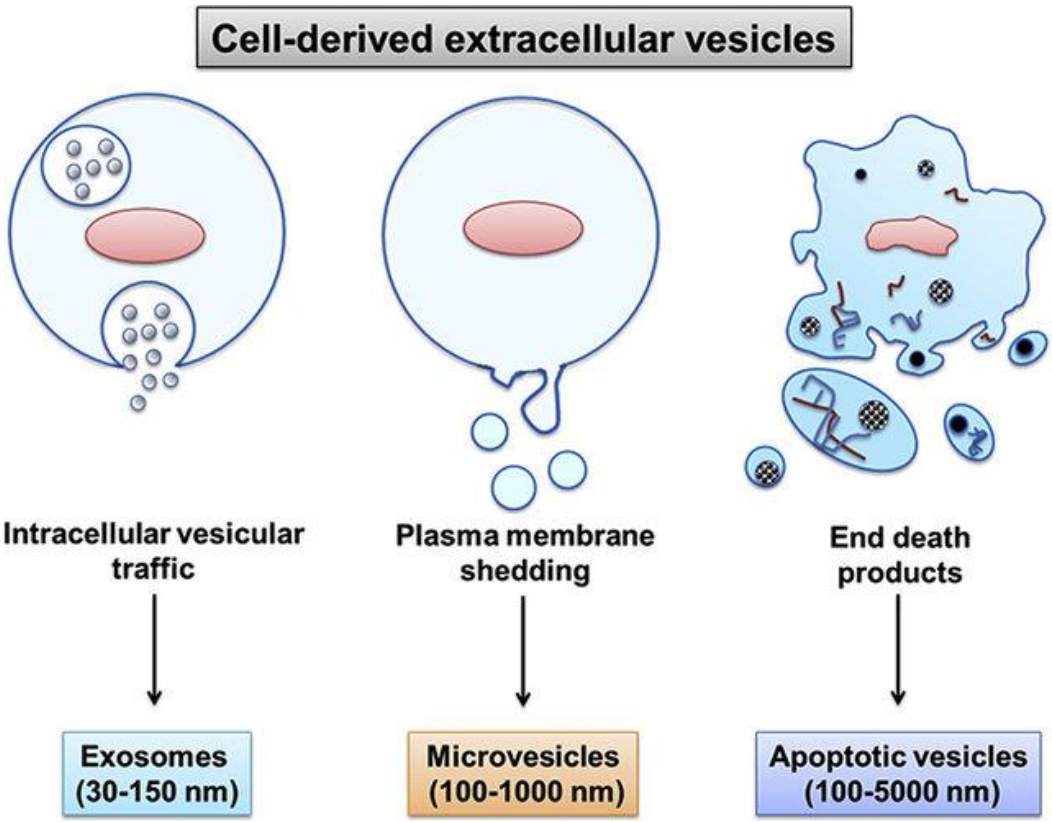

Figure 6. Classification of extracellular vesicles according to the mechanism of generation. Exosomes are generated intracellularly from multivesicular bodies. Microvesicles are produced by budding from the extracellular membrane. Apoptotic vesicles are released upon cell fragmentation during apoptotic cell death.

EVs role was related to removing biological waste from cells, while now it is indisputable their crucial role in intercellular communication, not only in normal body functions but also in pathological states such as cancer. Microvesicles are produced through the outer budding of the plasma membrane, while exosomes are generated by blending the multivesicular bodies into the plasma membrane. The biogenesis of exosome begins at endosome formation through the invagination of the plasma membrane. The endosomes are divided into three different compartments inside the cell during the endocytic process, and they are early recycling, and late endosomes. Early endosomes are formed after plasma membrane invagination and are able to fuse with endocytic vesicles leading to different cellular fates, e.g., recycling, secretion, or degradation. After sorting the recycled amount into recycling endosomes, the remaining early endosomes transform into late endosomes. Cytosolic molecular cargoes, including

proteins, lipids, and nucleic acids, are inserted into exosome during intraluminal vesicle formation, and the contents differ according to their different biogenesis pathways. Intraluminal vesicles are stored within multivesicular bodies before being degraded by lysosome or released as exosome through fusion with the plasma membrane.

The EV content can differ according to their biogenesis and cell of origin [132]. Proteins related to membrane function (e.g., ICAM1, integrins), EV biogenesis (TSG101, ALIX), uptake, and release (Annexins, Rab proteins) are commonly found in EVs. In addition, a large array of tetraspanins, e.g., CD9, CD37, CD53, CD63, CD81 and CD82; proteins related to antigen presentation, e.g. HLA-G, MHC; cytokines, e.g., VEGF-A, semaphorin 3A (Sema3A), TGF-beta and EGFRvIII could also be present. The complete composition of EVs lipid is fully revealed, but it is known that their lipid bilayer is enriched with sphingomyelin, cholesterol, phosphatidylcholine, phosphatidylinositol, phosphatidylethanolamine, phosphatidylserine, prostaglandin and ganglioside GM3. EV nucleic acid contents are diverse in nature, and they are usually fragmented. Most of them are small RNAs, especially rRNAs and tRNAs, but other small RNAs are also present, e.g., short and long non-coding RNAs, mRNAs, and miRNAs.

In GBM, tumor cells use EVs for their benefits to promote angiogenesis, clonogenicity, heighten cell proliferation, and invasion [133]. Through transferring non-coding RNAs, oncogenic EGFRvIII, histones, PTEN, and pro-migratory factors, EVs themselves can influence tumor microenvironment and convert normal cells into malignant cells. In vivo experiments also showed a change in phenotype of brain immune cells that had taken up GB-derived EVs [134]. These observations suggest that EVs can alter tumor microenvironment by exchanging signals between brain cells, which ultimately provide a suitable environment for tumor growth.

EVs are emerging as a promising source of biomarkers for diagnostic and prognostic purposes [133]. They can be noninvasively collected for longitudinal sampling; their large array of molecules allows the characterization of the global tumor genome and transcriptome; their short half-life enables detection of rapid changes in the tumor milieu. Besides, its inherent stability and capability to maintain the integrity of its contents allow researchers to analyze DNA, RNA, and proteins from solid tumors. It also

provides a potential link between tumor drug-resistance and metastasis. Noerholm et al. [135] showed that distinct RNA expression pattern is present in serum EVs of GB patients compared with controls. The miR-301a level in EVs is significantly increased and correlated with overall survival. In fact, nucleic acid variations could be detected in EVs collected from GB patients, e.g., IDH1, EGFRvIII, miR-21, miR-1587 and EPHA2. EV nucleic acids can also serve as a source of biomarkers that depicts chemotherapeutic resistance in GB patients. For example, O6-methylguanine-DNA-methyltransferase mRNA expression level was found to be increased in EVs collected from GB patients resistant to temozolomide.

Of note, TMZ affects EVs secretion and could confer drug resistance to recipient cells by transferring molecular cargos through EVs [136]. Mass spectrometry-based analysis reveals that protein levels related to cell adhesion, e.g., β1-integrin, are increased in EVs after TMZ treatment whereas TMZ resistant cell-derived EVs containing miR-151a are able to generate drug resistance in recipient cells [137]. It is, therefore, possible to monitor TMZ failure by analyzing the molecular components of GB tumor-derived EVs. Other EV surface proteins such as CD44 and CD133 may serve as biomarkers for chemoresistant GB patients [138]. GSCs responsible for chemoresistance and tumor recurrence also express the same cell surface markers [139].

2. RATIONALE AND AIM OF THE STUDY

Although the complex biomolecular framework that underlies GBM aggressiveness is not yet fully defined, an increasing amount of studies that aimed at identifying the mechanisms responsible for GBM progression, chemo/radiotherapy resistance, and high recurrence rate led to the identification of **GSCs** as an election target for anti-GBM therapy. The current GBM pathophysiological hypothesis involves GSCs being responsible for the formation, expansion, recurrence, and the high therapy resistance of GBM.

Several studies have suggested that gliomas, similar to most established malignant tumors, are characterized by a moderately **inflammatory environment**. The inflammatory process seems to be involved in all of the steps of tumorigenesis, promoting the genomic instability, proliferation, and survival of malignant cells, as well as angiogenesis, resistance to therapy, local or systemic immunosuppression, and also raising the metastatic process.

Aberrant **nitric oxide synthase 2 (NOS2)** expression and its enzymatic product nitric oxide (NO), which play a crucial role in the pathophysiology of several inflammatory disorders, have been implicated in the development, growth and progression of several human malignant tumors, including glioma. NOS2 has been reported highly expressed in grade III astrocytomas and glioblastomas, with a positive correlation between its expression and tumor grade. As recently reviewed, an overexpressed NOS2/NO system in the tumor cell induces invasion, angiogenesis, immunosuppression, differentiation, and therapeutic resistance in gliomas. The key roles of NOS2 in tumor development and vessel maturation in the C6 rat glioma cell line were also published.

GSCs have been shown to express high NOS2 levels, which were correlated with a poorer glioma patient survival. Furthermore, the silencing of NOS2 expression by RNA interference decreased in vitro brain glioma-initiating cells (GICs), highlighting the main role of NOS2 in GSC biology and maintenance. NOS2 knockdown by RNA interference strategy or by specific inhibitors negatively affected the proliferation and invasiveness of GBM cells, and was able to reduce the progression of subcutaneous and intracranial

human glioma xenografts in mice. The increase or the significant inhibition of tumor cell migration were respectively recorded after treating a co-culture of U87-MG and C6 glioma cell lines with the NO-donor sodium nitroprusside (SNP), or the NOS inhibitor NAME (Nω-nitro-l-arginine methyl ester).

NOS2 pharmacological inhibition might therefore have potential therapeutic value in the treatment of GBM. A major class of NOS2 inhibitors are amidine derivatives, such as L-NIL, the cyclic amidine ONO-1714, and the aromatic acetamidine 1400W. This latter is considered to be one of the most potent and **selective NOS2 inhibitors** reported to date, although it has never been approved into clinical use.

Many of the drugs that were tested to prevent GBM growth and invasiveness are able to kill tumor cells by inducing apoptosis, autophagic cell death or necrosis. Although **apoptosis** is considered to be the most common form of programmed cell death, there are significant literature data that attribute a noteworthy involvement of autophagic death in the tumorigenesis process.

Autophagy is a highly conserved catabolic process, by which cells can recycle organelles and long-lived intracellular proteins. The induction of autophagy can protect or kill metabolically active cancer cells, including GBM cells, depending upon the cellular microenvironment. Indeed, autophagy can either sustain cancer cells to evade death in response to stress conditions (i.e., starvation or deprivation of pro-survival signaling, hypoxia, apoptosis, heat or chemical stress, anti-cancer therapies) or support tumor progression as well as a dysregulated or excessive hyperactivation of autophagic flux can lead to non-apoptotic type II programmed cell death, which is known as autophagic cell death. Even with the awareness of its “double face”, autophagy induction has been proposed as another potential anti-tumoral mechanism to counteract several cancers, including GBM. Recent studies have highlighted the molecular pattern and regulatory pathways that are shared between autophagy and biogenesis of **extracellular vesicles (EVs),** suggesting that these processes are intimately linked.

The aims of the present study are below summarized:

- *To evaluate the macrophage infiltrate and M2-polarization as well as SOX-2 expression in human GBM sections.*
- *To assess the ability of GBM primary cultures to generate neurospheres and analyze the concordance with the level of SOX-2 expression and M2-polarization.*
- *To analyze the NOS2 expression and activity in neurospheres derived by both human GBM primary cells and GBM cell lines as well as its possible correlation with SOX-2 expression.*
- *To verify the potential functional role of NOS2 activity in glioma biology, through the use of 1400W, a specific NOS2 inhibitor, in terms of cell proliferation and migration rate, clonogenic potential, and capacity of generating neurospheres of GBM cell lines.*
- *To investigate the ability of 1400W to influence autophagic flux as well as the release of EVs by U87MG-derived GSCs.*
- *To assess the effects of EVs derived by 1400W-treated GSCs on adherent U87MG cells (recipient cells) in terms of proliferation index, migration rate, and autophagic flux.*

3. MATERIALS AND METHODS

3.1 Ethical statement and human glioblastoma samples

This study was ethically approved (Hospital Ethics Committee), and all patients affected by glioblastoma (GBM) (IV glioma grade), as confirmed by neuropathological examination, underwent a surgical exeresis, in accordance with fluorescence-guided tumor resection protocol (ALA-PDD assisted resection). Each patient gave written informed consent. 8 glioblastoma specimens were received from Neurosurgery Unit, San Salvatore Hospital of L'Aquila and processed in order to obtain sections for immunohistochemistry, primary cell cultures and relative neurospheres (NS).

3.2 Immunohistochemistry of GBM sections

Formalin-fixed paraffin-embedded tissue blocks from 8 GBM cases were included in this study. All materials were submitted for diagnostic or therapeutic purposes and were used in accordance with national ethical principles. No tissue sample has been collected solely for the purpose of this study. All histological diagnoses were reviewed before inclusion in this study. Whole tissue sections were used in all cases. For immunohistochemistry, blocks were sectioned at a thickness of 4 μm and then spunked, dehydrated and subjected to antigenic recovery with high temperature treatment in citrate buffer, pH 6, and finally immunostained with antibody anti-CD68, a cell surface antigen associated with M1 phenotype (clone PG-M1, Dako), and antibody anti-CD163, a cell surface antigen associated with M2 phenotype (clone 10D6, Novocastra). Section from tha same samples were stained with anti-SOX-2 antibody of rabbit, N/A clone, IgG histotype, (Spring Bioscience, USA), previously diluted with the Ventana antibody diluent in 1:50 ratio, using the ultraView Universal DAB Detection Kit Ventana with BenchMark GX Ventana immunosorbent. The ultraView Universal DAB Detection Kit is a highly sensitive 2-pass detection system based on the use of an enzyme (peroxidase) conjugated to a polymer that also binds some secondary antibody molecules. Sections of fetal brain tissue were used as positive controls. The tissue sections were initially placed in few drops of 3% H_2O_2 for 30 minutes at room temperature, then washed in PBS; incubated with 3% BSA for 30 minutes at room temperature; incubated with primary

antibody in BSA 3% overnight at 4° C, washed in PBS; incubated with the secondary antibody in BSA at 3% 1h at room temperature, washed in PBS; incubated with DAB for 1' at room temperature, washed in PBS; stained with Hematoxylin for 10", washed with fountain water; dehydrated with distilled H_2O, 70% ethanol, 95% ethanol, 100% ethanol, xylene (2' for each step), then mounted with the Canadian Balsam.

3.3 Primary GBM cell cultures and derived-neurosphere cultures

From each of 8 humans solid GBM, clinically and histologically characterized, we obtained primary cultures. Fresh surgical specimens were washed in PBS in order to remove adhering blood and visible necrotic portions. To obtain single cell suspensions, mechanical and enzymatic tissue dissociation by trypsin solution, was carried out; biopsy digestion was performed at 37°C for 20 min in a water bath by gentle stirring. A rate of recovered cells was cultured in serum-free medium containing DMEM supplemented with 10% FBS, 100 U/ml penicillin, 100 mg/ml streptomycin and 2 mM glutamine (Standard medium – "St-M"). To generate glioma stem cells (GSCs), another rate was suspended in DMEM/F12 medium supplemented with 20 mg/ml EGF and 20 mg/ml b-FGF and B27 ("GSC-M"). The generated GSCs appeared typically as free-floating structures called neurospheres (NS). All flasks were incubated in sterile conditions at 37°C in a 5% CO_2 atmosphere and the complete medium was totally replaced every three days. After reaching 80% confluence, GBM primary cultures were expanded, and their morphology was visualized and imaged by Nikon Eclipse TS100 microscope. Cell viability was determined using the trypan blue dye, (0.04% in PBS) in a Bürker chamber by using an optical microscopy (Eclipse 50i, Nikon Corporation, Japan). Tumor spheres were dissociated as single cells by Accutase™ solution and single cell suspensions counted. The cell number of live and dead cells was recorded.

3.4 Cell lines and treatments

The human glioma cell lines T98G (grade IV glioma, GBM), U87MG (grade IV glioma, GBM), U251MG (grade IV glioma, GBM), U373 MG (grade III astrocytoma), and LN229 (grade IV glioma, GBM) were obtained from ATCC (American Type Culture Collection, Georgetown, DC, USA) and were cultured in DMEM supplemented with

10% of Fetal Bovine Serum (FBS), 100U/ml penicillin, 100mg/ml streptomycin and 2mM glutamine (Standard medium – "St-M"). LN229 (ATCC) glioblastoma cell line was cultured in same medium DMEM supplemented with FBS 5%. All flasks were incubated in sterile conditions at 37°C in a humidified atmosphere with 5% CO_2. After reaching 80% confluence, adherent cell cultures were expanded after previous detachment with trypsin solution from bovine pancreas. The complete medium was totally replaced every three days. To evaluate the viability, the adherent cells at approximately 70% confluence, were treated or not with 1400W, a selective NOS2 inhibitor, N-(3-(aminomethyl)benzyl)acetamidine (Sigma Chemical Co., Milan, Italy), (1-10-100 μM) for 24 h. PBS at the same volume was added to the control conditions. Neurospheres viability, treated or not with the selective NOS2 inhibitor, 1400W at the concentration of 100 μM was evaluated after enzymatic dissociation with the Accutase™ solution for about 10 min at 37° C, ensuring a gentle and effective dissociation of cell aggregates and maintenance of surface proteins and epitopes. Afterward, cell number and viability were evaluated by trypan blue dye exclusion assay (0.04% in PBS) in a Bürker chamber by using an optical microscopy (Eclipse 50i, Nikon Corporation, Japan). The cell number of live and dead cells was recorded. Cell viability was also assessed by flow cytometric analysis, by incubating cells with propidium iodide (PI) for 30 min; then, both viable and dead cells were analyzed using a flow cytometer (BD Instruments Inc., San José, CA), and the BD CellQuest Software program (BD Instruments Inc.). Where specified, cells were treated with a NO-donor S-nitroso-N-acetylpenicillamine (SNAP) (Cayman Chemical-Ann Arbor, MI), as an exogenous NO source, at the concentration of 100 μM, as previously suggested [140]. The morphology of cell lines cultured in St-M and derived-NS was visualized and imaged by Nikon Eclipse TS100. Where not otherwise specified, the reagents and consumables were purchased from EuroClone (EuroClone, West York, UK).

Neurosphere size was evaluated in the absence or presence of 1400W (100 μM). Briefly, 10 bright field images, at 4× magnification, were randomly taken from each condition with an inverted microscope under phase contrast mode and analyzed using Image J software. The neurosphere average area, as expressed in mm^2, was planned by

dividing the total neurosphere area by the total number of neurospheres. Each experiment was performed in duplicate.

3.5 SOX-2 Immunophenotypic analysis by flow cytometry

Immunophenotypic characterization of GBM cell lines, glioma primary cultures and respective derived-NS was performed by FACSCalibur flow cytometry (Beckton Dickinson, Immunocytometry System, San Jose, CA) in order to analyze the SOX-2 stem cell marker expression. Tumor spheres were dissociated as single cells by Accutase™ solution and single cell suspensions were fixed for 15 min at room temperature with 2% formaldehyde in PBS. For SOX-2 intracellular staining, cells were permeabilized for 5 min at room temperature with 0.1% Triton-X-100 in PBS. Then, the cells were washed twice and at least $2x10^5$ cells for each experimental condition were incubated with a primary fluorochrome-conjugated monoclonal antibody for 1 h at room temperature in the dark. Samples were centrifuged at 400*xg* for 10 min and washed twice. 10,000 events were acquired for each sample. The population of interest was gating according to its Forward Scatter (FSC)/Side Scatter (SSC) criteria. Data were analyzed using CellQuest software (BD Biosciences).

3.6 Total RNA extraction and gene expression by RT-PCR

Total RNA from all GBM cells were extracted using Trizol Reagent according to the manufacturer's protocol. RNA for NOS2 positive control was obtained from immortalized human non-small cell lung cell lines A549 cells (ATCC) treated with inflammatory cytokines (IL-1β, TNF-α, IFN-γ) and LPS. RNA was spectrophotometrically quantified, and its quality was assessed by 1% agarose/Tris–Acetate–EDTA (TAE) gel electrophoresis. The gene expressions were quantified in a reverse transcription-polymerase chain reaction (RT-PCR). To prepare first-strand cDNA, 1 μg of total RNA was reverse transcribed with reverse transcriptase enzyme MLV-Reverse Transcriptase in 20 μl reaction mixture. For the reverse transcription reaction, a mixture of 20 μl including total RNA sample (1 μg), 0.5 μg/μl Oligo (dT)12–18 primer and 10 mM of the four deoxynucleoside triphosphates (dNTPs) for each sample was used. Samples were incubated at 65°C for 5 min followed 37°C for 2 min. A

reaction buffer containing 5X First Strand Buffer RT, 0.1 M dithiothreitol (DTT), 40 U/µl of a ribonuclease inhibitor was added to each sample. Following incubation at 37° C for 2 min, 200 U/µl of M-MLV Reverse Transcriptase was added in every sample. PCR products were synthesized from cDNA using specific primers for NOS2. A relative quantification method was employed where the mRNA level of a target gene was normalized with β-actin mRNA sequence (internal control) used as housekeeping gene. The oligonucleotide primers were designed from NOS2 sequence (GenBank accession number NM_153292) and from human cytoplasmic β-actin gene sequence (GenBank accession number M_10277). PCR step was carried out in a volume of 50 µl, including 10 µl of cDNA, 4 mM MgCl2, 10 mM of the dNTPs mix, buffer 10X, 5 U/µl of AmpliTaq DNA polymerase and 100 µM each of NOS2 and β-actin primers. The PCR products were analysed on 1.2% agarose gel and visualized by EuroSafe Nucleic Acid Staining. The PCR conditions for NOS2 and β-actin were: 35 cycles of denaturation at 94° C for 1 minute, annealing at 61° C for 1 min and extension at 72° C for 1 min. Densitometric analysis was performed using Image J Software to quantify the band intensities. Data represent average values ± SEM from three independent experiments.

3.7 Western Blot

Cell pellets were homogenized in ice-cold RIPA buffer (phosphate buffer saline pH 7.4 supplemented with 0.5% sodium deoxycolate, 1% NP40, 0.1% SDS, 5 mM of EDTA (Ethylenediaminetetraacetic acid), 100 mM of sodium fluoride, 2 mM of sodium pyrophosphate, 1 mM of PMSF (Phenylmethylsulfonyl fluoride), 2 mM of ortovanadate, 10 µg/mL of leupeptin, 10 µg/mL of aprotinin, 10 µg/mL of pepstatin). Homogenates were centrifuged at 600×g for 30 min at 4°C, and the protein content was quantified into supernatants using the BCA protein assay kit (Pierce, Rockford, IL, USA). Samples (40 µg/lane) were run on 8.5% SDS polyacrylamide gels according to standard procedures, and proteins were transferred onto nitrocellulose membranes. Non-specific binding sites were blocked with 5% non-fat dry milk for 1 hr at room temperature, and the membranes were incubated overnight at 4°C with primary antibody anti-NOS2 (Thermo Fisher Scientific, Waltham, Massachusetts, United States), and anti-β-actin (Bio-Rad, Hercules,

CA, USA). The detection of autophagy related proteins (microtubule-associated protein light chain 3 - LC3B and Beclin-1), was performed by Western Blot technique on lysates of untreated and 1400W-treated neurospheres. The detection of members of the tetraspanin protein family, CD63 and CD81, widely used as EVs markers [141] was performed by Western Blot technique on lysates of EVs. Moreover, the protein expression of known cell cycle regulators such as Cyclin D1, CDK4 and p27 has been also verified. For LC3B and Beclin-1 detection, 25 μg/lane of protein extracts were run on 12.5% SDS polyacrylamide gels according to standard procedures, and proteins were transferred onto nitrocellulose membranes. For CD63 and CD81 detection, equal amount of proteins (10 μg/lane) were resolved by 10% SDS polyacrylamide gels according to standard procedures, and proteins were transferred onto nitrocellulose membranes. Non-specific binding sites were blocked with 5% non-fat dry milk for 1 h at room temperature, and membranes were incubated overnight at 4°C with primary antibodies: anti-LC3B (Thermo Fisher, Waltham, Massachusetts, United States), anti-Beclin-1 (Origene, 9620 Medical Center Drive Suite 200 Rockville, MD, USA), anti-CD63 and anti-CD81 (Novus Biological, Briarwood Avenue, Centennial, United States), anti-Cyclin D1, anti-CDK4 and anti-p27 (Sigma-Aldrich, Saint Louis, MO, USA). Bands were visualized by ECL chemiluminescent substrate reagent according to the manufacturer instructions and acquired by UVItec Alliance (Cambridge, UK). Densitometric analysis was performed by software provided by the company. Protein band intensities were normalized to relative β-actin or GAPDH band. Specific secondary antibodies were used and immunoreactive bands were visualized by ECL chemiluminescent substrate reagent according to the manufacturer instructions and acquired by UVItec Alliance (Cambridge, UK). Densitometric analysis was performed by software provided by the company. Relative band intensity was normalized to respective β-actin bands. The murine macrophage cell line RAW 264.7 untreated or treated with LPS (1 μg/mL) and IFN-γ (100 ng/mL) for 24 hrs was used as the NOS2 negative and positive control, respectively.

3.8 Nitrite Level Assay

NOS2 activity measured through a colorimetric assay of nitrite levels (Nitrite Assay kit-Sigma-Aldrich Co., Milan, Italy) was also checked to verify the efficacy of 1400W as enzyme inhibitor. GBM cells were treated or not with 1400W (1-10-100 μM) for 24 h, and nitrite levels were assayed in the cell supernatants applied to a 96-well microtiter plate, according to the manufacturer's instructions. The absorbance was measured by spectrophotometric reading at 550 nm using a microplate reader (Bio-Rad, Hercules, CA USA). The nitrite content of each sample was evaluated with a standard curve obtained by linear regression made with sodium nitrite and expressed in μg/mL. Each sample was assayed in duplicate.

3.9 Cell proliferation assay

Cell proliferation was examined using Cell Counting Kit-8 assay (CCK-8, Sigma-Aldrich, Saint Louis, MO, USA) according to the manufacturer's instructions. Briefly, U87MG cells were seeded into 96-well plates at a density of $3x10^3$ cells per well in 100 μl culture medium, incubated overnight, then treated or not with 100μM 1400W for 24 and 48 h. Where indicated the cells were incubated for 24 and 48 h with EVs derived from not treated (EVs NT-NS) or 1400W-treated (EVs 1400W-NS) neurospheres for 48 h. 10 μl CCK-8 reagent was added to each well and incubated at 37°C for 2 h. The absorbance was recorded at a wavelength of 450 nm using a microplate reader (Bio-Rad, Hercules, CA, USA). A calibration curve has been prepared using the data obtained from the wells that contain known numbers of viable cells.

3.10 Clonogenic Assay

The ability of the glioma cells to generate *in vitro* colonies was determined using clonogenic assay. Briefly, U87MG, T98G cells were incubated in St-M in six-well plates at a concentration of 1.000 cells/well until colony formation. The medium was regularly changed. The cells were daily treated with 1400W (100 μM) or SNAP (100 μM). After 10 days for U87MG and T98G the supernatants were removed; then, colonies were gently washed with PBS, fixed with cold methanol for 20 min, and stained with crystal

violet 0.1% at room temperature for 10 min and air-dried. Images were captured and the total number of colonies/well was counted.

3.11 Cell Migration Assays

The effect of NOS2 inhibitor on glioma cell proliferation and migration was assessed using wound-healing assay, as previously described [140]. U87MG and T98G cell lines were plated at $6 \times 10^4/cm^2$ in six-well plates until reaching confluence. DMEM was removed, and cell monolayers were scratched using a 200μL pipet tip. Then, the cells were washed with PBS in order to remove debris, and cultures were incubated with fresh medium at 37°C in a 5% CO_2 humidified atmosphere in the absence or presence of 1400W (100 μM) or the NO chemical donor SNAP (100 μM). Images of cell migration were captured by an inverted light microscope (Eclipse TS 100, Nikon) (10× magnification) at different time points after the injury (0–24 h). The experiments were conducted in duplicate, and nine fields for each condition were analyzed. To calculate the percentage of wound closure, the images were analyzed quantitatively using the standalone TScratch software that automatically calculates the portion of the area occupied by the cells by a mathematical model [142]. The quantification of a relative scratched monolayer closure (wound closure) was performed according to the equation where Tn is a specific time point after the scratching:

$$\% \text{ Relative wound closure} = \frac{[\% \text{ of scratched area at T0} - \% \text{ of scratched area at Tn}] \ (\times 100)}{[\% \text{ of scratched area at T0}]}$$

3.12 Scanning Electron Microscopy

Scanning electron microscopy (SEM) was carried out on U87MG-derived neurosphere previously untreated or treated with 1400W and then let adhere overnight on coverslips pre-coated with poly-lysine ($1x10^3$ cells/cm^2) and fixed with 2% glutaraldehyde (Electron Microscopy Sciences, Hatfield, PA, USA) in PBS for 30 min. Coverslips were briefly rinsed with PBS and water and then dehydrated in ethanol solutions 30-50-70-90% in H_2O and three times 100%, for 10 min each. For HMDS drying, the samples were immersed for 3 min in 100% HMDS (Electron Microscopy Sciences) and then excess HMDS was blotted away by filter paper. The samples were then transferred to a desiccator for 25 min to avoid water contamination, mounted on

stubs, sputter-coated with chromium in a Quorumtech Q 150T ES Turbo chromium sputter, and detected via a Zeiss Gemini SEM 500.

3.13 Cell cycle profile and apoptosis analysis by flow cytometer

The cell cycle and apoptosis analysis were carried out by cell DNA staining with propidium iodide (PI). The neurospheres of U87MG, treated or not with 1400W at 100 μM for 48 h, were enzymatically dissociated by Accutase™ solution (acquired from PAA-GE Healthcare Life Sciences,) for about 10 min at 37°C and centrifuged (800xg for 10 min at 4°C). The pellets were washed in PBS and fixed in ice-cold ethanol (70%) at 4°C for 30 min. Fixed cells were transferred to plastic BD tubes (Becton Dickinson), washed with the ice-cold PBS, and stained with a mixture solution of PI (50 μg/ml), Nonidet-P40 (0.1% v/v), and RNase A (6 μg/10^6 cells) (all from Sigma-Aldrich) for 1 h in the dark at 4°C. Cell cycle phase distribution was analyzed using FACSCalibur (Beckton Dickinson, San Jose, CA) flow cytometry. Data from 10,000 events per sample were collected and analyzed using FACSCalibur instrument equipped with cell cycle analysis software (Modfit LT for Mac V3.0). The results were expressed as the percentage of cells in each phase of the cycle. Apoptotic cells were determined by their hypochromic subdiploid nuclei staining profiles and analyzed using Cell Quest software program (BD Instruments Inc.).

3.14 Detection and quantification of AVO by fluorescent staining

Adherent GBM U87MG cells were seeded on coverslips, treated as above described and then vital staining with acridine orange (AO) was performed. The disaggregated neurospheres were seeded on coverslips pre-coated with poly-lysine, treated as described above, and vital staining with AO was performed. Briefly, both adherent cells and neurospheres were stained with a final concentration of 0.01 μg/ml AO solution in PBS at room temperature for 10 minutes and with RNase A (6 μg/10^6 cells, Sigma Aldrich). The cells were washed and examined under a fluorescent microscope (Nikon Eclipse 50i) equipped with a digital camera. Orange/red-stained cells are visible through the accumulation of acidic vacuolar organelles (AVO) in the cytoplasmic compartment. To quantify the development of AVO, adherent cells (not treated or treated

with 100 mM 1400W) were stained, removed from the plate with trypsin-EDTA, and analyzed using a FACSCalibur flow cytometry equipped by Cell Quest software. Disrupted neurospheres were counted, stained and analyzed by flow cytometry. Cells were analyzed using the 488-nm excitation detector (green fluorescence/FL1) and the 540-nm emission detector (red fluorescence/FL3), which quantified the AVO development. U87MG cells subjected to serum withdrawal for 4 h have been used as a positive control of autophagy.

3.15 Isolation and characterization of NS-derived extracellular vesicles

EVs were isolated from U87MG-derived neurosphere cell media by ultracentrifugation. The supernatants from neurospheres cultures exposed or not to 1400W for 48 h were initially cleared of cellular debris/dead cells by centrifugation at 600xg for 10 min (to remove suspended cells), and then at 1,500xg for 30 min (to remove cell debris). The collected supernatants were centrifuged at 100,000xg (Rotor 70Ti, Quick-Seal Ultra-Clear tubes, kadj 221) for 2 h in an Optima XPN-110 Ultracentrifuge (Beckman Coulter). All centrifugations were performed at 4°C. Pelleted EVs were resuspended in PBS. The quantity of EVs was double measured by determining total protein concentration in the preparations using the BCA Protein Assay Kit (Pierce, Rockford, IL, USA) following the manufacturer's instructions. Samples were immediately used or stored at -20°C. Identification of purified EVs was achieved by morphological examination using a transmission electron microscope.

3.16 Nanoparticle tracking analysis (NTA)

The number and dimension of EVs released by U87MG-neurospheres were assessed by the nanoparticle tracking analysis (NTA). Using a NanoSight NS300 system (NanoSight Ltd., Amesbury, UK) equipped with a Blue488 laser and a digital camera sCMOS, EVs were visualized by laser light scattering. Briefly, EV-enriched pellets (derived from an equal volume of conditioned medium collected from cells originally seeded in the same number) were resuspended in 500 µl of 0.1 µm triple-filtered sterile PBS and five recordings of 30 sec were performed for each sample. The camera level and detection threshold were set at values of 13 and 5, respectively. Collected data were

analyzed with NTA 3.3 Dev Build 3.3.301 software, which provided high-resolution particle size distribution profiles and concentration measurements of the vesicles in solution.

3.17 Transmission Electron Microscopy

Transmission electron microscopy (TEM) on purified EV resuspended in PBS was performed, to analyze the ultrastructural morphology. According to proper dilutions, the samples were adsorbed to 300 mesh carbon-coated copper grids (Electron Microscopy Sciences) for 5 min in a humidified chamber at room temperature. EVs on grids were then fixed in 2% glutaraldehyde (Electron Microscopy Sciences) in PBS for 10 min and then rinsed in Milli-Qwater. Grids with adhered EVs were examined with a Zeiss Gemini SEM 500 equipped with a STEM detector at 20 kV and at a 3.0 mm working distance, after negative staining with 2% phosphotungstic acid, brought to pH 7.0 with NaOH.

3.18 Acid sphingomyelinase activity

After incubation with or without 1400W for 48 h, U87MG-derived neurospheres were lysed in 250 mM sodium acetate (pH 5.0) and 1% NP40 for 30 min in ice. The samples were then subjected to centrifugation at 10,000xg at 4°C for 10 min. The supernatant was isolated and protein concentration was measured by BCA protein assay kit (Pierce, Rockford, IL, USA). For each sample, 30 µg of protein was diluted in a buffer containing 250 mM sodium acetate, 1 mM EDTA, pH 5.0. The enzyme reaction was started by addition of 10 nmol of C12-NBD Sphingomyelin (N-[12-[(7-nitro-2-1,3-benzoxadiazol-4-yl)amino]dodecanoyl]-sphingosine-1-phosphocholine-Avanti Polar Lipids, Inc, Alabaster, Alabama) in the acid reaction buffer (250 mM sodium acetate, 1 mM EDTA and 0.2% Triton-X100, pH 5.0) in a total volume of 200 µl. After incubation at 37°C for 1 h, the reaction was stopped by the addition of 200 µl chloroform:methanol (2:1, v/v), samples were centrifuged for 10 min at 22,000xg, the organic phases were extracted and, at the aqueous phases, 400 µl chloroform:methanol (2:1, v/v) were added. Then, the samples were centrifuged, and the organic phases were added to organic lipid phases previously obtained. Organic lipid phases were evaporated under stream of N2 and then dissolved in chloroform (80 µl). The samples were spotted onto a thin-layer

chromatography (TLC) plate (Merck) and separated with chloroform:methanol:water (65:25:4, v/v/v) as a solvent. In these conditions, NBD-ceramide appeared as a single spot. The emission intensities of the fluorescent ceramide spots were determined by UVItec Alliance (Cambridge, UK). Densitometric analysis was performed by software provided by the company.

The amounts of pmol ceramide generated from NBD-SM by aSMase activity were obtained from interpoling the respective fluorescence intensities in the calibration plot of C12-NBD Ceramide (N-[12-[(7-nitro-2-1,3-benzoxadiazol-4-yl)amino]dodecanoyl]-D-erythro-sphingosine, Avanti Polar Lipids, Inc, Alabaster, Alabama) concentration vs fluorescence intensity. Activity of aSMase was expressed as picomoles ceramide produced/h/mg protein.

3.19 Statistical Analysis

Data were analyzed using Prism 6.0 GraphPad Software (GraphPad, San Diego, CA). Results are expressed as mean ± SEM from two or three independent experiments conducted in duplicate or triplicate, as specified. For comparison between two means, Student's unpaired *t*-test was used. For comparisons of the mean values among groups, a one-way or repeated measures two-way ANOVA followed by Bonferroni post hoc test were used. Statistical correlation was tested by calculating the Pearson correlation coefficient (Pearson's test). Values of P less than 0.05 were accepted as significant.

4. RESULTS

4.1 Immunohistochemistry on glioblastoma sections

As said above, the GBM microenvironment includes tumor cells and also other cell types, including infiltrating inflammatory cells such as macrophages. Macrophages are mobilized and recruited by tumor-derived factors and undergo to polarization process that defines the acquisition of specific phenotypes. Tumor-associated macrophages (TAMs) can be classified into M1, and M2 subtypes based on their polarization status and play different roles: M1 phenotype exhibits tumor-suppressive functions and M2 phenotype promotes tumor-infiltrating leukocytes, tumor initiation, progression as well as the metastatic process. In the present study, we performed immunohistochemical staining on sections of GBM tissue obtained from surgical resection of eight patients diagnosed with grade IV GBM, for CD80, a cell surface antigen associated with M1 phenotype, and CD163, a cell surface antigen associated with M2 phenotype. In **Figure 8 A and B** representative images of two GBM sections stained for M1 marker are shown. We observed a weak positivity for M1 in all analyzed specimens. Differently, 6 out of 8 GBM specimens were highly positive for CD163 staining. A representative field for the positive M2 specimen and a representative field for negative M2 specimens are shown in **Figure 8 C and D**, respectively.

Ye et al. [143] have demonstrated a positive correlation between the number of M2-TAMs and glioma development, particularly glioma stem-like cells. Zhengzheng et al. [144] have evaluated the contribution of M2-TAMs to the stemness and migration abilities of glioma cells, demonstrating that TGF-β1 in the tumor microenvironment secreted from M2-TAMs activated the SMAD2/3 pathway and then increased the expression levels of SOX4 and SOX-2. SOX-2 has been shown to be important in the maintenance of stem cell activity, particularly for cancer stem cells [145] and that the downregulation of SOX-2 in glioma stem cells impairs their proliferation and tumor formation ability. According to scientific evidence, we also performed immunohistochemical staining on sections of GBM tissue obtained from surgical resection of eight patients diagnosed with grade IV GBM for SOX-2, a stemness marker.

The results indicated a highly SOX-2 positivity in 6 of out 8 patients, as shown in **Figure 9**.

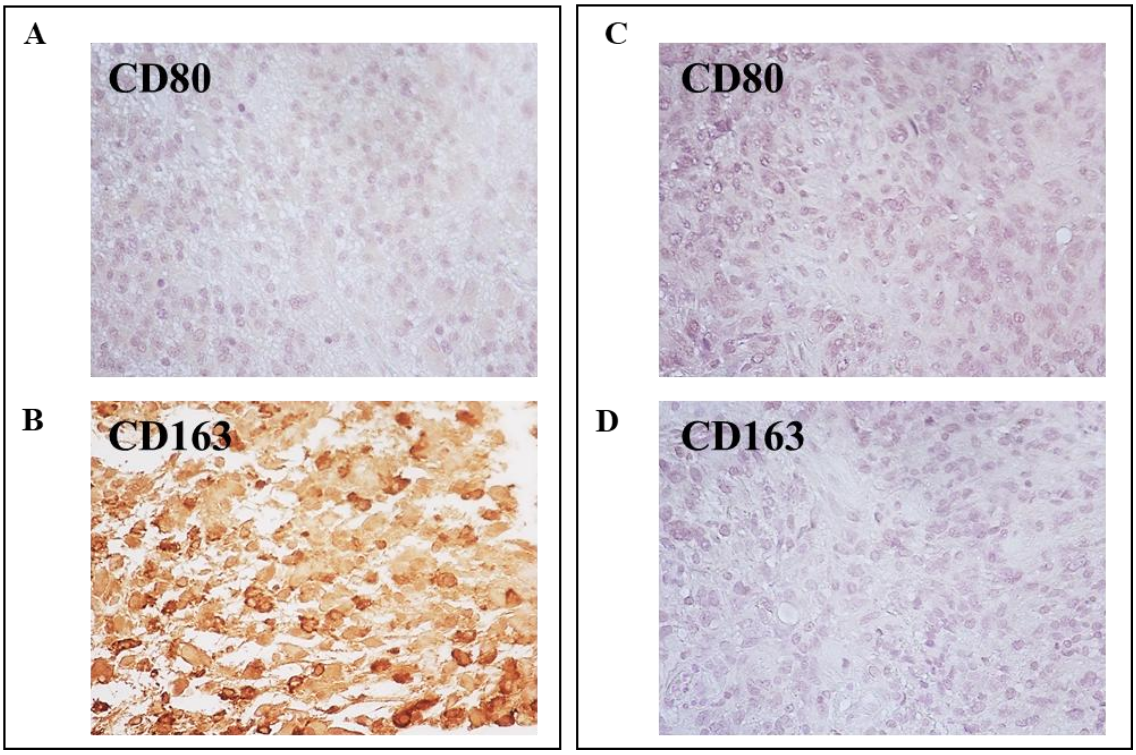

Figure 8: Immunohistochemical analysis of M1 and M2 macrophage polarization in glioblastoma (GBM) sections. The patient sections were immunostained using anti-CD80 (M1 marker) (A and C) and anti-CD163 (M2 marker) (B and D) antibodies. The brown color indicates positive staining. Images were taken at 40× magnification. Representative images relative to two out of eight GBM specimens (A and B: sample n.4; C and D: sample n.7) analyzed are shown.

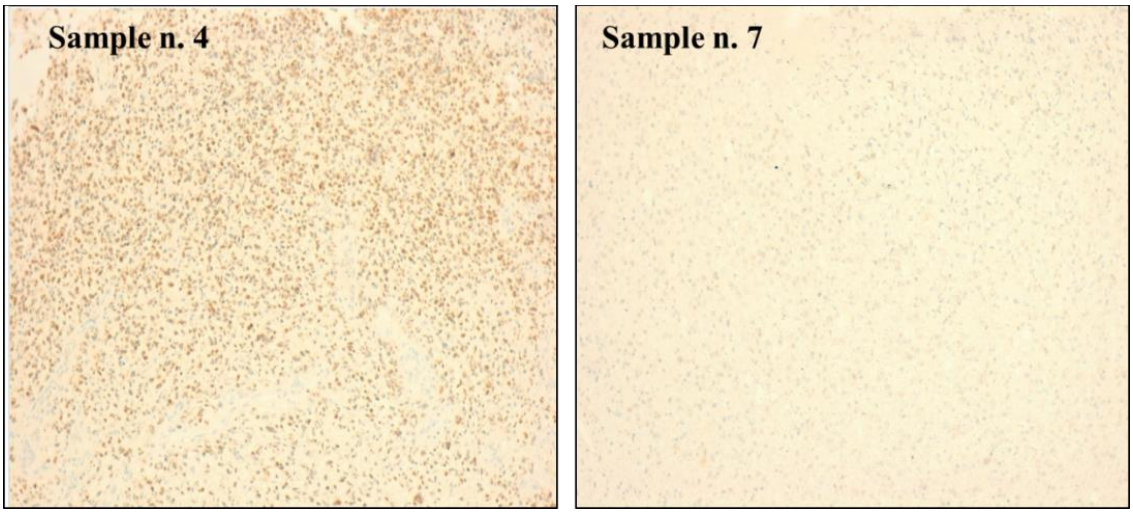

Figure 9. Representative immunohistochemical staining of SOX-2 in human GBM sections. (A) Intense SOX-2 expression detected in sample n.4. (B) Absent SOX-2 expression evaluated in sample n.7.

In **Table 3**, a summary of the immunohistochemical analysis of CD163 and SOX-2 on GBM sections and relative diagnosis is reported.

Table 1. Summary of immunohistochemistry analysis of SOX-2 expression in glioblastoma (GBM) fixed paraffin-embedded sections.

Case	Diagnosis	SOX-2 HIC expression	CD163 HIC expression
1	**Glioblastoma (IV)**	**Absent**	**Absent**
2	**Glioblastoma (IV)**	**Intense**	**Intense**
3	**Glioblastoma (IV)**	**Intense**	**Intense**
4	**Glioblastoma (IV)**	**Intense**	**Intense**
5	**Glioblastoma (IV)**	**Weak /Mod**	**Moderate**
6	**Glioblastoma (IV)**	**Intense**	**Intense**
7	**Glioblastoma (IV)**	**Absent**	**Absent**
8	**Glioblastoma (IV)**	**Moderated**	**Intense**

4.2 Human glioma primary cultures and neurosphere generation

A group of 8 glioma post-surgical specimens (GBM IV grade) was enzymatically digested and obtained cells were cultured both in standard culture medium (DMEM supplemented with FCS 10% - “St-M”) and in culture medium for GSC generation (DMEM/F12 medium serum free with EGF, b-FGF and B27 supplement - “GSC-M”), and observed by contrast phase microscopy. In Figure 3 representative images from all the 8 GBM primary cultures acquired in both conditions (St-M and GSC-M) are shown. A morphological heterogeneity was observed in St-M primary cultures: astrocytic-shaped cells with long cellular processes, fibroblastic-shaped cells, epithelioid-like cells and spindle-shaped cells. A morphological variability was also detected in GSC-M cultures: spheres of different sizes were observed, some of them with a well-defined spherical

shape, or showing irregular cell clusters. As showed in **Figure 10**, 6 out from 8 primary GSC-M cultures (sample n.2-3-4-5-6-8) had the ability to generate neurosphere (GSC+), whereas 2 remaining cultures (samples n. 1-7) were not able to generate neurospheres (GSC-). The GSC- cultures appeared as a fraction of suspended not proliferative single cells not joined to shape neurospheres (**Figure 10, samples n.1 and 7**).

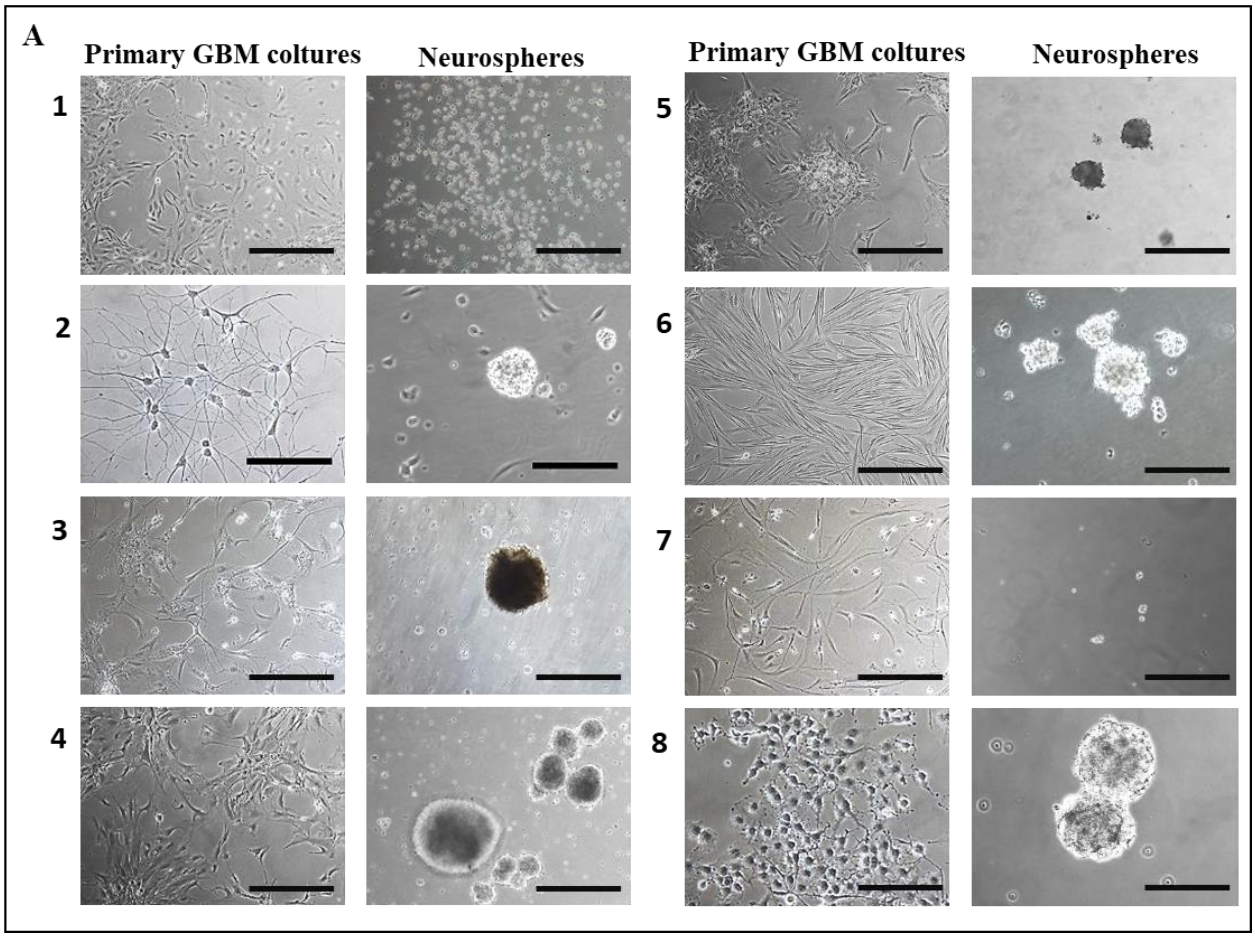

Figure 10: GBM primary cultures kept in standard culture medium (St-M) and in DMEM/F12 medium serum free with EGF, b-FGF and B27 supplement for neurospheres' growth (GSC-M). Representative images from each primary culture are shown (Original magnification 10X, scale bar = 100 μm).

Flow cytometric analysis of primary cells cultured in St-M and in GSC-M revealed heterogeneous levels of the stemness SOX-2 marker, in particular GSC+ cultures showed higher levels than that recorded in GSC- (**Table 4**).

SOX-2 positive cells (%)		
Sample	**St-M**	**GSC-M**
1	14.5 ± 0.73	/
2	90,4 ± 4.52	97.68 ± 3.73
3	69.33 ± 3.47	84.01 ± 3.70
4	82.03 ± 4.10	84.71 ± 2.94
5	69.30 ± 3.47	80.30 ± 3.02
6	81.00 ± 3.05	65.73 ± 3.29
7	13.78 ± 0.69	/
8	79.84 ± 2.45	91.02 ± 4.12

Table 4: SOX-2 cytofluorimetric analysis performed in GBM primary cultures kept in St-M and GSC-M. The cytofluorimetric results are from one representative of two independent experiments are shown.

The **Table 5** showed the concordance between immunohistochemical SOX-2 expression, neurospheres' generation and SOX-2 expression levels detected by cytofluorimetric analysis.

Case	SOX-2 (IHC)	Neurospheres	SOX-2 (FACS)	M2MΦ	Concordance	Survival (months)
1	**No**	**No**	**5.62%**	**No**	**Yes**	**25**
2	**Yes**	**Yes**	**91.24%**	**Yes**	**Yes**	**4**
3	**Yes**	**Yes**	**69.30%**	**Yes**	**Yes**	**6**
4	**Yes**	**Yes**	**92.93%**	**Yes**	**Yes**	**11**
5	**Yes**	**Yes**	**56.07%**	**Yes**	**Yes**	**15**
6	**No**	**No**	**28.53%**	**Yes**	**Yes**	**27**
7	**No**	**No**	**29.54%**	**No**	**Yes**	**29**
8	**Yes**	**Yes**	**59.02%**	**Yes**	**Yes**	**17**

Table 5. Concordance between immunohistochemical SOX-2 expression, neurosphere generation and SOX-2 expression levels detected by cytofluorimetric analysis.

4.3 Neurosphere generation and immunophenotypic analysis of glioma cell lines

The glioma cell lines, U251MG, T98G, U87MG, U373MG, LN229, were cultured both in St-M and in GSC-M. **Figure 11** shows the morphology of glioma cell lines and respective derived-neurospheres observed by contrast phase microscope. All cell lines kept in GSC medium were able to generate *in vitro* neurospheres at different times-points. In particular, the U87MG cell line started to organize in neurospheres after 8-10 days, LN229 after 12-15 days, T98G after 16-18 days, U373MG and U251MG after 20-22 days.

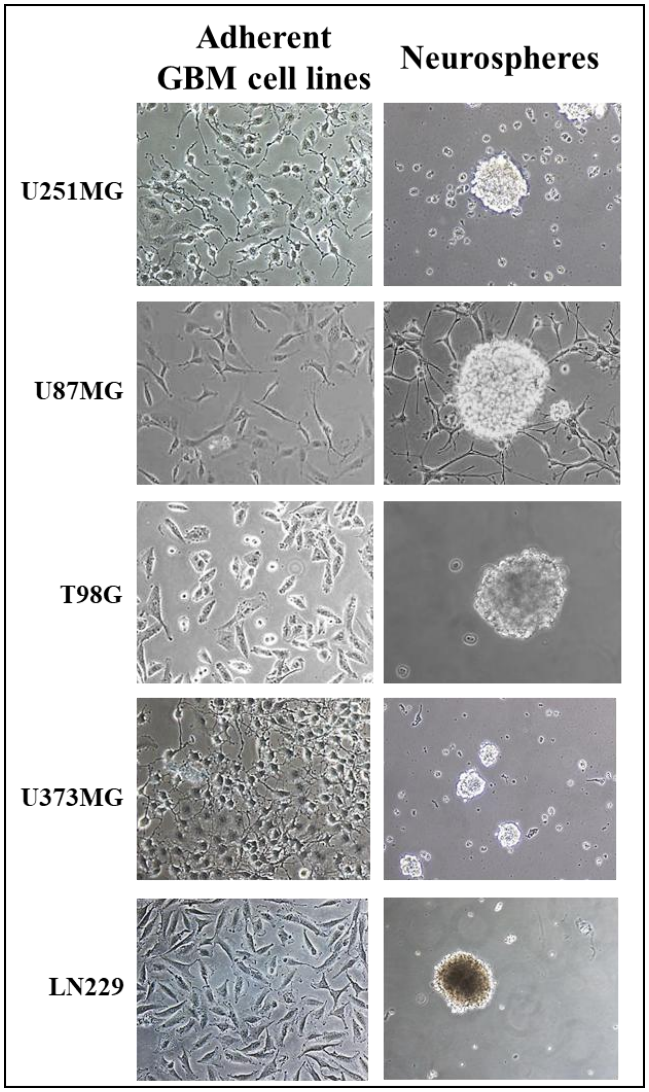

Figure 11. Glioma cell lines cultured in standard culture medium (St-M) and in DMEM/F12 medium serum free with EGF, b-FGF and B27 supplement for neurospheres' growth (GSC-M). Representative images from the analyzed glioma cell lines are shown (Original magnification 20X).

Moreover, we examined the stemness marker SOX-2 by immunofluorescence analysis, in all cell lines cultured in St-M or GSC-M, and the data expressed as SOX-2 Median Fluorescence Intensity (MFI) values are reported in **Figure 12**. Of interest, the mean levels of MFI in GSC-M (mean ± SEM, 105.56±14.30) resulted significantly higher ($P<0.001$) when compared to St-M (mean ± SEM, 45.77±4.72).

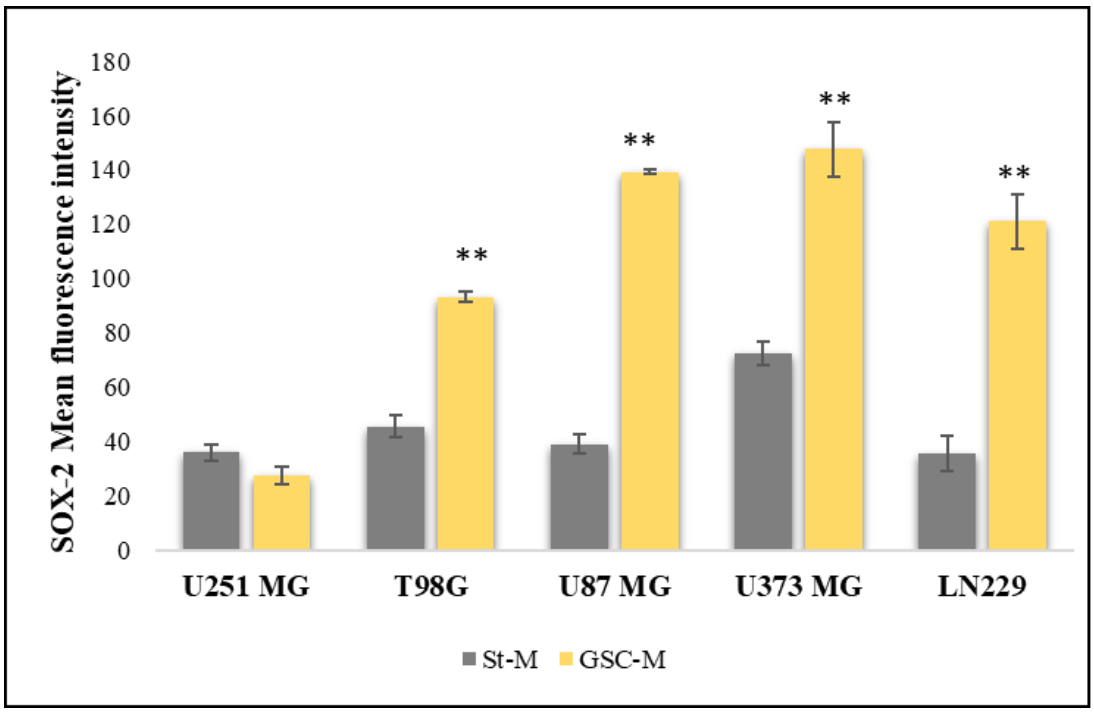

Figure 12. SOX-2 immunostaining analysis of glioma cell lines. Values of Median Fluorescence Intensity (MFI) of SOX-2 in glioma cell lines maintained both in St-M and GSC-M conditions. Data are from one representative out of two independent experiments in duplicates ± SD.

4.4 NOS2 mRNA expression in glioma cell lines

As reviewed in Tran et al. [90] the overexpressed NOS2/NO system in the tumor cell induces invasion, angiogenesis, immunosuppression, differentiation, and therapeutic resistance in gliomas. Moreover, GSCs have been shown to express high NOS2 levels, a key player in tumor inflammation, and this expression was associated with a worse glioma patient survival [86]. According to this scientific evidence, here the NOS2 expression, evaluated by RT-PCR technique in glioma cell lines (U251MG, T98G,

U87MG, U373MG, and LN229) cultured in St-M and GSC-M was evaluated. The representative images of three independent RT-PCR experiments showed higher levels of NOS2 mRNA in neurosphere cultures (GSC+) when compared to the respective cells in St-M (**Figure 13**). The electrophoretic bands of glioma cell lines maintained at St-M exhibited a basal expression of the gene encoding NOS2. In figure 6B, the densitometric analysis showed that NOS2 mRNA levels in neurosphere cultures (GSC+) from T98G, U87MG, and U373MG were significantly higher when compared to respective St-M cell lines.

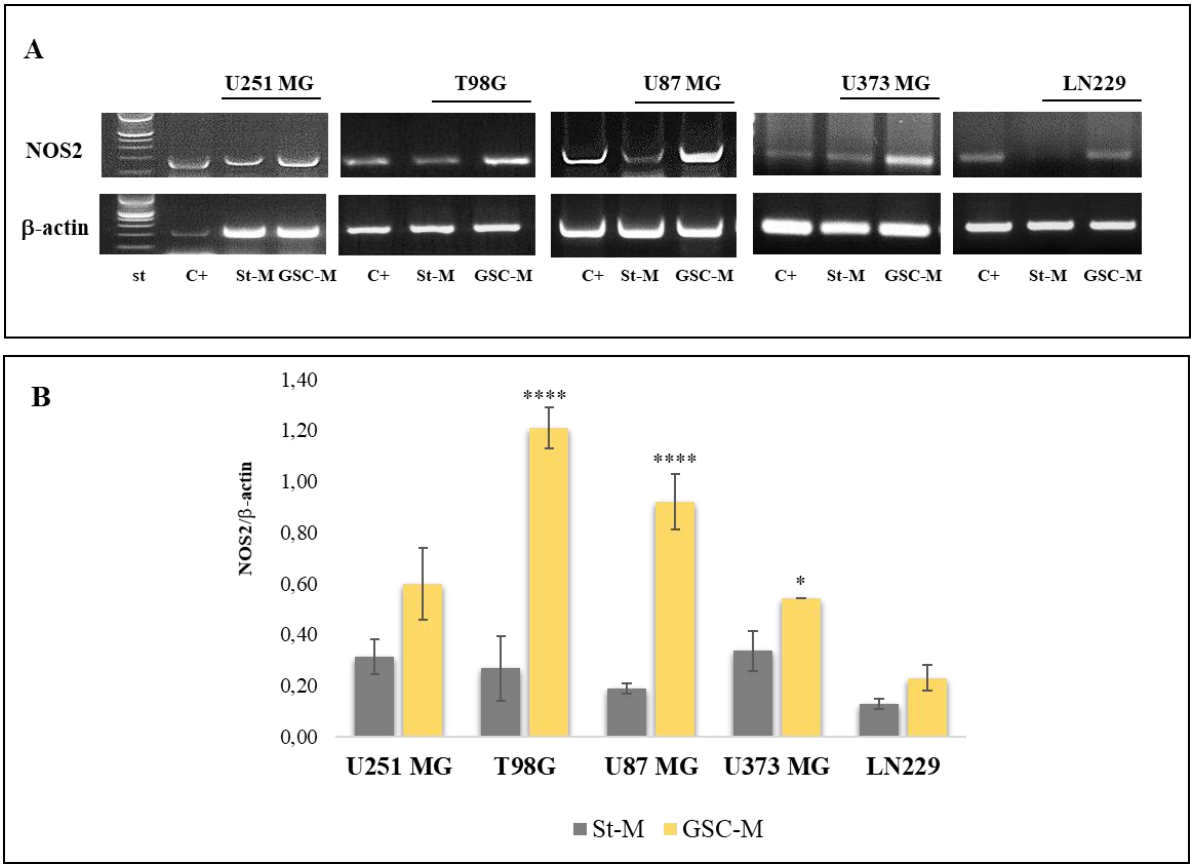

Figure 13. NOS2 expression in adherent glioma cell lines and derived-neurospheres. (A) The graph shows the mean values obtained from ratio of NOS2 expression density to β-actin ± SEM of three independent experiments performed in duplicate. (B) Images from one representative out of three independent experiments of NOS2 expression in glioma cell lines maintained in St-M and in GSC-M are shown. Standard= DNA ladder (100 bp), C+=Positive control (human A549 cells treated with inflammatory cytokines and LPS). β-actin was used as the internal control.

To verify a statistical relationship among NOS2 expression levels and SOX-2 positive cells (%) in all cell lines kept in St-M, a correlation analysis was conducted. Pearson's

test revealed a positive, statistically significant, and strong correlation between NOS2 expression levels and % SOX-2 positive cells (R= 0.94; p<0.001) (**Figure 14**).

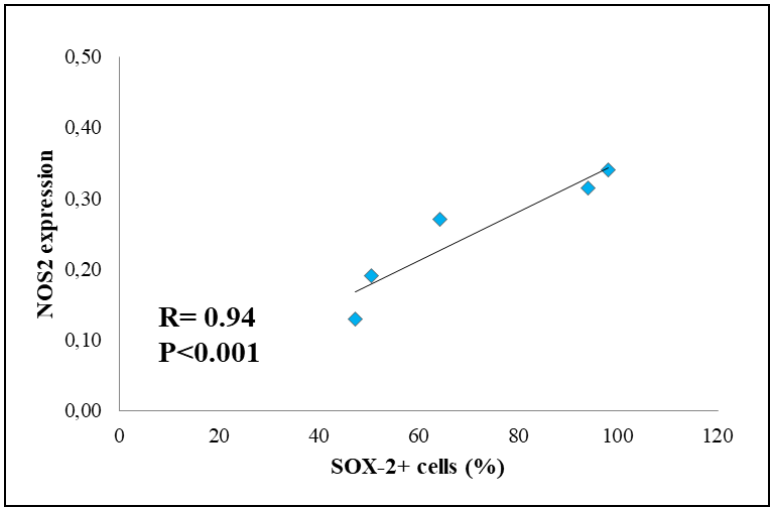

Figure 14. Statistical correlation between NOS2 and SOX-2. Correlation between NOS2 level expressed as mean values of NOS2/β-actin ratio and percentage of SOX-2 positive cells (mean values) detected in analyzed GBM cell lines (U-251 MG, T98G, U-87 MG, U-373 MG, LN229) kept in standard conditions (St-M) and analyzed by Pearson's test.

4.5 NOS2 expression and activity in adherent U87MG and T98G cell lines

To study the NOS2 involvement on glioma cell growth, clonogenic potential, and neurosphere generation, enzymatic activity inhibition of NOS2 by 1400W, a selective inhibitor, was used in U87MG and T98G cell lines, showing higher NOS2 levels. To examine the effect of 1400W on the human GBM cell lines, a dose-response curve was firstly performed to define the more effective concentration able to inhibit NOS2 activity. NOS2 enzymatic activity, evaluated as nitrite levels, was assayed in the culture media of the untreated (NT) and 1400W-treated cells at different concentrations (1 μM, 10 μM, and 100 μM) for 24 h. In **Figure 15**, the results expressed as percentage vs NT are presented. The addition of a NOS2 inhibitor at 100 μM significantly reduced the basal nitrite levels evaluated after 24 h in U87MG (P<0.05 vs NT and 10 μM) and in T98G (P<0.01 vs NT) cultures.

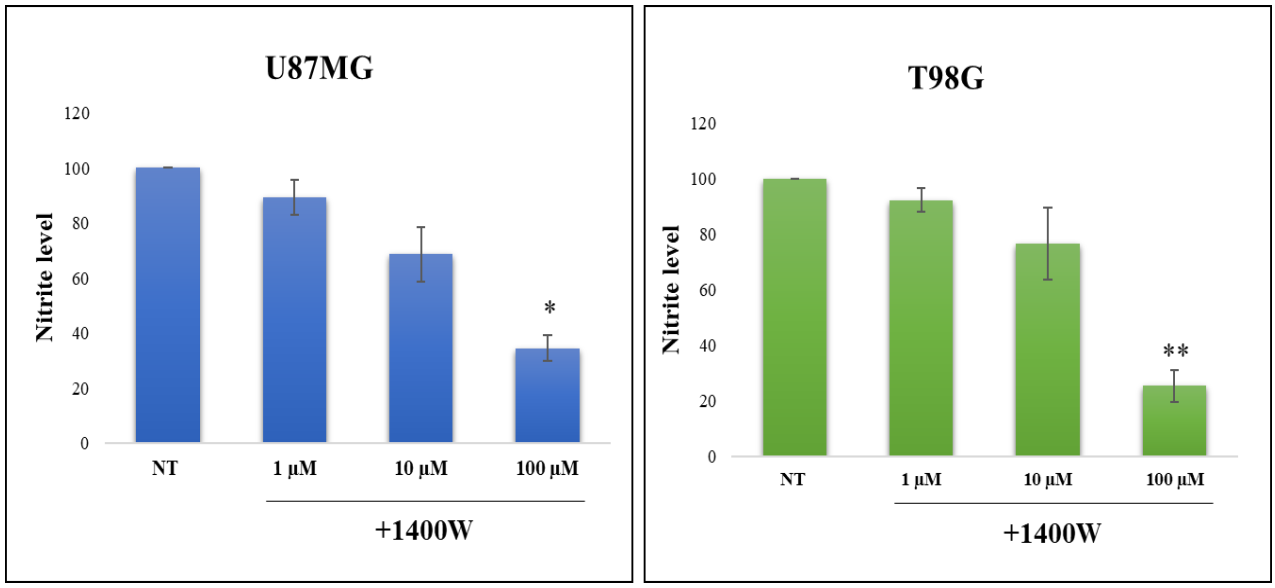

Figure 15. Nitrite levels in media from adherent U87MG and T98G human glioblastoma (GBM) cell lines cultured for 24 h without (not treated, NT) or with NOS2 inhibitor, 1400W a nitric oxide synthase 2 (NOS2) inhibitor (1 µM,10 µM, and 100 µM). The results presented as percentage *vs.* NT are expressed as the mean ± SEM from two independent experiments in triplicate. For comparative analysis of groups of data, one-way ANOVA followed by Bonferroni post hoc test was used (*P <0.05 vs NT and **P<0.01 vs NT).

After 1400W treatment, the viable cells were significantly reduced with the concentration of 100 µM 1400W for 24 h, as analysed by the Trypan blue dye exclusion test (P<0.05) in both cell lines. It is of note that the dead cell number was not influenced by any different concentration of 1400W in U87MG as well as T98G (**Figure 16A and B**). The propidium iodide (PI) staining by cytofluorimetry confirmed that the percentage of dead cells at all used concentrations was not different from that of the control cells in both cell lines, underlining that the 1400W inhibitor did not cause a cytotoxic effect (**Figure 16C and D**). A considerable decrease in the cell number and nitrite levels of 1400W was obtained with 100 µM; hence, the following experiments were performed with the single 1400W concentration (100 µM), as previously reported [86].

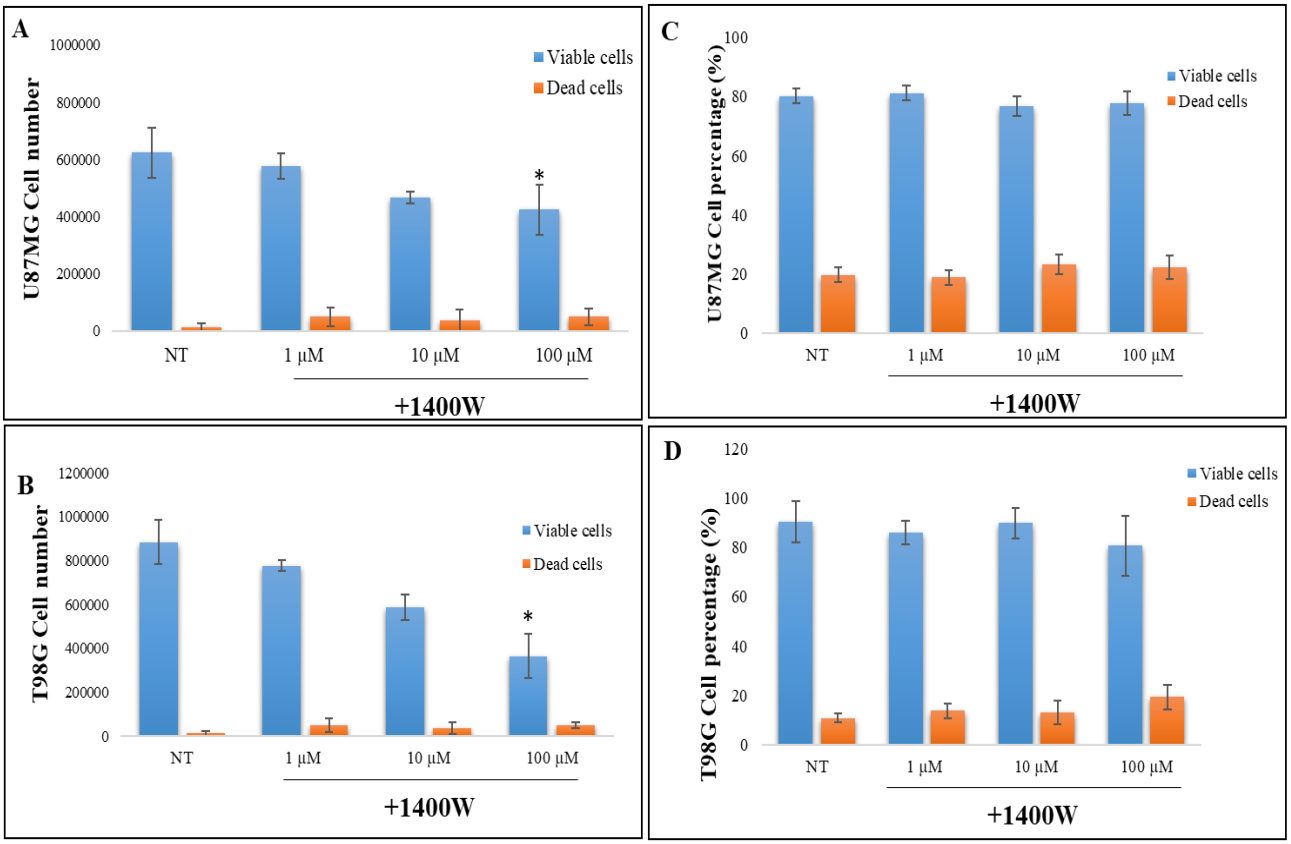

Figure 16. Effect of 1400W on viability of adherent U87MG- and T98G. U87MG and T98G cells were treated with 1400W at 1µM, 10µM,100 µM, or PBS (NT) for 24 h, and the number of viable and dead cells was assessed by Trypan blue exclusion test (A) and (**B**) respectively. The percentage of viable and dead cells was assessed in both cell lines by cytofluorimetry after propidium iodide (PI) staining (C and D). Results are presented as the mean ± SEM of two independent experiments in triplicate. For comparative analysis of groups of data, one-way ANOVA followed by Bonferroni post hoc test was used (*P<0.05).

To further confirm the RT-PCR results as above reported, NOS2 protein levels were evaluated in adherent U87MG and T98G cells after 24 h of culture. As expected, both cell lines basally expressed NOS2 protein, and the exposure to the 1400W inhibitor did not affect the NOS2 protein expression, as evident in the representative Western blot and relative densitometric analysis shown in Figure **17A and B**. For these experiments, RAW 264.7 cells that were either unstimulated or stimulated with LPS and IFN-γ were used as the negative and positive control, respectively. Also, for this cell line, no cytotoxic effect was detected when treated with 1400W for up to 100 µM (data not shown).

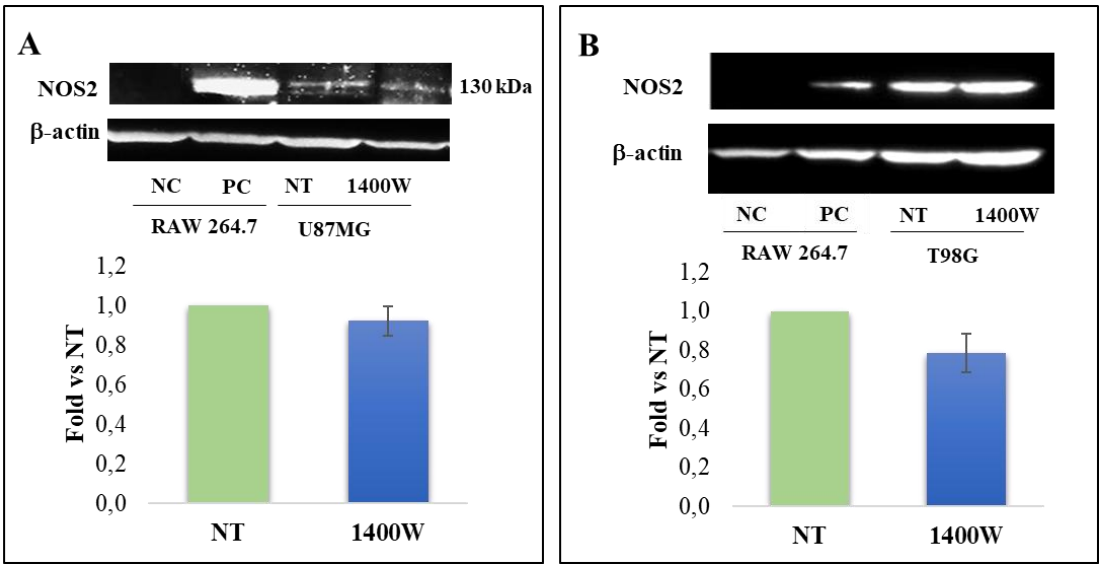

Figure 17. NOS2 protein expression in adherent U87MG and T98G cell lines following 1400W treatment. Representative western blot of NOS2 and β-actin protein detected in U87MG cells (A) and T98G (B) treated or not with 1400W (100 μM) for 24 hrs. Quantification analysis of blots by densitometry is expressed as fold increase vs NT. NC (negative control): Untreated RAW 264.7; PC (positive control): RAW 264.7 treated with LPS (Lipopolysaccharide) (1 μg/mL) and IFN-γ (Interferon- γ) (100 ng/mL) for 24 h. The results from three independent experiments in duplicate are presented and expressed as mean ± SEM. For comparison between two means, Student's unpaired t-test was used.

4.6 NOS2 inhibition strongly affects proliferation of U87MG and T98G

The clonogenic potential of U87MG and T98G treated daily with 1400W for 10 days was significantly lower than that in the control group ($P < 0.0001$ in U87MG vs NT; $P < 0.05$ in T98G vs NT), (**Figure 18B and D**) suggesting the crucial role of NOS2 activity on the capacity of the glioma cell line to produce progeny. On the other hand, NO-donor SNAP (100 μM) induced a significant increase of the clonogenic potential when compared to control in U87MG cell line ($P < 0.0001$ versus vs not treated and 1400W-treated cells) (**Figure 18B**). The addition of NO exogenous improved the clonogenic potential in T98G culture ($P < 0.01$ versus vs 1400W-treated cells) (**Figure 18D**). In **Figure 18A and C**, representative microscopy images of clonogenic assay are presented.

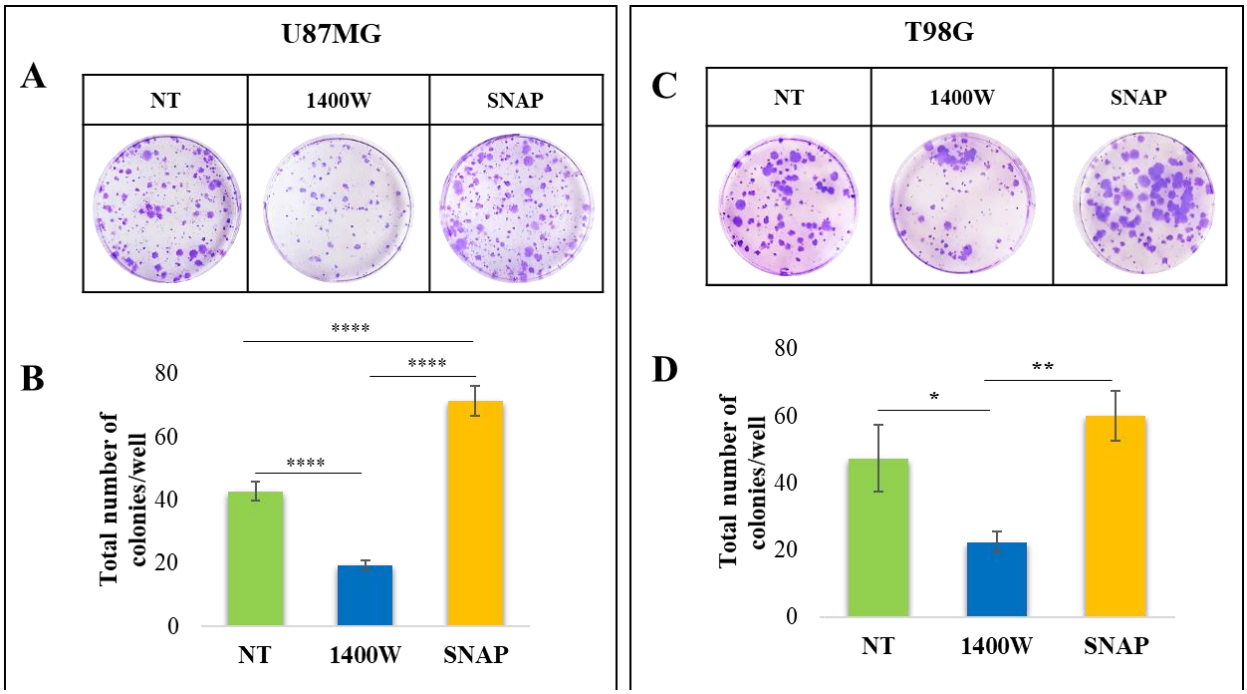

Figure 18. Clonogenic ability of U87MG and T98G exposed to 1400W. Representative microscopic images of clonogenic assay of U87MG and T98G cell lines (A) and (C) after daily treatment for 10 days with 1400W (100 μM) or nitric oxide (NO)-donor S-nitroso-N-acetylpenicillamine (SNAP) (100 μM). NT = not treated. Quantitative results of clonogenic assay expressed as total number of surviving colonies/well (B) and (D). Viable colonies with diameter >0.3 mm were counted with an ocular micrometer (mean ± SEM of three independent experiments in triplicate). For comparative analysis of groups of data, one-way ANOVA followed by Bonferroni post hoc test was used (*P<0.05, **P<0.01, ****P<0.0001).

As invasiveness is one of the pathophysiological features of human GBM, to analyse the functional role of the NOS2/NO system in our cell models, the migration and proliferation abilities of U87MG and T98G cells cultured with or without 1400W (100 μM) were also studied through an in vitro scratch wound assay. The images obtained by inverted light microscope were acquired at different time points after scratching and converted to % closure by using a mathematical system calculating automatically the portion of the area occupied by the cells. In all experiments, the scratched monolayers of control cells (untreated) were closed at 28–30 h (not shown). The effect of NO-donor SNAP (100 μM) was also evaluated to verify the ability of NO to positively influence both migration and proliferation rate in our cell models. The results showed that the migration and proliferation abilities of U87MG and T98G cells were strongly and significantly impaired by 1400W inhibitor, as reported in **Figure 19A and C**, where representative microscopy images of the scratch-wound healing assay acquired at 0 (T0),

18 h, or 24 h, are shown. Moreover, the U87MG and T98G quantitative analysis of the wound-closure rate from two independent experiments in duplicate are presented in **Figure 19B and D**. The addition of 1400W significantly and negatively affected the closure rate of a scratched U87MG monolayer both at 18 h ($P < 0.01$) and at 24 h ($P < 0.001$). Similar results were obtained in scratched T98G monolayer (at 18 h $P < 0.05$ and at 24 h ($P < 0.01$). This finding could be due to the effect on cell proliferation even if a slowed cell migration could not be excluded. Accordingly, with the results above described, treatment with NO-donor SNAP was able to strongly and positively influence the basal wound closure rate either at 18 hours or 24 hours in both cell lines, as reported in **Figure 19A-D**.

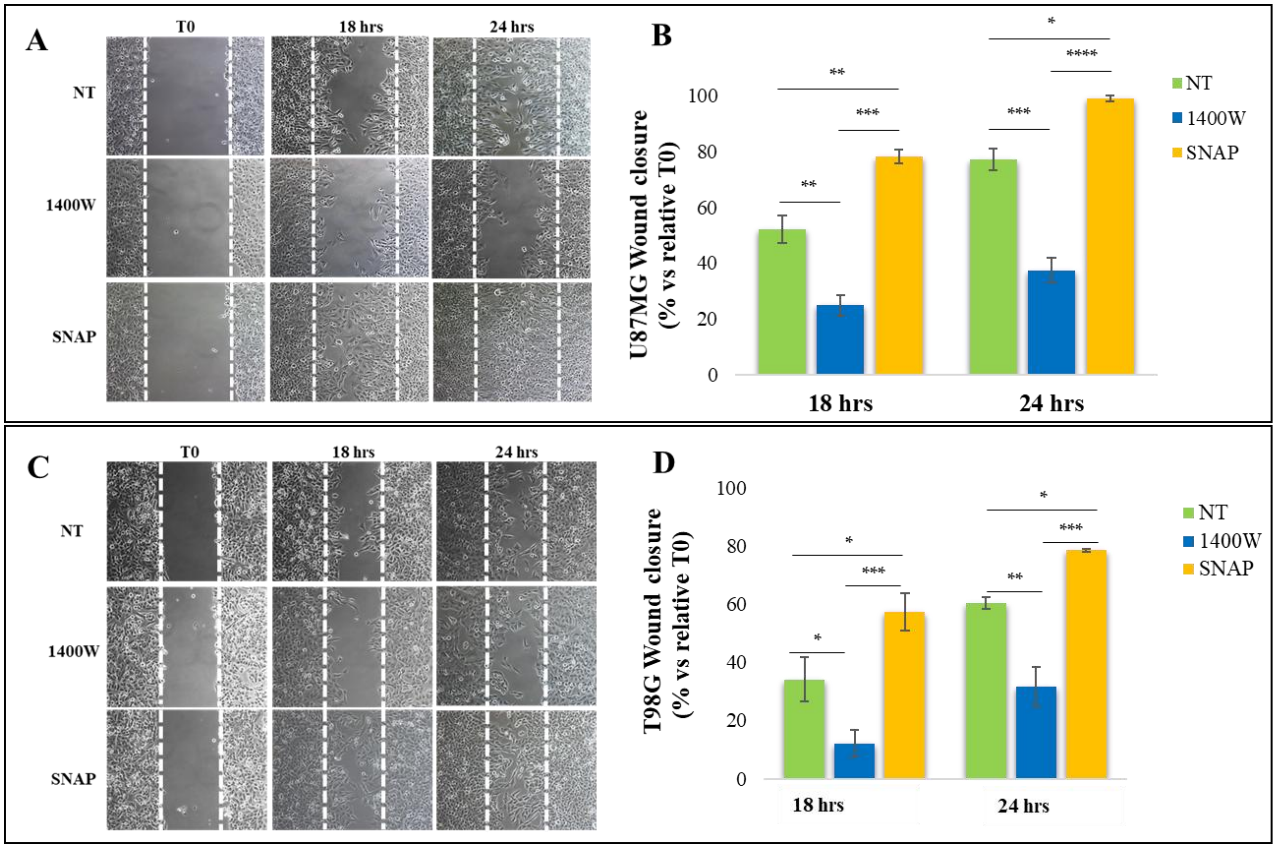

Figure 19. Scratch-wound healing ability of GBM cell lines cells following 1400W treatment. Representative microscopy of scratched U87MG (A) and T98G (C) monolayers incubated without (not treated, NT) or with NOS2 inhibitor 1400W (100 µM) or NO-donor SNAP (100 µM) for the indicated times after injury (10× magnification). The extent of the wound closure rate for each cell lines was calculated as described and expressed as % closure versus relative T0 at 18 hrs and 24 hrs (B) and (D). Data are expressed as the mean ± SEM of two independent experiments in duplicate. For a comparative analysis of groups of data, repeated measures two-way ANOVA followed by a Bonferroni post hoc test was used (*P<0.05, **P<0.01, ***P<0.001, ****P<0.0001).

4.7 NOS2 inhibition affects neurosphere generation from U87MG and T98G

The ability of U87MG and T98G cells to generate neurospheres, which is a main feature of GSC self-renewal, was also significantly affected by the presence of 1400W at 20 and 30 days of incubation, thus supporting the functional role of the NOS2/NO system in the sphere-forming ability of tumor stem cells. Representative images captured with the phase contrast microscope are shown in **Figure 20A and C**. The data of neurosphere mean area expressed as fold versus NT are shown in **Figure 20B and D**, as mean ± SEM (U87MG $P<0.05$ at 20 and 30 days; T98G $P<0.01$ at 20 and $P<0.05$ at 30 days).

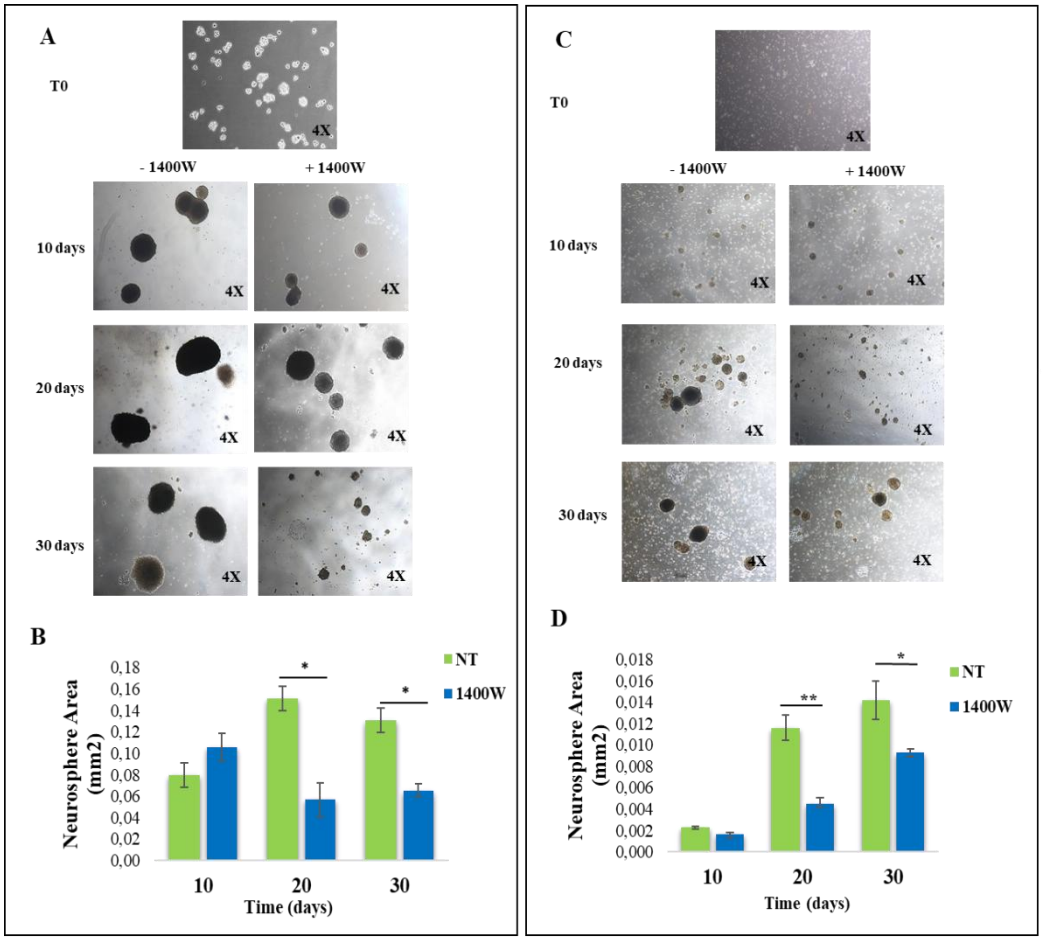

Figure 20. Effect of NOS2 inhibition on U87MG and T98G neurospheres' generation. Representative phase contrast images (4× magnification) of both GBM cell lines maintained in GSC-M to allow neurospheres' generation in the absence (not treated, NT) or presence of NOS2 activity inhibitor 1400W (100 µM), added daily for 10, 20 and 30 days (A) and (C), respectively. Baseline condition (NT) at five-

day culture is shown. Quantification analysis of neurosphere mean area expressed as fold vs NT (B) and (D). Data represent mean ± SEM of two independent experiments in duplicate. For comparison between two means, Student's unpaired t-test was used (*P<0.05 vs NT; **P<0.01 vs NT).

We also investigated the NOS2/NO system in neurospheres derived from U87MG and T98G cell culture measuring NOS2 protein levels at 20 days of incubation being the shortest time with the highest significance. The Western blot analysis showed the NOS2 protein expression in U87MG- and T98G-derived neurospheres at 20 days of culture and the addition of 1400W to the both cell cultures did not influence the expression levels of NOS2 when compared to untreated neurospheres (**Figure 21A and C**). As observed in adherent U87MG and T98G cells (St-M), NOS2 inhibitor was also able to reduce the cell number of neurosphere-forming cells in GSC-M, (U87MG P<0.05 vs NT neurospheres; T98G P<0.01 vs NT neurospheres) without affecting cell viability, which registered >95% (**Figure 21B and D**).

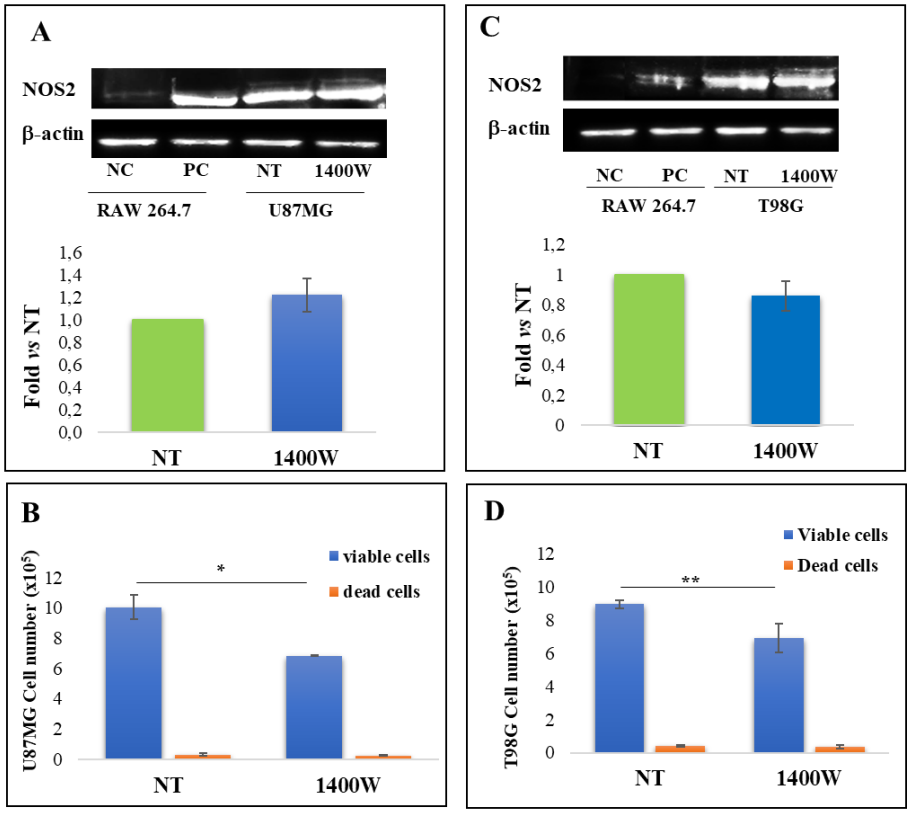

Figure 21. NOS2 protein expression and viability in U87MG- and T98G-derived neurospheres. (A) and (C) U87MG and T98G neurospheres were incubated in the absence (not treated, NT) or presence of 1400W (100 μM) daily added for 20 days and representative Western blot of NOS2 and β-actin are shown. Quantification analysis by densitometry are expressed as fold vs. NT. The results from three independent experiments in duplicate are presented and expressed as mean ± SEM. NC (negative control): untreated RAW 264.7; PC (positive control): RAW 264.7 treated for 24 h with LPS (1 μg/mL) and IFN-γ(100

ng/mL). (C) and (D) Effect of NOS2 inhibitor 1400W (100 μM) on U87MG- and T98G-derived neurosphere viability after 20-day culture. Data are expressed as the mean ± SEM of two independent experiments performed in duplicate. For comparison between two means, Student's t-test was used.

4.8 1400W reduces growth of glioma stem cells by inducing S-phase cell cycle arrest

To further investigate the involvement of NOS2 activity in the GBM biology, U87MG cell line was uniquely used for the remarkable efficiency in generating neurospheres. To analyse the effect of 1400W (100 μM) on neurosphere growth, we used GSC previously generated after a 7-day culture of adherent U87MG cells in GSC-M and treated for 48 h. The GSC growth as assayed by measuring the sphere average area in mm^2, was significantly reduced by 1400W exposure ($P<0.05$). Of note, the addition of 1400W led to a ~22-23% decrease of GSC mean area vs relative T0, instead the average surface of untreated GSC after 48 h culture was increasing by >10%, as shown in Figure 15A. Representative phase contrast images (4x magnification) of NS not treated or treated with 1400W for 48 h are shown in **Figure 22A and B**.

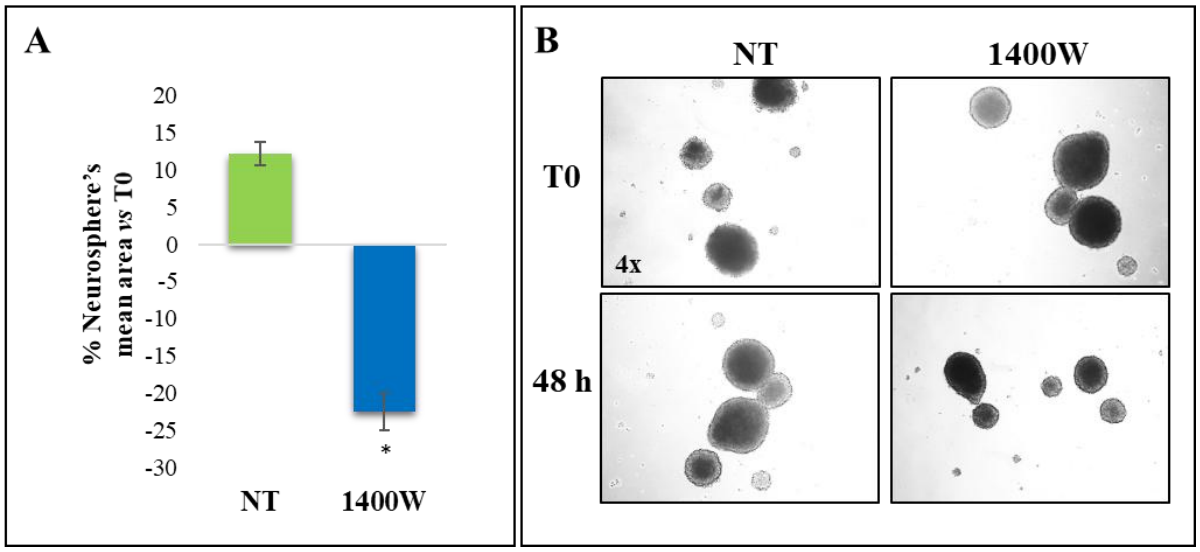

Figure 22. Effect of 1400W on U87MG-derived neurospheres (NS) growth. (A) U87MG cells were maintained for 7 days in a GSC-M to allow neurospheres generation, afterwich neurospheres were incubated in the absence (not treated, NT) or presence of 1400W (100 μM) for 48 h. Quantitative analysis of neurospheres mean area is expressed as percentage vs relative T0. The results representative of two independent experiments are expressed as mean values of duplicates ± SD. For comparison between two means, Student's unpaired t-test was used (*$P<0.05$). (B) Representative phase contrast images (4× magnification) of U87MG-derived neurospheres in the absence (NT) or presence of 1400W (100 μM) for 48 h.

With low magnification (2,000x) SEM imaging, NS surfaces showed more thickened cells in the controls (NT) than in 1400W-treated GSC. Moreover, a smaller size of the 1400W-treated NS when compared to controls (NT) was evident, thus confirming above results (**Figure 23**). Interestingly, at high magnification, the 1400W-treated spheres appeared grapes-like, with a mostly rough-surface with protrusions and vesicular formations more numerous than in NT (Figure 16, images on the middle (10,000x) and right (20,000x).

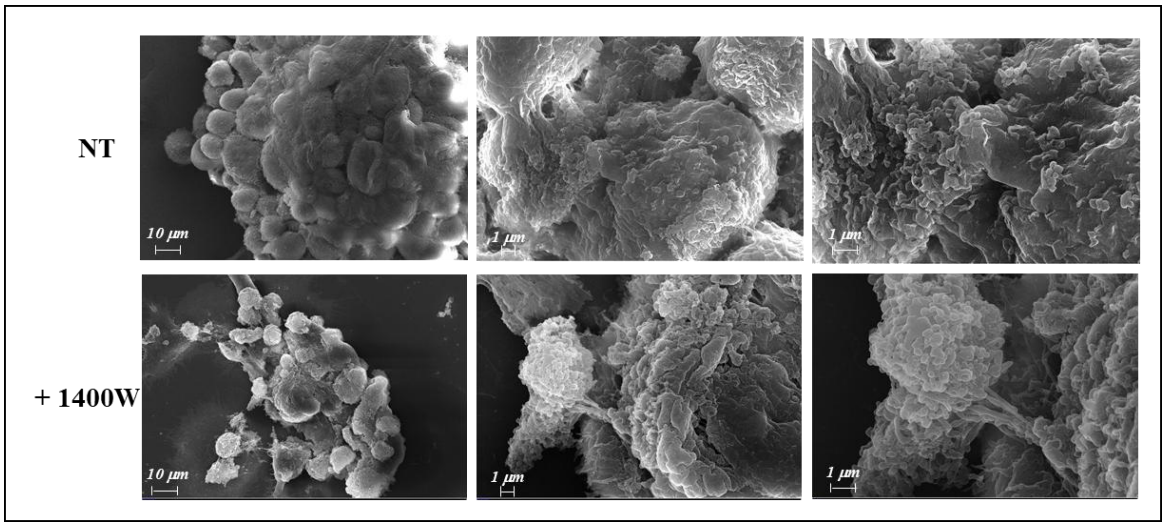

Figure 23. Representative scanning electron micrograph images of untreated (NT) or 1400W-treated neurospheres (from left to right: 2,000×, 10,000×, 20,000× magnification).

The inhibition of growth of 3D-cultured GSCs was also confirmed by the analysis of cellular distribution in cell cycle phases, assessed by flow cytometry, which disclosed a cell cycle arrest characterized by an cell accumulation in S-phase after 1400W treatment for 48 h (16.91% in 1400W treated cells and 10.22% in NT) and by a concomitant decrease in G2/M cell percentage in the 1400W-treated cells when compared to control cells (0.78% vs 8.95%) (**Figure 24A**). Furthermore, 1400W was not able to induce significant levels of apoptosis in GSCs after 48 h of treatment (7.31% vs 7.40% of not treated cells), in **Figure 24B** the representative cytofluorimetric profiles are shown. The cell cycle arrest was confirmed by specific cell cycle regulation proteins (Cyclin D1, cyclin-dependent kinase 4, CDK4 and cyclin-dependent kinase (CDK)-inhibitor, p27) detection. According to cell cycle distribution results, 1400W treatment effectively

induced a down-regulation of the expression of both Cyclin D1 and CDK4 which was associated to an increased expression of p27 thus halting the cells in S-phase (**Figure 24C**).

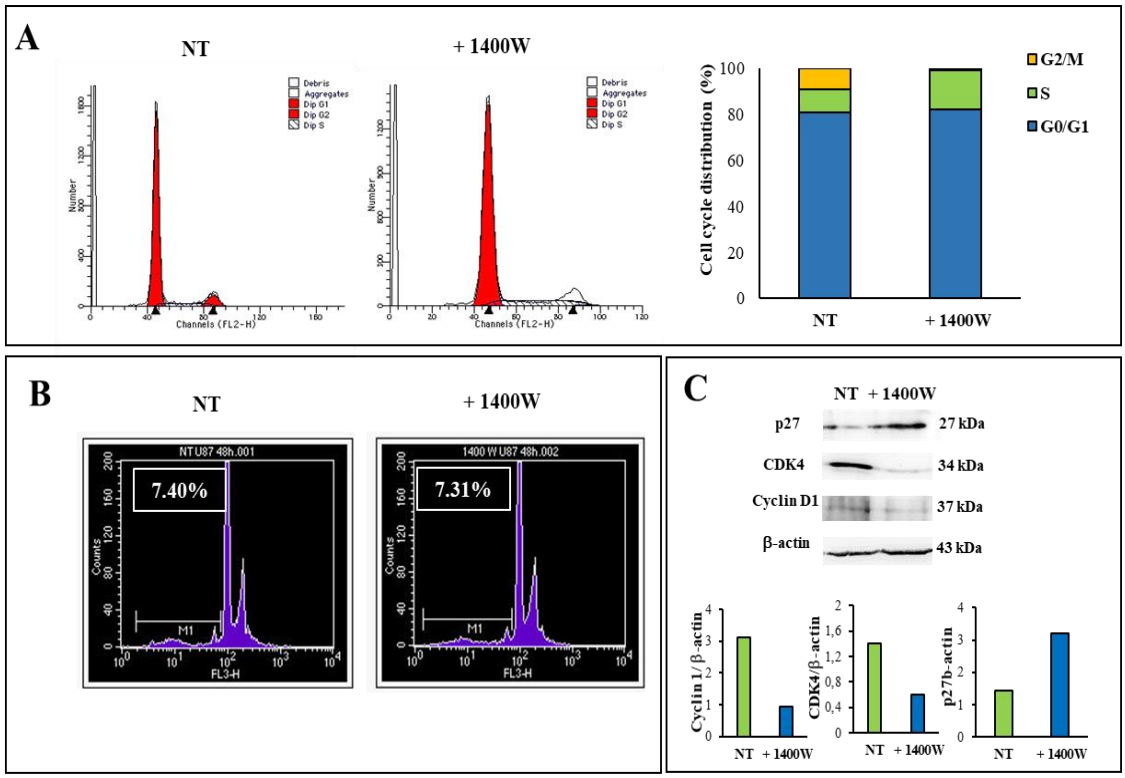

Figure 24. Effects of 1400W on U87MG-derived NS cell cycle. (A) Cell cycle profiles of neurospheres-forming cells after 48 h incubation without (NT) or with 1400W (100 μM). Cell cycle distribution (%) is also reported in the histogram. Results are representative of three independent experiments. (B) Flow cytometric profiles of apoptosis level analysis in neurospheres-forming cells after 48 h incubation without (NT) or with 100 μM 1400W. Results are representative of three independent experiment. (C) Representative images of western blot analysis of cell cycle-related proteins Cyclin D1, CDK4, and p27 in extracts of neurospheres after 48 h incubation without (NT) or with 1400W (100 μM). The results of densitometric analysis of bands expressed as ratio vs β-actin band intensity are reported in the histograms. Data are representative of two independent experiments.

4.9 1400W induces autophagy of glioma stem cells

In order to verify whether 1400W could induce the autophagic pathway in GBM stem cells, Acridine Orange (AO) staining of the U87MG neurospheres was assessed to visualize acidic compartments, lysosomal structures named acidic vesicular organelles (AVO) and considered as marker of autophagic process. AO-stained disaggregated U87MG-derived neurospheres were visualized by fluorescence microscopy and relative quantification was performed by FACS analysis. In untreated cells, the cytoplasm and

nuclei fluoresced bright green, otherwise, 1400W treatment at 100 μM for 48 h, caused a marked induction of AVOs developed in the cell cytoplasm of disaggregated neurospheres, clearly shown by the bright orange/red acidic compartments (**Figure 25A**). As a positive control of the autophagic process, U87MG cells subjected to serum withdrawal for 4 h have been used (data not shown). Furthermore, we quantified the AVOs presence with FACS analysis, and a significant increase of fluorescence intensity as compared to untreated cells has been registered (91.37% vs 23.93%) (**Figure 25B**). To confirm whether 1400W induced autophagic flux in GBM cells the classical autophagy-related proteins, including LC3-I/II and Beclin-1 were analyzed by western blot. Consistent with the AO staining, both proteins were observed to be upregulated indicating that 1400W promoted autophagy in GSCs. Representative western blots of autophagic markers in U87MG are shown in **Figure 25C**.

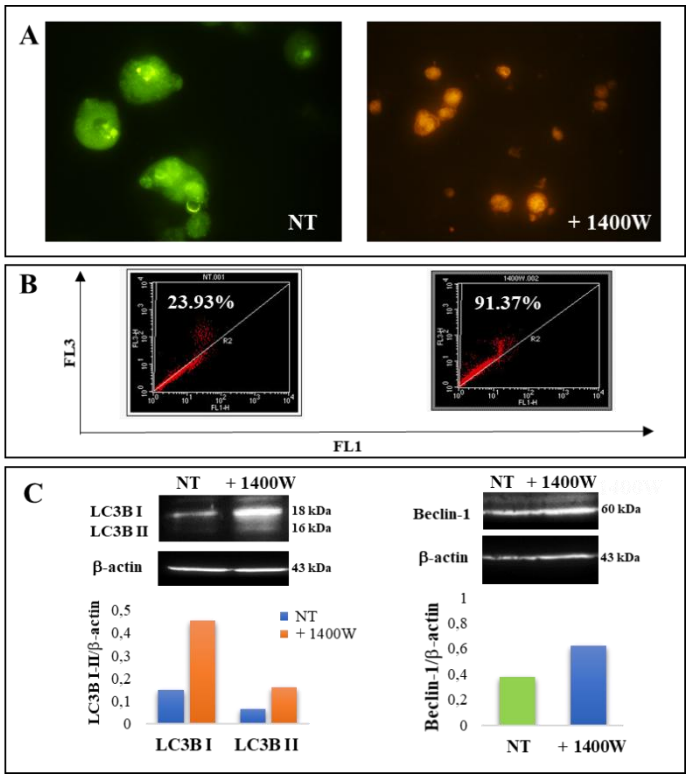

Figure 18. Detection of autophagy by acridine orange staining. (A) Representative images of acidic vacuolar organelles (AVO) fluorescence staining in not treated (NT), and 1400W-treated NS-forming cells (100 μM for 48 h) (magnification 100×). (B) Flow cytometric analysis of AVO in NS-forming cells exposed or not to 1400W (100 μM) for 48 h. AVO were measured using the 488-nm excitation detector (green fluorescence/FL1) and the 540-nm emission detector (red fluorescence/FL3). The results are representative of two independent experiments. (C) Representative images of western blot analysis of autophagic markers LC3B I/II and Beclin-1 in neurospheres treated or not with 1400W (100 μM) for 48 h

are shown. The results of densitometric analysis expressed as ratio vs β-actin band intensity are reported in the histograms. The results are representative of three independent experiments.

4.10 1400W influences the release of extracellular vesicles by glioma stem cells

Taking into account the known association between autophagy and EV biogenesis through shared molecular machinery or organelles [60,146] and also based on the SEM images that showed a significant membrane activity in the 1400W-treated neurospheres, the ability of 1400W inhibitor to modulate EVs shedding by U87MG-derived neurospheres was evaluated. For this purpose, U87MG-derived neurosphere cultures were exposed to 1400W at 100 μM for 48 h and then EV isolated from neurospheres' supernatants, were firstly characterized by transmission electron microscopy (TEM). TEM images of fresh EVs isolated from U87MG-derived neurospheres confirmed the classical morphological features: an unbroken bilayer membrane with a typical rounded morphology (**Figure 26A**). Size and concentrations of EVs, determined by nanoparticle tracking analysis (NTA) are reported in **Figure 26B** (graph and table). Of note, the total number of EVs (size 30.5-700.5 nm) resulted strongly enhanced after treatment with NOS2 inhibitor, with a % increase >110%. In particular, both small (30.5-130.5 nm) and large (131.5-700.5 nm) vesicle concentrations were increased by 1400W treatment, even if the small vesicle number/ml resulted noticeably higher (>180% increase) when compared to large vesicle number/ml (>90% increase). Furthermore, the tetraspanins CD63 and CD81, specific EV markers reported in MISEV 2018 [141] were expressed in all isolated EVs without significant difference between untreated and 1400W-treated cells. Representative western blots for EVs derived from U87MG- and T98G-neurospheres treated and untreated, are showed in **Figure 26C**.

Taken together, these results demonstrated that the EVs fractions were successfully isolated from the both GBM neurospheres media with high purity.

According to the literature data on the involvement of acid sphingomyelinase (aSMase) in the vesicle biogenesis in different cell systems treated with various stimuli [147], the ability of 1400W to influence the aSMase activity in U87MG-derived NS was

evaluated. A significant increase of more than 200% of the level of ceramide, hydrolysis product of aSMase activity was detected in presence of 1400W ($P<0.05$) (**Figure 26D**).

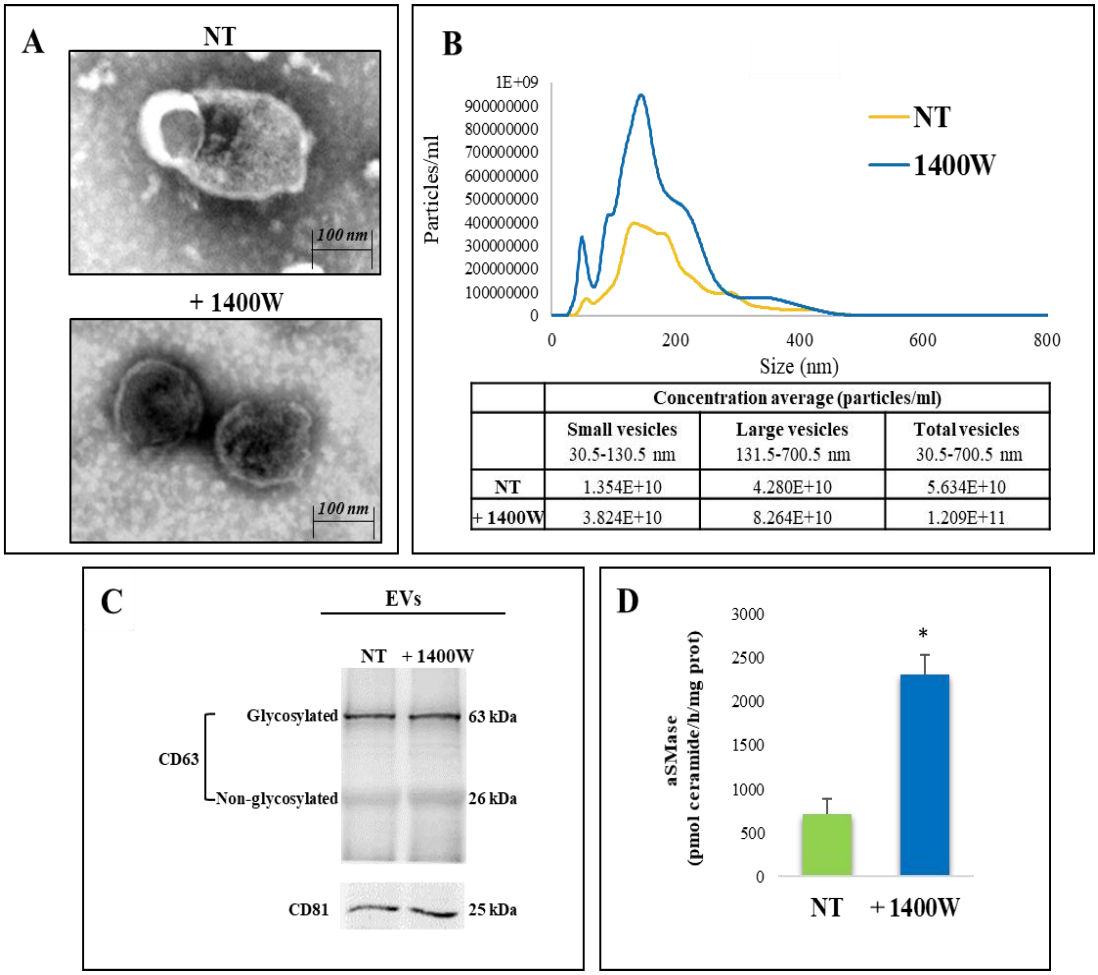

	Concentration average (particles/ml)		
	Small vesicles 30.5-130.5 nm	**Large vesicles** 131.5-700.5 nm	**Total vesicles** 30.5-700.5 nm
NT	1.354E+10	4.280E+10	5.634E+10
+ 1400W	3.824E+10	8.264E+10	1.209E+11

Figure 26. Characterization of extracellular vesicles (EVs) released by U87MG-derived NS after 48 h incubation without or with 1400W. (A) Morphological analysis of EVs from U87MG-derived neurospheres, treated or not with 1400W (100 µM) for 48 h, was evaluated using transmission electron microscopy (TEM) (scale bar 100 nm). Pictures show membrane bound vesicles with a spheroid shape. (B) Size distribution of EVs from U87MG-derived neurospheres by Nanoparticles Tracking Analysis (NTA). Concentration average of particles per ml is reported in the table. (C) Representative western blots of EVs markers, CD63 (core protein, 26 kDa; glycosylated protein, 63 kDa) and CD81, in neurospheres-released EVs. (D) Acid SMase activity in U87MG-derived neurospheres treated or not with 1400W (100 µM) for 48 h. Data are expressed as pmol ceramide/h/mg protein (mean ± SD) and they are representative of four independent experiments in duplicate. For comparison between two means, Student's unpaired t-test was used (*$P< 0.05$).

4.11 Effect of EVs by 1400W-treated GSC on U87MG proliferation and migration

To test whether the EVs released by U87MG-derived neurospheres were able to affect the proliferation and migration of adherent GBM recipient cells, we firstly verified the effects of direct addition of 1400W on U87MG cell proliferation and migration ability. In **Figure 27A** a significant reduction of the cell number was observed in the presence of 100 µM 1400W (**P<0.01 vs NT at 24 h; ***P<0.001 vs NT at 48 h).

EVs derived from cancer stem cells in many tumors, including GBM, could be involved in the tumorigenic effects [148], therefore we evaluated the effect of EVs released by NS in our cell model. The adherent GBM cells were incubated for 48 h with the EVs secreted by U87MG-derived NS previously treated for 48 h with 1400W (EVs 1400W-NS) or not (EVs NT-NS). We observed that the presence of EVs secreted by NS not treated (EVs NT-NS) exerted a stimulatory effect (~ 25% increase) on cell growth, instead the addition of EVs 1400W-NS had an impairment effect (~ 23-28% reduction) on the growth of adherent U87MG cells (**Figure 27B**).

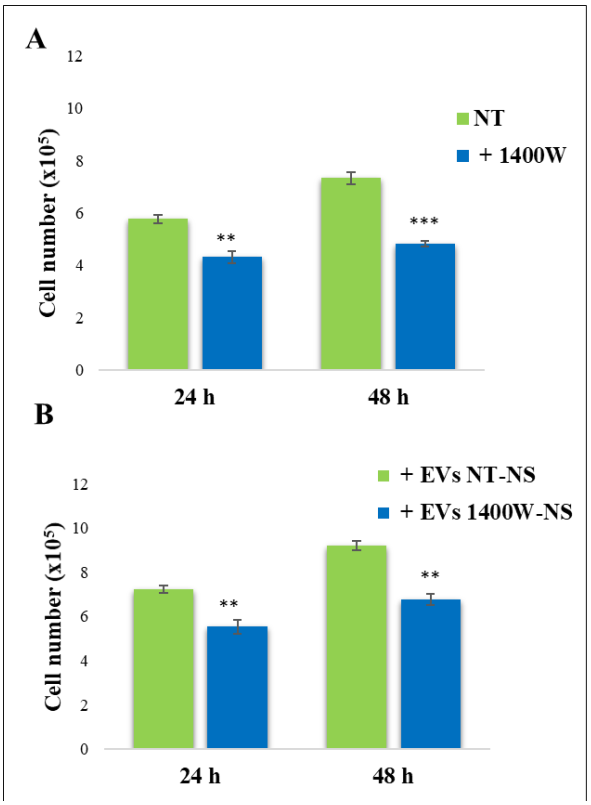

Figure 27. Proliferation assay of adherent U87MG cells treated with 1400W or EVs released by not treated neurospheres (NT-NS) or treated with 1400W (1400W-NS). (A) Adherent U87MG cells were treated with 1400W (100 µM) for 24 and 48 h and proliferation rate was measured using Cell Counting Kit-8 assay

(CCK-8) assay. Data expressed as total cell number are representative of two experiments in duplicate (**P<0.01, ***P<0.001 compared to relative NT). (B) Adherent U87MG cells were incubated with EVs that were released from not treated (EVs NT-NS) and 1400W-treated (EVs 1400W-NS) NS and proliferation assay was assessed at 24 and 48 h. Data that are expressed as total number of cells are representative of two experiments in duplicate (**P<0.01 vs NT).

It is known that GBM cells are characterized by a remarkable proliferation and, also, by a high migration ability. The capability of NOS2 inhibitor to influence tumor invasiveness was evaluated using an *in vitro* artificial wound model. The rate of scratched monolayer closure in the absence or presence of 100 μM of 1400W was evaluated by measuring the repopulated area between the wound edges at different time points after the mechanical lesion. **Figure 28, panels A and B**, shows representative microscopy images at T0, 8 h, and 24 h, and the quantitative analysis of wound closure rate for GBM adherent U87MG cell line. The results are expressed as percentages of wound closure vs relative T0 from two independent experiments in duplicate. In all experiments, the scratched monolayers of control cells (untreated - NT) were closed at about 28 h. Treatment with selective NOS2 inhibitor alone significantly delayed the U87MG monolayer migration both at 8 h (22.41 ± 2.43 NT vs 5.40 ± 1.72 1400W) (P<0.01) and 24 h (58.44 ± 4.57 NT vs 33.92 ± 5.83 1400W) compared to untreated control (P<0.01) (**Figure 28A and B**). These data highlighted that the migration of both GBM cell line was significantly delayed by NOS2 inhibitor addition.

On the other hand, the addition of EVs 1400W-NS on scratched U87MG monolayer of U87MG, caused a reduction of the wound closure rate similarly to that observed after the direct addition of 1400W to cell cultures. As reported in **Figure 28C and D**, the addition of EVs derived from 1400W-treated NS significantly reduced the repair rate of the scratched monolayer at 24 h as compared to U87MG cells treated with EVs secreted by not treated NS (71.00 ± 2.30 NT vs 43.14 ± 2.56 1400W) (**P<0.01).

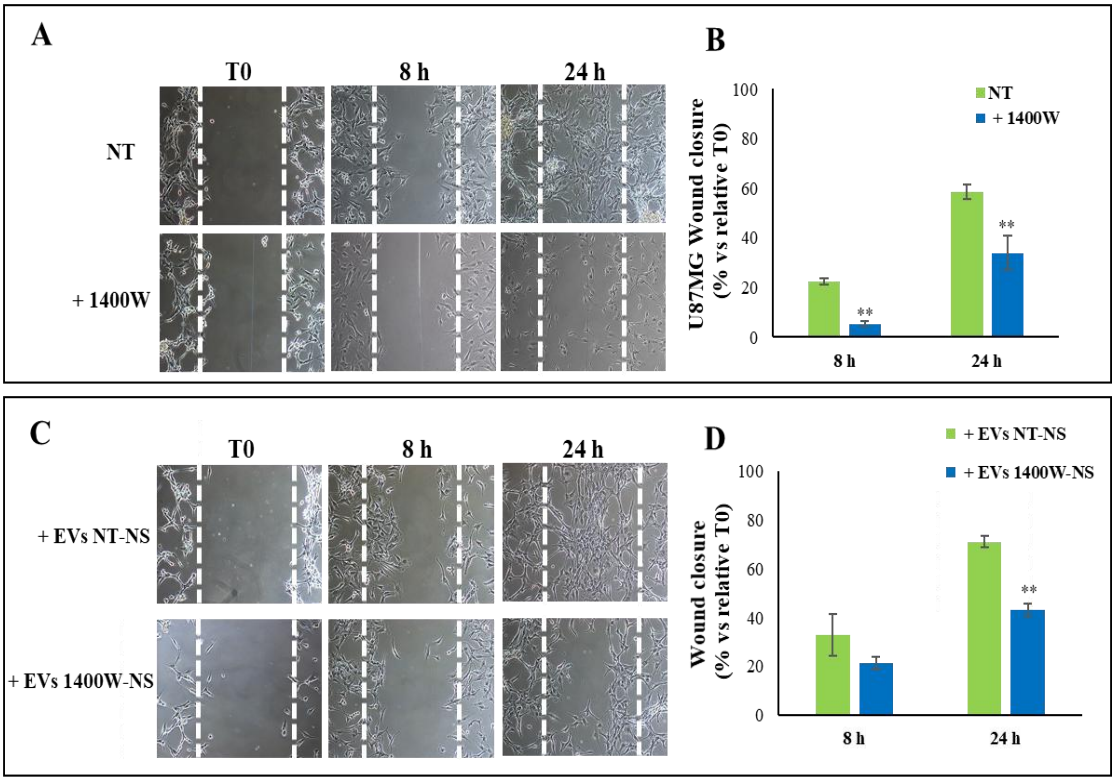

Figure 28. Cell migration ability of adherent U87MG cells treated with 1400W or EVs released by NT-NS or 1400W-NS. (A) Scratched monolayers of adherent U87MG cells were incubated up to 48 h without (NT) or with 1400W (100 μM) to quantify cell motility by measuring the wound closure. Representative microscopy images captured at 0, 8, and 24 h are shown (10× magnification). (B) The quantitative results expressed as % wound closure vs relative T0 (mean ± SD) are representative from two independent experiments in duplicate. For comparative analysis of groups of data, repeated measures two-way ANOVA followed by Bonferroni post hoc test was used (**P< 0.01). (C) Wound healing assay performed on adherent U87MG after incubation with EVs derived from untreated NS (EVs NT-NS) and 1400W-treated NS (EVs 1400W-NS). Images of scratched monolayers were acquired for the indicated times after injury (10x magnification). Additionally, in this case, the wound closure rates expressed as % closure at 8 and 24 h vs relative T0 (mean ± SD) and shown in the histogram in panel (D). Representative microscopy images captured at 0, 8, and 24 h are shown (10× magnification). For comparative analysis of groups of data, repeated measures two-way ANOVA followed by Bonferroni post hoc test was used (**P< 0.01).

4.12 EVs by 1400W-treated GSC promote autophagy of U87MG cells

Exposure to NOS2 inhibitor 1400W alone led to an AVO level increase in adherent U87MG cell line as visualized by orange/red spots (**Figure 29A**). On the other hand, untreated cells showed a bright green fluorescence, thus indicating a lack of AVO. To further confirm the ability of EVs secreted from 1400W-treated neurospheres to cause autophagy in adherent cell line, U87MG were exposed for 48 h to purified EVs from not treated neurospheres (EVs NT-NS) and from 1400W-treated neurospheres (EVs 1400W-

NS). As reported in the **Figure 29B**, the addition of EVs 1400W-NS caused high levels of AVO's accumulation as highlighted by a diffuse orange/red fluorescence in the recipient adherent cells. As expected, EVs from NT-NS did not lead to any formation of AVO.

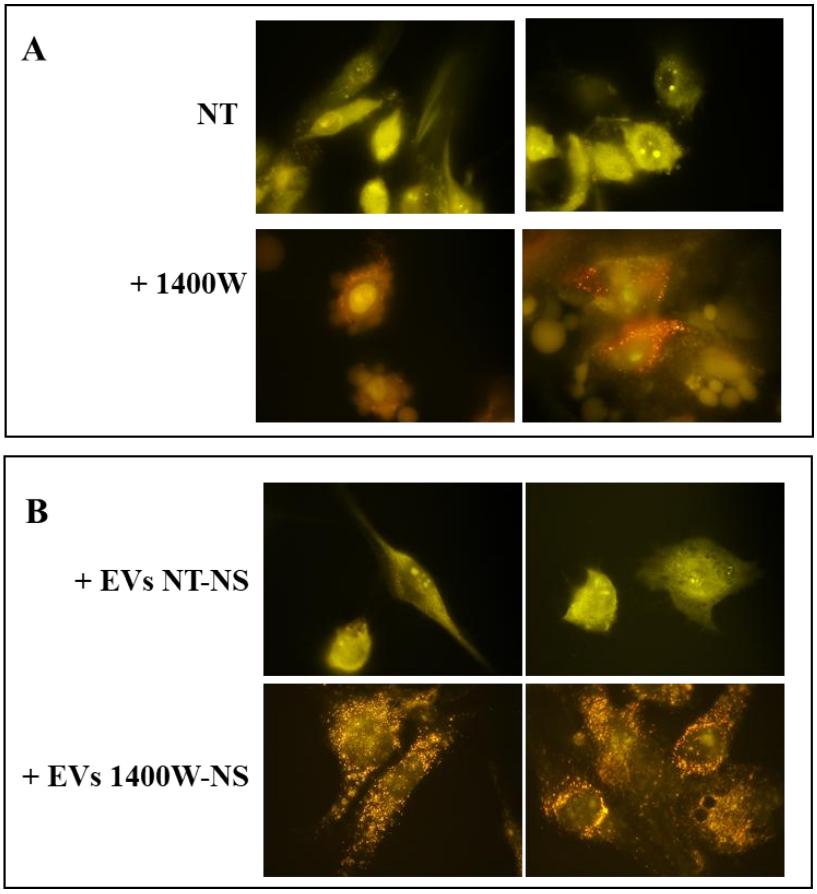

Figure 29. Induction of autophagy by 1400W in adherent U87MG cells. (A) U87MG cells were treated or not with 1400W (100 μM) for 48 h and then stained with AO to assess the content of acidic vacuoles (orange/red spots) by fluorescence microscopy. Two images for each condition are shown (magnification 100×) and are representative of two independent experiments. (B) U87MG cells were treated for 48 h with EVs derived from NT (EVs NT-NS) and 1400W-treated (EVs 1400W-NS) neurospheres. After treatment cells were stained as above described. Also in this case, two images for each condition are shown and are representative of two independent experiments.

5. DISCUSSION

GBM, like many other malignant tumors, is characterized by a moderately inflammatory microenvironment that promotes all stages of tumorigenesis, tumor progression, and invasiveness, as well as resistance to therapy [149]. In this context, the results of different groups concerning the expression of NOS2, either as a potential GBM molecular profile marker or interesting therapeutic target, assume particular relevance [86,149].

The potential correlation between NOS2 and SOX-2, a stemness marker aberrantly upregulated in GBM [75,150,151], was also verified. The potential role of NOS2 as a key regulator in the aberrant upregulation of master genes such as SOX-2, involved in sustaining self-renewal of glioma initiating cells should be further investigated. In this context, in fact, the literature data are still scarce and involve different systems of stem cells. In particular, Kim et al. [91] found that irradiation of glioma cells promotes GSC through NOS2-mediated NO production. They reported that downregulation of NOS2 led to a reduced GSC population as well as decreased radiotherapy resistance by preventing NO generation. Of interest, siRNA targeting NOS2 blocked the increase in SOX-2, Notch-2 and β-catenin expression in irradiated U87 glioma cells, thus inhibiting the stemness machinery for malignant progression.

Actually, GSCs are mainly considered to be responsible for high resistance to therapies and tumor recurrence. NOS2 was shown to play an important role in GSC survival, proliferation, stemness expression, and therapy resistance. Fractionated radiotherapy has been reported to increase SOX-2 and Notch expression through NOS2/NO system upregulation, leading to glioma resistance to radiotherapy [91]. NO signaling has been involved in the ID4 (inhibitor of differentiation-4)-induced enhancing effect on SOX-2 expression and the resistance of GSC to chemotherapy [152,153].

NOS2 expression was shown to promote the induction of stem cell properties in GBM cells [154]. The positive regulatory circuit that is associated with platelet-derived growth factor (PDGF)–NO–ID4 signaling has been suggested to play a pivotal role in regulating the self-renewal and glioma-initiating cells (GICs).

According to a recent article, the upmodulation of NOS2, among other inflammatory enzymes (i.e., COX-2), is associated with cell survival mechanisms during an oxidative stress condition by which GBM cells adapted themselves to aberrant metabolic activities [155].

A crucial role of the NOS2/NO system in immunosuppression has also been evidenced [156,157]. Recently, in a model system of GBM—non-ionizing photodynamic therapy—the reported findings indicated that suppressing NOS2 expression markedly increased the efficacy of anti-tumor therapy [158]. Recently, the ability of temozolomide (TMZ), alone or in combination with thymoquinone (TQ), to reduce NO production by U-87 MG cells has been suggested as a potential mechanism underlying its anti-glioma activity [159,160]. The pharmacological inhibition of NOS by L-NMMA (NG-Monomethyl-L-arginine) has been reported to enhance chemotherapy response in triple negative breast cancer (TNBC) models, significantly reducing tumor volume growth and increasing the survival rate [161].

A previous study showed evidence that several NO-releasing chemical compounds were able to decrease endogenous LC3-II in rat primary cortical neurons and HeLa cells, thus suggesting that NO could inhibit autophagy by impairing autophagosome generation [162]. Accordingly, the same authors reported that the inhibition of NO synthesis by L-NAME, which is a broad-spectrum NOS inhibitor, induced autophagy, thus delineating a crucial role of NO in regulating the autophagic process with a number of implications in the context of its multiple cellular functions.

Collectively, all of these studies, among others, suggest that NO signaling plays an important role in GSC maintenance and resistance to anticancer therapies. Thus, the NOS2/NO system as a biomarker for glioma and/or as a potential pharmacological target is extremely promising. In this context, the inhibition of NO production may have a significant therapeutic potential also to improve conventional treatment, even if the clinical studies are still limited [163].

With the aim to further evaluate the role of inflammatory profile in GBM biology, in the present work we first showed the concordance between M2-polarization of GBM-infiltrating macrophages, SOX-2 expression, and ability to generate neurospheres by

GBM primary cultures. A high and significant correlation resulted between NOS2 expression level and SOX-2 positive cells in all cell cultures maintained in standard conditions. GBM primary culture-derived neurospheres expressed significantly higher levels of NOS2 expression and activity when compared to the cells cultured in standard conditions. Also, NOS2 levels were significantly increased in neurospheres derived by SOX-2 positive GBM primary cultures, while all primary cultures unable to generate neurospheres expressed low levels of NOS2, highlighting its possible relevance in glioma pathology as supposed by other groups [86,87,90,91]. These results were also confirmed by using five different GBM cell lines [94].

In an effort to highlight the functional role of the NOS2/NO system in glioma biology, in the current study we also explored the effect of the NOS2 inhibitor 1400W at no cytotoxic concentrations toward the proliferation and migration rate, clonogenic potential, and neurosphere generation ability of glioma cells expressing high levels of NOS2. NOS2, being basically expressed in the U87 MG, T98G glioma cell lines, and human glioma primary cells, was confirmed to be upmodulated in the relative neurospheres generated in specific culture conditions. Of note, 1400W, at an effective concentration to inhibit NO generation, was able to significantly reduce the proliferation, migration, colony formation, and neurosphere generation abilities of glioma cells, thus supporting the emerging relevance of NOS2 as a functional player in glioma biology. Results from experiments that aimed to investigate the effect of the NO chemical donor SNAP also support a functional role for NO in the glioma cell survival and proliferation rates as well as clonogenic potential.

With the aim of highlighting the functional role of NOS2 in GBM biology, we have explored the possible involvement of the autophagic process and associated vesicle biogenesis in the in vitro anti-tumoral actions of a selective NOS2 inhibitor, 1400W on U87MG cell line, which basically expresses high levels of NOS2 [164]. In our experimental conditions, the NOS2 inhibitor was able to cause greater induction of autophagy markers, including a relevant number of autophagy vacuoles and the upregulation of proteins that are associated to autophagosome generation, i.e., LCB3 and Beclin-1, where overexpression in the U87MG cells has been already related to cellular

autophagy [165]. The autophagic flux induced by 1400W was associated with membrane blebbing, cell cycle arrest, and decreased cell proliferation and migration rate. 1400W-induced autophagy was accompanied by a noteworthy increase of the EV secretion by GSCs, as well as by the upregulation of common protein markers of autophagosome biogenesis such as CD63 and CD81. Additionally, the activity of the acidic SMase, an enzyme involved in the budding of EV by converting sphingomyelin into ceramide [147,166], was significantly increased in NS-forming GSCs after the addition of 1400W. The results of the experiments designed to explore the effects of EVs released by glioma stem cells previously incubated with 1400W on adherent U87MG cells showed a strongly negative influence on the recipient cells, with a strictly reduced proliferation rate and migration ability. These results were associated with a relevant autophagy level. On the contrary, the adherent U87MG cells receiving EVs secreted by untreated GSCs were induced to an increase of proliferation index and migration ability. No autophagy was detectable in this condition.

Altogether, these findings (schematized in **Figure 30**) lead us to hypothesize that the effect induced by the direct addition of 1400W to GSCs or adherent U87MG cells could be mediated by anti-tumoral molecular messages induced by NOS2 inhibition in the origin cells and then transferred to the surrounding recipient cells through the EVs. On the other hand, NOS2 inhibition could induce GSCs to release EVs with a modified cargo that is able to alter and manipulate the tumor inflammatory microenvironment in order to make it less advantageous to tumor growth and invasiveness.

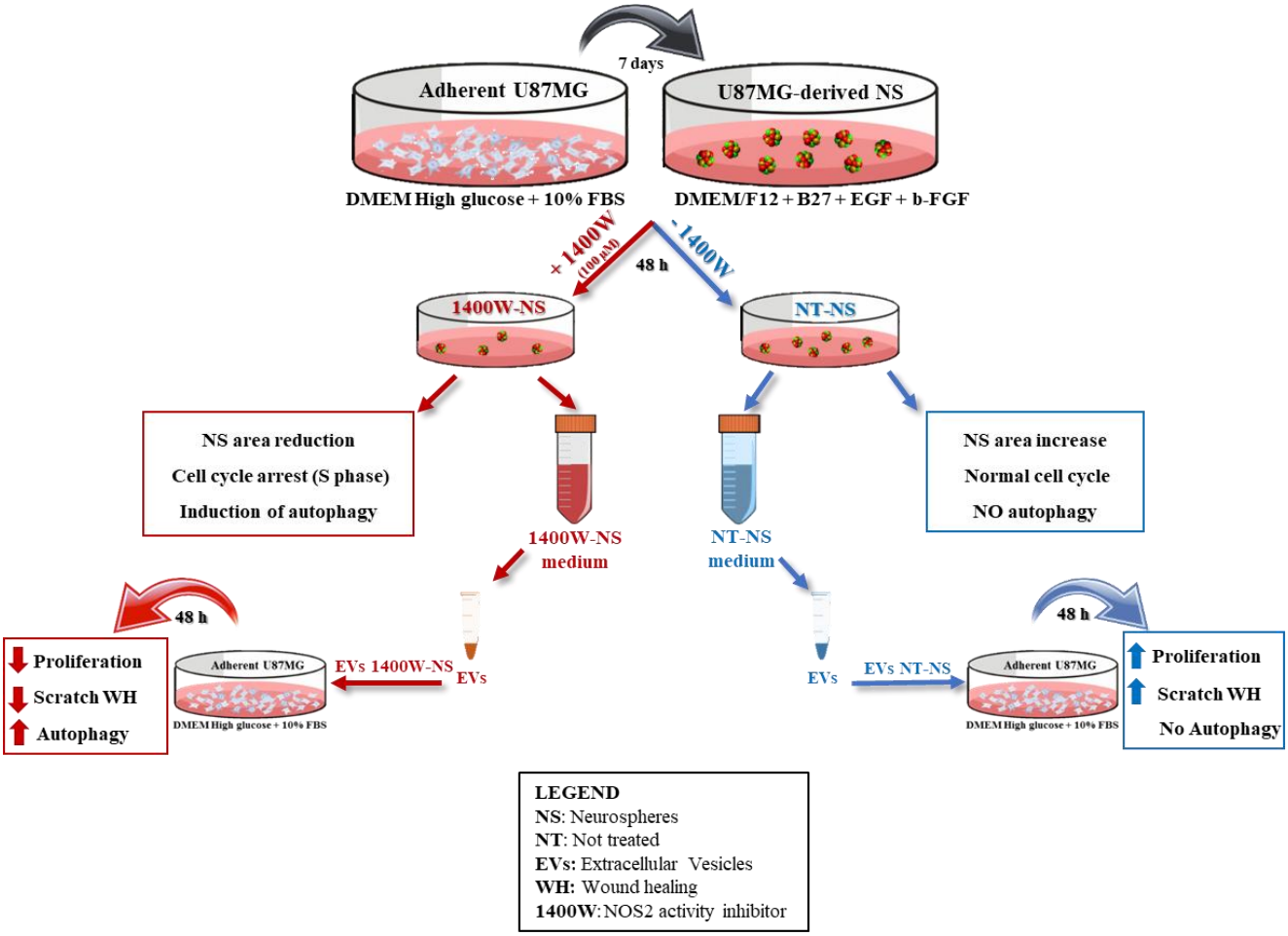

Figure 30. Scheme of experimental design and obtained results.

It will be of interest to explore in our experimental system the possible influence of 1400W on PI3K-Akt/mTOR system, a key signaling pathway mainly involved in modulating autophagy and associated to malignancy grade of gliomas [167,168]. In this respect, it is worth noting that the U87MG cell line is expressing mutant PTEN (phosphatase and tensin homolog), which is an important negative regulator of the Akt/mTOR pathway [122].

In conclusion, our findings could represent a useful contribution to the development of potential therapeutic approaches for the treatment of glioma based on knowledge of the signaling pathways involved in the NO-mediated glioma cell regulation. Studies are in progress to investigate the role of the glioma-associated inflammatory profile with the aim to identify the upstream mechanisms of NOS2

induction which in turn might underlie the overexpression of stemness markers such as SOX-2 and the consequent abnormal expansion of glioma initiating stem cells.

In addition, the methodological approaches used in this work to study proliferation and migration, together with those aimed at verifying the tumor potential of developing spheres, appear useful for the screening of new and increasingly specific NOS2 inhibitors such as acetamidines, which have been recently discovered and are structurally related to the 1400W [97]. Even if further studies are required to gain insights into the signaling networks involved in NOS2/NO system expression and overexpression, which in turn might underlie the abnormal expansion of GICs, our findings could represent a useful contribution to the development of potential therapeutic approaches for the treatment of glioma based on knowledge of the signaling pathways involved in the NO-mediated glioma cell regulation.

6. REFERENCES

1. Louis DN, Perry A, Reifenberger G, von Deimling A, Figarella-Branger D, Cavenee WK, Ohgaki H, Wiestler OD, Kleihues P, Ellison DW. The 2016 World Health Organization Classification of Tumors of the Central Nervous System: a summary. Acta Neuropathol 2016, 131, 803-820, doi:10.1007/s00401-016-1545-1.
2. Wang Y, Liu X, Guan G, Zhao W, Zhuang M A. Risk Classification System With Five-Gene for Survival Prediction of Glioblastoma Patients. Front Neurol 2019, 10, 745, doi:10.3389/fneur.2019.00745.
3. Molinaro AM, Taylor JW, Wiencke JK, Wrensch MR. Genetic and molecular epidemiology of adult diffuse glioma. Nat Rev Neurol 2019, 15, 405-417, doi:10.1038/s41582-019-0220-2.
4. Ostrom QT, Gittleman H, Stetson L, Virk S, Barnholtz-Sloan JS. Epidemiology of Intracranial Gliomas. Prog Neurol Surg 2018, 30, 1-11, doi:10.1159/000464374.
5. Miranda-Filho A, Pineros M, Soerjomataram I, Deltour I, Bray F. Cancers of the brain and CNS: global patterns and trends in incidence. Neuro Oncol 2017, 19, 270-280, doi:10.1093/neuonc/now166.
6. Weller M, van den Bent M, Tonn JC, Stupp R, Preusser M, Cohen-Jonathan-Moyal E, Henriksson R, Rhun EL, Balana C, Chinot O, Bendszus M, Reijneveld JC, Dhermain F, French P, Marosi C, Watts C, Oberg I, Pilkington G, Baumert BG, Taphoorn MJB, Hegi M, Westphal M, Reifenberger G, Soffietti R, Wick W. European Association for Neuro-Oncology (EANO) guideline on the diagnosis and treatment of adult astrocytic and oligodendroglial gliomas. Lancet Oncol 2017, 18, e315-e329, doi:10.1016/S1470-2045(17)30194-8.
7. Perus LJM, Walsh LA. Microenvironmental Heterogeneity in Brain Malignancies. Front Immunol 2019, 10, 2294, doi:10.3389/fimmu.2019.02294.
8. Ostrom QT, Gittleman H, Xu J, Kromer C, Wolinsky Y, Kruchko C, Barnholtz-Sloan JS. CBTRUS Statistical Report: Primary Brain and Other Central Nervous System Tumors Diagnosed in the United States in 2009-2013. Neuro Oncol 2016, 18, v1-v75, doi:10.1093/neuonc/now207.
9. Shergalis A, Bankhead A 3rd, Luesakul U, Muangsin N, Neamati N. Current Challenges and Opportunities in Treating Glioblastoma. Pharmacol Rev 2018, 70, 412-445, doi:10.1124/pr.117.014944.
10. Stoyanov GS, Dzhenkov D, Ghenev P, Iliev B, Enchev Y, Tonchev AB. Cell biology of glioblastoma multiforme: from basic science to diagnosis and treatment. Medical oncology 2018, 35, 27, doi:10.1007/s12032-018-1083-x.
11. Thakkar JP; Dolecek TA; Horbinski C; Ostrom QT; Lightner DD; Barnholtz-Sloan JS; Villano JL. Epidemiologic and molecular prognostic review of glioblastoma. Cancer epidemiology, biomarkers & prevention: a publication of the American Association for Cancer Research, cosponsored by the American Society of Preventive Oncology 2014, 23, 1985-1996, doi:10.1158/1055-9965.EPI-14-0275.
12. Dirkse A; Golebiewska A; Buder T; Nazarov PV; Muller A; Poovathingal S; Brons NHC; Leite S; Sauvageot N; Sarkisjan D, Seyfrid M, Fritah S, Stieber D, Michelucci A, Hertel F, Herold-Mende C, Azuaje F, Skupin A, Bjerkvig R, Deutsch A, Voss-Böhme A, Niclou SP. Stem cell-associated heterogeneity in Glioblastoma results from intrinsic tumor plasticity shaped by the microenvironment. Nature communications 2019, 10, 1787, doi:10.1038/s41467-019-09853-z.
13. Garnier D; Renoult O; Alves-Guerra MC; Paris F; Pecqueur C. Glioblastoma Stem-Like Cells, Metabolic Strategy to Kill a Challenging Target. Frontiers in oncology 2019, 9, 118, doi:10.3389/fonc.2019.00118.

14. Wrensch W, Fisher JL, Schwartzbaum A, Bondy M, Berger M, Aldape KD. Molecular epidemiology of gliomas in adults. Neurosurgical Focus. 2005;19(5):1–11.
15. Schwartzbaum JA, Fisher JL, Aldape KD, Wrensch M. Epidemiology and molecular pathology of Glioblastoma multiforme. Nat Clin Pract Neurol. 2006;2:494–503.
16. Brenner AV, Butler MA, Wang SS, Ruder AM, Rothman N, Schulte PA, Chanock SJ, Fine HA, Linet MS, Inskip PD. Single-nucleotide polymorphisms in selected cytokine genes and risk of adult glioma. Carcinogenesis. 2007;28(12):2543–47.
17. Lachance DH, Yang P, Johnson DR, Decker PA, Kollmeyer TM, McCoy LS, Rice T, Xiao Y, Ali-Osman F, Wang F, Stoddard SM, Sprau DJ, Kosel ML, Wiencke JK, Wiemels JL, Patoka JS, Davis F, McCarthy B, Rynearson AL, Worra JB, Fridley BL, O'Neill BP, Buckner JC, Il'yasova D, Jenkins RB, Wrensch MR. Associations of high-grade glioma with glioma risk alleles and histories of allergy and smoking. Am J Epidemiol. 2011;174(5):574–81.
18. Scheurer ME, Amirian S, Davlin TL, Rice T, Wrensch M, Bondy ML. Effects of antihistamine and anti-inflammatory medication use on risk of specific glioma histologies. Int J Cancer. 2011;129(9):2290–6.
19. Chakrabarti I, Cockburn M, Cozen W, Wang YP, Preston-Martin S. A population-based description of glioblastoma multiforme in Los Angeles County, 1974–1999. Cancer. 2005;104:2798–06.
20. Kitahara CM, Wang SS, Melin BS, Wang Z, Braganza M, Inskip PD, Albanes D, Andersson U, Beane Freeman LE, Buring JE, Carreón T, Feychting M, Gapstur SM, Gaziano JM, Giles GG, Hallmans G, Hankinson SE, Henriksson R, Hsing AW, Johansen C, Linet MS, McKean-Cowdin R, Michaud DS, Peters U, Purdue MP, Rothman N, Ruder AM, Sesso HD, Severi G, Shu XO, Stevens VL, Visvanathan K, Waters MA, White E, Wolk A, Zeleniuch-Jacquotte A, Zheng W, Hoover R, Fraumeni JF Jr, Chatterjee N, Yeager M, Chanock SJ, Hartge P, Rajaraman P. Association between adult height, genetic susceptibility and risk of glioma. Int J Epidemiol. 2012 Aug;41(4):1075–85.
21. Deltour I, Auvinen A, Feychting M, Johansen C, Klaeboe L, Sankila R, et al. Mobile phone use and incidence of glioma in the Nordic countries 1979–2008: Consistency check. Epidemiology. 2012;23(2):301–7.
22. Benson VS, Pirie K, Schuz J, Reeves GK, Beral V, Green J. Mobil phone use and risk of brain neoplasms and other cancers: Prospective study. Int J Epidemiol. 2013;43(3):792–802.
23. Nieder C, Grosu A, Astner S, Molls M. Treatment of unresectable glioblastoma multiforme. Anticancer Res. 2005;1(25):4605–10.
24. Gerlinger M, Swanton C. How Darwinian models inform therapeutic failure initiated by clonal heterogeneity in cancer medicine. Br J Cancer. 2010;103:1139–43. http://dx.doi.org/10.1038/sj.bjc.6605912
25. Glioblastoma, 2017. Edited by Steven De Vleeschouwer, Codon Publications, Brisbane, QLD 4122, Australia. ISBN: 978-0-9944381-2-6, DOI: http://dx.doi.org/10.15586/codon.glioblastoma.
26. Verhaak RG, Hoadley KA, Purdom E, Wang V, Qi Y, Wilkerson MD, Miller CR, Ding L, Golub T, Mesirov JP, Alexe G, Lawrence M, O'Kelly M, Tamayo P, Weir BA, Gabriel S, Winckler W, Gupta S, Jakkula L, Feiler HS, Hodgson JG, James CD, Sarkaria JN, Brennan C, Kahn A, Spellman PT, Wilson RK, Speed TP, Gray JW, Meyerson M, Getz G, Perou CM, Hayes DN; Cancer Genome Atlas Research Network. Integrated genomic analysis identifies clinically relevant subtypes of glioblastoma characterized by abnormalities in PDGFRA, IDH1, EGFR, and NF1. Cancer Cell. 2010;17(1):98–110. http://dx.doi.org/10.1016/j.ccr.2009.12.020.
27. Feng H, Hu B, Jarzynka MJ, Li Y, Keezer S, Johns TG, Tang CK, Hamilton RL, Vuori K, Nishikawa R, Sarkaria JN, Fenton T, Cheng T, Furnari FB, Cavenee WK, Cheng SY.

Phosphorylation of dedicator of cytokinesis 1 (Dock180) at tyrosine residue Y722 by Src family kinases mediates EGFRvIII-driven glioblastoma tumorigenesis. Proc Natl Acad Sci U S A. 2012;109(8):3018–23. http://dx.doi.org/10.1073/pnas.1121457109.

28. Wiencke JK, Zheng S, Jelluma N, Tihan T, Vandenberg S, Tamguney T, Baumber R, Parsons R, Lamborn KR, Berger MS, Wrensch MR, Haas-Kogan DA, Stokoe D. Methylation of the PTEN promoter defines low-grade gliomas and secondary glioblastoma. Neuro Oncol. 2007 Jul;9(3):271–9. http://dx.doi.org/10.1215/15228517-2007-003
29. McNamara MG, Sahebjam S, Mason WP (2013) Emerging biomarkers in glioblastoma. Cancers 5(3):1103–1119.
30. Lam PY, Di Tomaso E, Ng HK, Pang JC, Roussel MF, Hjelm NM. (2000) Expression of p19INK4d, CDK4, CDK6 in glioblastoma multiforme. Br J Neurosurg 14(1):28–32.
31. Crespo I, Vital AL, Gonzalez-Tablas M, Patino Mdel C, Otero A, Lopes MC, de Oliveira C, Domingues P, Orfao A, Tabernero MD. Molecular and Genomic Alterations in Glioblastoma Multiforme. Am J Pathol. 2015 Jul;185(7):1820-33. doi: 10.1016/j.ajpath.2015.02.023. Epub 2015 May 11.
32. Reifenberger G, Liu L, Ichimura K, Schmidt EE, Collins VP. Amplification and overexpression of the MDM2 gene in a subset of human malignant gliomas without p53 mutations. Cancer Res. 1993;53(12):2736–9.
33. Biernat W, Kleihues P, Yonekawa Y, Ohgaki H. Amplification and overexpression of MDM2 in primary (de novo) glioblastomas. J Neuropathol Exp Neurol. 1997;56(2):180–5. http://dx.doi.org/10.1097/00005072-199702000-00009
34. Stott FJ, Bates S, James MC, McConnell BB, Starborg M, Brookes S, Palmero I, Ryan K, Hara E, Vousden KH, Peters G. The alternative product from the human CDKN2A locus, p14(ARF), participates in a regulatory feedback loop with p53 and MDM2. EMBO J. 1998;17(17):5001–14. http://dx.doi.org/10.1093/emboj/17.17.5001
35. Sturm D, Bender S, Jones DT, Lichter P, Grill J, Becher O, Hawkins C, Majewski J, Jones C, Costello JF, Iavarone A, Aldape K, Brennan CW, Jabado N, Pfister SM. Paediatric and adult glioblastoma: Multiform (epi)genomic culprits emerge. Nat Rev Cancer. 2014;14:92–107. http://dx.doi.org/10.1038/nrc3655.
36. Yap TA, Gerlinger M, Futreal PA, Pusztai L, Swanton C. Intratumor heterogeneity: Seeing the wood for the trees. Sci Transl Med. 2012;4:127ps110. http://dx.doi.org/10.1126/scitranslmed.3003854.
37. Lombard A, Goffart N, Rogister B. Glioblastoma circulating cells: Reality, trap or illusion? Stem Cell Int. 2015;2015:182985. http://dx.doi.org/10.1155/2015/182985
38. Aubry M, de Tayrac M, Etcheverry A. “From the core to beyond the margin”: A genomic picture of glioblastoma intratumor heterogeneity. Oncotarget. 2015;6(14):12094–109. http://dx.doi.org/10.18632/oncotarget.3297
39. Brabletz T, Jung A, Spaderna S, Hlubek F, Kirchner T. Migrating cancer stem cells—An integrated concept of malignant tumour progression. Nat Rev Cancer. 2005;5(9):744–9. http://dx.doi.org/10.1038/nrc1694
40. Radisky DC. Epithelial-mesenchymal transition. J Cell Sci. 2005;118(19):4325–6. http://dx.doi.org/10.1242/jcs.02552
41. Kalluri R, Weinberg RA. The basics of epithelial-mesenchymal transition. J Clin Invest. 2009;119(6):1420. http://dx.doi.org/10.1172/JCI39104
42. Gaoliang Ouyang (2011). Epithelial-Mesenchymal Transition and Cancer Stem Cells, Cancer Stem Cells - The Cutting Edge, Prof. Stanley Shostak (Ed.), ISBN: 978-953-307-580-8, InTech, Available from:http://www.intechopen.com/books/cancer-stem-cells-the-cutting-edge/epithelial- mesenchymaltransition-andcancer-stem-cells.

43. Zhang X, Chen T, Zhang J, Mao Q, Li S, Xiong W, Qiu Y, Xie Q, Ge J. Notch1 promotes glioma cell migration and invasion by stimulating β-catenin and NF-κB signaling via AKT activation. Cancer Sci. 2012;103(2):181–90. http://dx.doi.org/10.1111/j.1349-7006.2011.02154.x
44. Carro MS, Lim WK, Alvarez MJ, Bollo RJ, Zhao X, Snyder EY, Sulman EP, Anne SL, Doetsch F, Colman H, Lasorella A, Aldape K, Califano A, Iavarone A. The transcriptional network for mesenchymal transformation of brain tumours. Nature. 2009;463(7279):318–25. http://dx.doi.org/10.1038/nature08712
45. Mani SA, Guo W, Liao M, Eaton EN, Ayyanan A, Zhou AY, Brooks M, Reinhard F, Zhang CC, Shipitsin M, Campbell LL, Polyak K, Brisken C, Yang J, Weinberg RA. The epithelialmesenchymal transition generates cells with properties of stem cells. Cell. 2008;133(4):704–15. http://dx.doi.org/10.1016/j.cell.2008.03.027
46. Merzak A, Koocheckpour S, Pilkington GJ. CD44 mediates human glioma cell adhesion and invasion in vitro. Cancer Res. 1994;54(15):3988–92.
47. Cheng W, Kandel JJ, Yamashiro DJ, Canoll P, Anastassiou D. A multi-cancer mesenchymal transition gene expression signature is associated with prolonged time to recurrence in glioblastoma. PLoS One. 2012;7(4):e34705. http://dx.doi.org/10.1371/journal.pone.0034705
48. Bouck N. P53 and angiogenesis. Biochim Biophys Acta. 1996;1287(1):63–6. http://dx.doi.org/10.1016/0304-419x(96)00005-4
49. Long DM. Capillary ultrastructure and the blood-brain barrier in human malignant brain tumors. J Neurosurg. 1970;32(2):127. http://dx.doi.org/10.3171/jns.1970.32.2.0127
50. Ricci-Vitiani L, Pallini R, Biffoni M, Todaro M, Invernici G, Cenci T, Maira G, Parati EA, Stassi G, Larocca LM, De Maria R. Tumour vascularization via endothelial differentiation of glioblastoma stem-like cells. Nature. 2010;468(7325):824–8. http://dx.doi.org/10.1038/nature09557
51. Semenza GL. Targeting HIF-1 for cancer therapy. Nat Rev Cancer. 2003;3(10):721–32. http://dx.doi. org/10.1038/nrc1187
52. Bao S, Wu Q, Sathornsumetee S, Hao Y, Li Z, Hjelmeland AB, Shi Q, McLendon RE, Bigner DD, Rich JN. Stem cell-like glioma cells promote tumor angiogenesis through vascular endothelial growth factor. Cancer Res. 2006;66(16):7843–8. http://dx.doi.org/10.1158/0008-5472.CAN-06-1010
53. Bergers G, Benjamin LE. Tumorigenesis and the angiogenic switch. Nat Rev Cancer. 2003;3(6):401–10. http://dx.doi.org/10.1038/nrc1093
54. Carmeliet P, Jain RK. Molecular mechanisms and clinical applications of angiogenesis. Nature. 2011;473(7347):298–307. http://dx.doi.org/10.1038/nature10144
55. Weis SM, Cheresh DA. Tumor angiogenesis: Molecular pathways and therapeutic targets. Nat Med. 2011;17(11):1359–70. http://dx.doi.org/10.1038/nm.2537
56. Norden AD, Drappatz J, Wen PY. Novel anti-angiogenic therapies for malignant gliomas. Lancet Neurol. 2008;7(12):1152–60. http://dx.doi.org/10.1016/S1474-4422(08)70260-6
57. Zhang X, Ding K, Wang J, Li X, Zhao P. Chemoresistance caused by the microenvironment of glioblastoma and the corresponding solutions. Biomedicine & Pharmacotherapy. Volume 109, January 2019, Pages 39-46; https://doi.org/10.1016/j.biopha.2018.10.063.
58. Jhaveri N, Chen TC, Hofman FM. Tumor vasculature and glioma stem cells: Contributions to glioma progression.Cancer Lett. 2016 Oct 1;380(2):545-51. doi: 10.1016/j.canlet.2014.12.028. Epub 2014 Dec 16.
59. Matias D, Balça-Silva J, da Graça GC, Wanjiru CM, Macharia LW, Nascimento CP, Roque NR, Coelho-Aguiar JM, Pereira CM, Dos Santos MF, Pessoa LS, Lima FRS, Schanaider A, Ferrer VP; Tania Cristina Leite de Sampaio e Spohr, Moura-Neto V. Microglia/Astrocytes-

Glioblastoma Crosstalk: Crucial Molecular Mechanisms and Microenvironmental Factors. Front Cell Neurosci. 2018 Aug 3;12:235. doi: 10.3389/fncel.2018.00235. eCollection 2018.
60. Brandao M, Simon T, Critchley G, Giamas G. Astrocytes, the rising stars of the glioblastoma microenvironment. Glia. 2019 May;67(5):779-790. doi: 10.1002/glia.23520. Epub 2018 Sep 21.
61. Liberti MV, Locasale JW. The warburg effect: How does it denefit cancer cells? Trends Biochem Sci. 2016;41(3):211–18. http://dx.doi.org/10.1016/j.tibs.2015.12.001.
62. Monteiro AR, Hill R, Pilkington GJ, Madureira PA. The Role of Hypoxia in Glioblastoma Invasion. Cells. 2017 Nov 22;6(4). pii: E45. doi: 10.3390/cells6040045.
63. Nguyen HS, Shabani S, Awad AJ, Kaushal M, Doan N. Molecular Markers of Therapy-Resistant Glioblastoma and Potential Strategy to Combat Resistance. Int J Mol Sci. 2018 Jun 14;19(6). pii: E1765. doi: 10.3390/ijms19061765.
64. Tomiyama A, Ichimura K. Signal transduction pathways and resistance to targeted therapies in glioma. Semin Cancer Biol. 2019 Oct;58:118-129. doi: 10.1016/j.semcancer.2019.01.004. Epub 2019 Jan 24.
65. Zhang Y, Dube C, Gibert M Jr, Cruickshanks N, Wang B, Coughlan M, Yang Y, Setiady I, Deveau C, Saoud K, Grello C, Oxford M, Yuan F, Abounader R. The p53 Pathway in Glioblastoma. Cancers (Basel). 2018 Sep 1;10(9). pii: E297. doi: 10.3390/cancers10090297.
66. Morgan MA, Canman CE. Replication Stress: An Achilles' Heel of Glioma Cancer Stem-like Cells. Cancer Res. 2018 Dec 15;78(24):6713-6716. doi: 10.1158/0008-5472.CAN-18-2439. Epub 2018 Nov 29.
67. Lee SY. Temozolomide resistance in glioblastoma multiforme. Genes & Diseases 2016, 3, 198-210, doi:10.1016/j.gendis.2016.04.007.
68. Salazar-Ramiro A, Ramírez-Ortega D, Pérez de la Cruz V, Hérnandez-Pedro NY, González-Esquivel DF, Sotelo J, Pineda B1 Role of Redox Status in Development of Glioblastoma. Front Immunol. 2016 Apr 26;7:156. doi: 10.3389/fimmu.2016.00156. eCollection 2016.
69. He Y, Su J, Lan B, Gao Y, Zhao J. Targeting off-target effects: endoplasmic reticulum stress and autophagy as effective strategies to enhance temozolomide treatment. Onco Targets Ther. 2019 Mar 7;12:1857-1865. doi: 10.2147/OTT.S194770. eCollection 2019.
70. Audia A, Conroy S, Glass R, Bhat KPL. The Impact of the Tumor Microenvironment on the Properties of Glioma Stem-Like Cells. Front Oncol. 2017 Jul 10;7:143. doi: 10.3389/fonc.2017.00143. eCollection 2017.
71. Sattiraju A, Sai KKS, Mintz A. Glioblastoma Stem Cells and Their Microenvironment. Adv Exp Med Biol. 2017;1041:119-140. doi: 10.1007/978-3-319-69194-7_7.
72. Germano IM, Binello E. Stem cells and gliomas: past, present, and future. J Neurooncol. 2014 Sep;119(3):547-55. doi: 10.1007/s11060-014-1498-y. Epub 2014 Aug 1.
73. Wuebben EL, Rizzino A. The dark side of SOX2: cancer - a comprehensive overview. Oncotarget. 2017 Jul 4;8(27):44917-44943. doi: 10.18632/oncotarget.16570.
74. Sampetrean O, Saya H. Characteristics of glioma stem cells. Brain Tumor Pathol. 2013 Oct;30(4):209-14. doi: 10.1007/s10014-013-0141-5. Epub 2013 Apr 13.
75. Gangemi RM, Griffero F, Marubbi D, Perera M, Capra MC, Malatesta P, Ravetti GL, Zona GL, Daga A, Corte G. SOX2 silencing in glioblastoma tumor-initiating cells causes stop of proliferation and loss of tumorigenicity.Stem Cells. 2009 Jan;27(1):40-8. doi: 10.1634/stemcells.2008-0493.
76. Annovazzi L, Mellai M, Caldera V, Valente G, Schiffer D. SOX2 expression and amplification in gliomas and glioma cell lines. Cancer Genomics Proteomics. 2011 May-Jun;8(3):139-47.

77. Landskron G, De la Fuente M, Thuwajit P, Thuwajit C, Hermoso MA. Chronic inflammation and cytokines in the tumor microenvironment. J Immunol Res. 2014;2014:149185. doi: 10.1155/2014/149185. Epub 2014 May 13.
78. Arcuri C, Fioretti B, Bianchi R, Mecca C, Tubaro C, Beccari T, Franciolini F, Giambanco I, Donato R. Microglia-glioma cross-talk: a two way approach to new strategies against glioma. Front Biosci (Landmark Ed). 2017 Jan 1;22:268-309.
79. Mantovani A, Allavena P, Sica A, Balkwill F. Cancer-related inflammation. Nature. 2008 Jul 24;454(7203):436-44. doi: 10.1038/nature07205.
80. Tanaka T, Watanabe M, Yamashita K. Potential therapeutic targets of TP53 gene in the context of its classically canonical functions and its latest non-canonical functions in human cancer. Oncotarget. 2018 Mar 23;9(22):16234-16247. doi: 10.18632/oncotarget.24611. eCollection 2018 Mar 23.
81. Cohen AL, Holmen SL, Colman H. IDH1 and IDH2 mutations in gliomas. Curr Neurol Neurosci Rep. 2013 May;13(5):345. doi: 10.1007/s11910-013-0345-4.
82. Aghili M, Zahedi F, Rafiee E. Hydroxyglutaric aciduria and malignant brain tumor: a case report and literature review. J Neurooncol. 2009 Jan;91(2):233-6. doi: 10.1007/s11060-008-9706-2. Epub 2008 Oct 18.
83. Dang L, White DW, Gross S, Bennett BD, Bittinger MA, Driggers EM, Fantin VR, Jang HG, Jin S, Keenan MC, Marks KM, Prins RM, Ward PS, Yen KE, Liau LM, Rabinowitz JD, Cantley LC, Thompson CB, Vander Heiden MG, Su SM. Cancer-associated IDH1 mutations produce 2-hydroxyglutarate. Nature. 2009 Dec 10;462(7274):739-44. doi: 10.1038/nature08617.
84. Christofides A, Kosmopoulos M, Piperi C. Pathophysiological mechanisms regulated by cytokines in gliomas. Cytokine. 2015 Feb;71(2):377-84. doi: 10.1016/j.cyto.2014.09.008. Epub 2014 Nov 4.
85. López-Sánchez LM, Aranda E, Rodríguez-Ariza A. Nitric oxide and tumor metabolic reprogramming. Biochem Pharmacol. 2019 Dec 17:113769. doi: 10.1016/j.bcp.2019.113769. [Epub ahead of print].
86. Eyler CE, Wu QL, Yan K, MacSwords JM, Chandler-Militello D, Misuraca KL, Lathia JD, Forrester MT, Lee J, Stamler JS, Goldman SA, Bredel M, McLendon RE, Sloan AE, Hjelmeland AB, Rich JN. Glioma Stem Cell Proliferation and Tumor Growth Are Promoted by Nitric Oxide Synthase-2. Cell 2011, 146, 53–66, doi:10.1016/j.cell.2011.06.006.
87. Jahani-Asl A, Bonni A iNOS: a potential therapeutic target for malignant glioma. Curr Mol Med. 2013 Sep;13(8):1241-9.
88. Bogdan C. Nitric oxide synthase in innate and adaptive immunity: An update. Trends Immunol. 2015, 36, 161–178.
89. Vannini F, Kashfi K, Nath N. The dual role of iNOS in cancer. Redox Biol. 2015, 6, 334–343.
90. Tran AN, Boyd NH, Walker K, Hjelmeland AB. NOS Expression and NO Function in Glioma and Implications for Patient Therapies. Antioxid. Redox Signal. 2017, 26, 986-999, doi:10.1089/ars.2016.6820.
91. Kim RK, Suh Y, Cui YH, Hwang E, Lim EJ, Yoo KC, Lee GH, Yi JM, Kang SG, Lee SJ. Fractionated radiation-induced nitric oxide promotes expansion of glioma stem-like cells. Cancer Sci. 2013 Sep;104(9):1172-7. doi: 10.1111/cas.12207. Epub 2013 Jun 24.
92. Shen SC, Wu MS, Lin HY, Yang LY, Chen YH, Chen YC. Reactive oxygen species-dependent nitric oxide production in reciprocal interactions of glioma and microglial cells. J. Cell Physiol. 2014, 229, 2015–2026.

93. Papaevangelou E, Whitley GS, Johnstone AP, Robinson SP, Howe FA. Investigating the role of tumour cell derived iNOS on tumour growth and vasculature in vivo using a tetracycline regulated expression system. Int. J. Cancer 2016, 138, 2678–2687.
94. Palumbo P, Miconi G, Cinque B1, Lombardi F, La Torre C, Dehcordi SR, Galzio R, Cimini A, Giordano A, Cifone MG. NOS2 expression in glioma cell lines and glioma primary cell cultures: correlation with neurosphere generation and SOX-2 expression. Oncotarget. 2017 Apr 11;8(15):25582-25598. doi: 10.18632/oncotarget.16106.
95. Re N, Fantacuzzi M, Maccallini C, Paciotti R, Amoroso R. Recent developments of amidine-like compounds as selective NOS inhibitors. Curr. Enzyme Inhib. 2016, 12, 30–39.
96. Fedorov R, Hartmann E, Ghosh DK, Schlichting I. Structural basis for the specificity of the nitric-oxide synthase inhibitors W1400 and Nu-propyl-L-argfor the inducible and neuronal isoforms. J. Biol. Chem. 2003, 278, 45818–45825.
97. Maccallini C, Di Matteo M, Gallorini M, Montagnani M, Graziani V, Ammazzalorso A, Amoia P, De Filippis B, Di Silvestre S, Fantacuzzi M, Giampietro L, Potenza MA, Re N, Pandolfi A, Cataldi A, Amoroso R. Discovery of N-{3-[(ethanimidoylamino)methyl]benzyl}-l-prolinamide dihydrochloride: A new potent and selective inhibitor of the inducible nitric oxide synthase as a promising agent for the therapy of malignant glioma.Eur J Med Chem. 2018 May 25;152:53-64. doi: 10.1016/j.ejmech.2018.04.027. Epub 2018 Apr 13.
98. Garvey EP, Oplinger JA, Furfine ES, Kiff RJ, Laszlo F, Whittle BJR, Knowles RG. 1400W is a slow, tight binding, and highly selective inhibitor of inducible nitric-oxide synthase in vitro and in vivo. J. Biol. Chem. 1997, 272, 4959–4963.
99. Patel P, Qi WN, Allen DM, Chen LE, Seaber AV, Stamler JS, Urbaniak JR. Inhibition of iNOS with 1400W improves contractile function and alters nos gene and protein expression in reperfused skeletal muscle. Microsurgery 2004, 24, 324–331.
100. Maccallini C, Patruno A, Besker N, Ali JI, Ammazzalorso A, De Filippis B, Franceschelli S, Giampietro L, Pesce M, Reale M, Tricca ML, Re N, Felaco M, Amoroso R. Synthesis, biological evaluation, and docking studies of N-substituted acetamidines as selective inhibitors of inducible nitric oxide synthase. J. Med. Chem. 2009, 52, 1481–1485.
101. Maccallini C, Patruno A, Lannutti F, Ammazzalorso A, De Filippis B, Fantacuzzi M, Franceschelli S, Giampietro L, Masella S, Felaco M, Re N, Amoroso R. N-Substituted acetamidines and 2-methylimidazole derivatives as selective inhibitors of neuronal nitric oxide synthase. Bioorg. Med. Chem. Lett. 2010, 20, 6495–6499.
102. Fantacuzzi M, Maccallini C, Lannutti F, Patruno A, Masella S, Pesce M, Speranza L, Ammazzalorso A, De Filippis B, Giampietro L, Re N, Amoroso R. Selective inhibition of iNOS by benzyl- and dibenzyl derivatives of N-(3-aminobenzyl)acetamidine. Chem. Med. Chem. 2011, 6, 1203–1206.
103. Maccallini C, Montagnani M, Paciotti R, Ammazzalorso A, De Filippis B, Di Matteo M, Di Silvestre S, Fantacuzzi M, Giampietro L, Potenza MA, Re N, Pandolfi A, Amoroso R. Selective acetamidine-based nitric oxide synthase inhibitors: Synthesis, docking, and biological studies. ACS Med. Chem. Lett. 2015, 6, 635–640.
104. Trejo-Solis C, Serrano-Garcia N, Escamilla-Ramirez A, Castillo-Rodriguez RA, Jimenez-Farfan D, Palencia G, Calvillo M, Alvarez-Lemus MA, Flores-Najera A, Cruz-Salgado A, Sotelo J. Autophagic and Apoptotic Pathways as Targets for Chemotherapy in Glioblastoma. Int. J. Mol. Sci. 2018, 19, 3773.
105. Howarth A, Madureira PA, Lockwood G, Storer LCD, Grundy R, Rahman R, Pilkington GJ, Hill R. Modulating autophagy as a therapeutic strategy for the treatment of paediatric high-grade glioma. Brain Pathol. 2019 Nov;29(6):707-725. doi: 10.1111/bpa.12729. Epub 2019 May 13.

106. Huang X, Bai HM, Chen L, Li B, Lu YC. Reduced expression of LC3B-II and Beclin 1 in glioblastoma multiforme indicates a down-regulated autophagic capacity that relates to the progression of astrocytic tumors. J. Clin. Neurosci. 2010, 17, 1515–1519.
107. Jo GH, Bogler O, Chwae YJ, Yoo H, Lee SH, Park JB, Kim YJ, Kim JH, Gwak HS. Radiation-induced autophagy contributes to cell death and induces apoptosis partly in malignant glioma cells. Cancer Res. Treat. 2015, 47, 221–241.
108. Ge P, Luo Y, Fu S, Ji X, Ling F. Autophagy: A strategy for malignant gliomas' resistance to therapy. Med. Hypotheses 2009, 73, 45–47.
109. Ito H; Daido S, Kanzawa T, Kondo S, Kondo Y. Radiation-induced autophagy is associated with LC3 and its inhibition sensitizes malignant glioma cells. Int. J. Oncol. 2005, 26, 1401–1410.
110. Lomonaco SL, Finniss S, Xiang C, Decarvalho A, Umansky F, Kalkanis SN, Mikkelsen T, Brodie C. The induction of autophagy by gamma-radiation contributes to the radioresistance of glioma stem cells. Int. J. Cancer 2009, 125, 717–722.
111. Padmakrishnan CJ, Easwer HV, Vijayakurup V, Menon GR, Nair S, Gopala S. High LC3/Beclin Expression Correlates with Poor Survival in Glioma: A Definitive Role for Autophagy as Evidenced by In Vitro Autophagic Flux. Pathol. Oncol. Res. 2019, 25, 137–148.
112. Shao N, Mao J, Xue L, Wang R, Zhi F, Lan Q. Carnosic acid potentiates the anticancer effect of temozolomide by inducing apoptosis and autophagy in glioma. J Neurooncol 2019, 141, 277-288, doi:10.1007/s11060-018-03043-5.
113. Catalano M, D'Alessandro G, Lepore F, Corazzari M, Caldarola S, Valacca C, Faienza F, Esposito V, Limatola C, Cecconi F, Di Bartolomeo S. Autophagy induction impairs migration and invasion by reversing EMT in glioblastoma cells. Mol Oncol. 2015 Oct;9(8):1612-25. doi: 10.1016/j.molonc.2015.04.016. Epub 2015 May 13.
114. Strickland M, Stoll EA. Metabolic Reprogramming in Glioma. Front Cell Dev Biol. 2017 Apr 26;5:43. doi: 10.3389/fcell.2017.00043. eCollection 2017.
115. Mowers EE, Sharifi MN, Macleod KF. Functions of autophagy in the tumor microenvironment and cancer metastasis. FEBS J. 2018 May;285(10):1751-1766. doi: 10.1111/febs.14388. Epub 2018 Feb 1. Review.
116. Hsu SPC, Kuo JS, Chiang HC, Wang HE, Wang YS, Huang CC, Huang YC, Chi MS, Mehta MP, Chi KH. Temozolomide, sirolimus and chloroquine is a new therapeutic combination that synergizes to disrupt lysosomal function and cholesterol homeostasis in GBM cells. Oncotarget. 2018 Jan 3;9(6):6883-6896. doi: 10.18632/oncotarget.23855. eCollection 2018 Jan 23.
117. Shen J, Zheng H, Ruan J, Fang W, Li A, Tian G, Niu X, Luo S, Zhao P. Autophagy inhibition induces enhanced proapoptotic effects of ZD6474 in glioblastoma. Br J Cancer. 2013 Jul 9;109(1):164-71. doi: 10.1038/bjc.2013.306. Epub 2013 Jun 25.
118. Yuan G, Yan S, Xue H, Zhang P, Sun J, Li G. JSI-124 suppresses invasion and angiogenesis of glioblastoma cells in vitro. PLoS One. 2015 Mar 19;10(3):e0118894. doi: 10.1371/journal.pone.0118894. eCollection 2015.
119. García-Prat L, Martínez-Vicente M, Muñoz-Cánoves P. Autophagy: a decisive process for stemness. Oncotarget. 2016 Mar 15;7(11):12286-8. doi: 10.18632/oncotarget.7766. Review.
120. Nabissi M, Morelli MB, Amantini C, Liberati S, Santoni M, Ricci-Vitiani L, Pallini R, Santoni G. Cannabidiol stimulates Aml-1a-dependent glial differentiation and inhibits glioma stem-like cells proliferation by inducing autophagy in a TRPV2-dependent manner. Int J Cancer. 2015 Oct 15;137(8):1855-69. doi: 10.1002/ijc.29573. Epub 2015 May 8.

121. Zhuang W, Long L, Zheng B, Ji W, Yang N, Zhang Q, Liang Z. Curcumin promotes differentiation of glioma-initiating cells by inducing autophagy. Cancer Sci. 2012 Apr;103(4):684-90. doi: 10.1111/j.1349-7006.2011.02198.x. Epub 2012 Jan 30.
122. Jawhari S, Ratinaud MH, Verdier M. Glioblastoma, hypoxia and autophagy: a survival-prone 'ménage-à-trois'.Cell Death Dis. 2016 Oct 27;7(10):e2434. doi: 10.1038/cddis.2016.318.
123. Dolma S, Selvadurai HJ, Lan X, Lee L, Kushida M, Voisin V, Whetstone H, So M, Aviv T, Park N, Zhu X, Xu C, Head R, Rowland KJ, Bernstein M, Clarke ID, Bader G, Harrington L, Brumell JH, Tyers M, Dirks PB. Inhibition of Dopamine Receptor D4 Impedes Autophagic Flux, Proliferation, and Survival of Glioblastoma Stem Cells. Cancer Cell. 2016 Jun 13;29(6):859-873. doi: 10.1016/j.ccell.2016.05.002.
124. Gewirtz DA. The four faces of autophagy: implications for cancer therapy. Cancer Res. 2014 Feb 1;74(3):647-51. doi: 10.1158/0008-5472.CAN-13-2966. Epub 2014 Jan 23. Review.
125. Cj P, Hv E, Vijayakurup V, R Menon G, Nair S, Gopala S. High LC3/Beclin Expression Correlates with Poor Survival in Glioma: a Definitive Role for Autophagy as Evidenced by In Vitro Autophagic Flux. Pathol Oncol Res. 2019 Jan;25(1):137-148. doi: 10.1007/s12253-017-0310-7. Epub 2017 Oct 11.
126. Colella B, Faienza F, Di Bartolomeo S. EMT Regulation by Autophagy: A New Perspective in Glioblastoma Biology. Cancers (Basel). 2019 Mar 6;11(3). pii: E312. doi: 10.3390/cancers11030312.
127. Zitvogel L, Kepp O, Galluzzi L, Kroemer G. Inflammasomes in carcinogenesis and anticancer immune responses. Nat Immunol. 2012 Mar 18;13(4):343-51. doi: 10.1038/ni.2224.
128. Galluzzi L, Pietrocola F, Bravo-San Pedro JM, Amaravadi RK, Baehrecke EH, Cecconi F, Codogno P, Debnath J, Gewirtz DA, Karantza V, Kimmelman A, Kumar S, Levine B, Maiuri MC, Martin SJ, Penninger J, Piacentini M, Rubinsztein DC, Simon HU, Simonsen A, Thorburn AM, Velasco G, Ryan KM, Kroemer G. Autophagy in malignant transformation and cancer progression. Embo J 2015, 34, 856-880, doi:10.15252/embj.201490784.
129. Yang ZJ, Chee CE, Huang S, Sinicrope FA. The role of autophagy in cancer: therapeutic implications. Mol Cancer Ther. 2011 Sep;10(9):1533-41. doi: 10.1158/1535-7163.MCT-11-0047. Epub 2011 Aug 30.
130. Whitehead CA, Kaye AH, Drummond KJ, Widodo SS, Mantamadiotis T, Vella LJ, Stylli SS. Extracellular vesicles and their role in glioblastoma. Crit Rev Clin Lab Sci. 2019 Dec 22:1-26. doi: 10.1080/10408363.2019.1700208. [Epub ahead of print]
131. Colombo M, Raposo G, Théry C. Biogenesis, secretion, and intercellular interactions of exosomes and other extracellular vesicles. Annu Rev Cell Dev Biol. 2014;30:255-89. doi: 10.1146/annurev-cellbio-101512-122326. Epub 2014 Aug 21.
132. Latifkar A, Hur YH, Sanchez JC, Cerione RA, Antonyak MA. New insights into extracellular vesicle biogenesis and function. J Cell Sci. 2019 Jul 1;132(13). pii: jcs222406. doi: 10.1242/jcs.222406.
133. Quezada C, Torres Á, Niechi I, Uribe D, Contreras-Duarte S, Toledo F, San Martín R, Gutiérrez J, Sobrevia L.Role of extracellular vesicles in glioma progression. Mol Aspects Med. 2018 Apr;60:38-51. doi: 10.1016/j.mam.2017.12.003. Epub 2017 Dec 13.
134. Azam Z, Quillien V, Wang G, To ST. The potential diagnostic and prognostic role of extracellular vesicles in glioma: current status and future perspectives. Acta Oncol. 2019 Mar;58(3):353-362. doi: 10.1080/0284186X.2018.1551621. Epub 2019 Jan 11. Review.
135. Noerholm M, Balaj L, Limperg T, Salehi A, Zhu LD, Hochberg FH, Breakefield XO, Carter BS, Skog J. RNA expression patterns in serum microvesicles from patients with glioblastoma multiforme and controls. BMC Cancer. 2012 Jan 17;12:22. doi: 10.1186/1471-2407-12-22.

136. Garnier D, Meehan B, Kislinger T, Daniel P, Sinha A, Abdulkarim B, Nakano I, Rak J. Divergent evolution of temozolomide resistance in glioblastoma stem cells is reflected in extracellular vesicles and coupled with radiosensitization. Neuro Oncol. 2018 Jan 22;20(2):236-248. doi: 10.1093/neuonc/nox142.
137. Zeng A, Wei Z, Yan W, Yin J, Huang X, Zhou X, Li R, Shen F, Wu W, Wang X, You Y. Exosomal transfer of miR-151a enhances chemosensitivity to temozolomide in drug-resistant glioblastoma. Cancer Lett. 2018 Nov 1;436:10-21. doi: 10.1016/j.canlet.2018.08.004. Epub 2018 Aug 10.
138. Zhang G, Zhang Y, Cheng S, Wu Z, Liu F, Zhang J. CD133 positive U87 glioblastoma cells-derived exosomal microRNAs in hypoxia- versus normoxia-microenviroment. J Neurooncol. 2017 Oct;135(1):37-46. doi: 10.1007/s11060-017-2566-x. Epub 2017 Sep 25.
139. Sun X, Ma X, Wang J, Zhao Y, Wang Y, Bihl JC, Chen Y, Jiang C. Glioma stem cells-derived exosomes promote the angiogenic ability of endothelial cells through miR-21/VEGF signal. Oncotarget. 2017 May 30;8(22):36137-36148. doi: 10.18632/oncotarget.16661.
140. La Torre C, Cinque B, Lombardi F, Miconi G, Palumbo P, Evtoski Z, Placidi G, Fanini D, Cimini AM, Benedetti E, Giuliani M, Cifone MG. Nitric Oxide Chemical Donor Affects the Early Phases of In Vitro Wound Healing Process. J Cell Physiol. 2016 Oct;231(10):2185-95. doi: 10.1002/jcp.25331. Epub 2016 Mar 6.
141. Thery C, Witwer KW, Aikawa E, Alcaraz MJ, Anderson JD, Andriantsitohaina R, Antoniou A, Arab T, Archer F, Atkin-Smith GK, et al. Minimal information for studies of extracellular vesicles 2018 (MISEV2018): a position statement of the International Society for Extracellular Vesicles and update of the MISEV2014 guidelines. J Extracell Vesicles 2018, 7, 1535750, doi:10.1080/20013078.2018.1535750.
142. Gebäck T, Schulz MM, Koumoutsakos P, Detmar M. TScratch: A novel and simple software tool for automated analysis of monolayer wound healing assays. Biotechniques 2009 46, 265–274, doi:10.2144/000113083.
143. Ye XZ, Xu SL, Xin YH, Yu SC, Ping YF, Chen L, Xiao HL, Wang B,Yi L, Wang QL, Jiang XF, Yang L, Zhang P, Qian C, Cui YH, Zhang X, Bian XW. Tumor-associated microglia/macrophages enhance the invasion of glioma stem-like cells via TGF-beta1 signaling pathway. J Immunol 189: 444-453, 2012.
144. Liu Z, Kuang W, Zhou Q and Zhang Y. TGF-β1 secreted by M2 phenotype macrophages enhances the stemness and migration of glioma cells via the SMAD2/3 signalling pathway. Int J Molec Med 42: 3395-3403, 2018. DOI: 10.3892/ijmm.2018.3923
145. Garros-Regulez L, Aldaz P, Arrizabalaga O, Moncho-Amor V Carrasco-Garcia E, Manterola L, Moreno-C ugnon L, Barrena C, Villanua J, Ruiz I, Pollard S, Lovell-Badge R, Sampron N, Garcia I, Matheu A. mTOR inhibition decreases SOX2-SOX9 mediated glioma stem cell activity and temozolomide resistance.Expert Opin Ther Targets 20: 393-405, 2016.
146. Ponpuak M, Mandell MA, Kimura T, Chauhan S, Cleyrat C, Deretic V. Secretory autophagy. Current opinion in cell biology 2015, 35, 106-116, doi:10.1016/j.ceb.2015.04.016.
147. Loidl A, Claus R, Deigner HP, Hermetter A. High-precision fluorescence assay for sphingomyelinase activity of isolated enzymes and cell lysates. Journal of lipid research 2002, 43, 815-823.
148. Giusti I, Di Francesco M, Dolo V. Extracellular Vesicles in Glioblastoma: Role in Biological Processes and in Therapeutic Applications. Current cancer drug targets 2017, 17, 221-235, doi:10.2174/1568009616666160813182959.
149. D'Alessio A, Proietti G, Sica G, Scicchitano BM. Pathological and Molecular Features of Glioblastoma and Its Peritumoral Tissue.Cancers (Basel). 2019 Apr 3;11(4). pii: E469. doi: 10.3390/cancers11040469.

150. Berezovsky AD, Poisson LM, Cherba D, Webb CP, Transou AD, Lemke NW, Hong X, Hasselbach LA, Irtenkauf SM, Mikkelsen T, deCarvalho AC. Sox2 promotes malignancy in glioblastoma by regulating plasticity and astrocytic differentiation. Neoplasia. 2014 Mar;16(3):193-206, 206.e19-25. doi: 10.1016/j.neo.2014.03.006. Epub 2014 Apr 13.
151. Schmitz M, Temme A, Senner V, Ebner R, Schwind S, Stevanovic S, Wehner R, Schackert G, Schackert HK, Fussel M, Bachmann M, Rieber EP, Weigle B. Identification of SOX2 as a novel glioma-associated antigen and potential target for T cell-based immunotherapy. Br J Cancer. 2007 Apr 23;96(8):1293-301. Epub 2007 Mar 20.
152. Jeon HM, Sohn YW, Oh SY, Kim SH, Beck S, Kim S, Kim H. ID4 imparts chemoresistance and cancer stemness to glioma cells by derepressing miR-9-mediated suppression of SOX2. Cancer Res. 2011 May 1;71(9):3410-21. doi: 10.1158/0008-5472.CAN-10-3340.
153. Jeon HM, Kim SH, Jin X, Park JB, Kim SH, Joshi K6, Nakano I, Kim H. Crosstalk between glioma-initiating cells and endothelial cells drives tumor progression. Cancer Res. 2014 Aug 15;74(16):4482-92. doi: 10.1158/0008-5472.CAN-13-1597. Epub 2014 Jun 24.
154. Eun K, Jeon HM, Kim SO, Choi SH, Lee SY, Jin X, Kim SC, Kim H. A cell-autonomous positive-signaling circuit associated with the PDGF-NO-ID4-regulatory axis in glioblastoma cells. Biochem Biophys Res Commun. 2017 Apr 29;486(2):564-570. doi: 10.1016/j.bbrc.2017.03.089. Epub 2017 Mar 19.
155. Cholia RP, Kumari S, Kumar S, Kaur M, Kumar R, Dhiman M, Mantha AK. An in vitro study ascertaining the role of H2O2 and glucose oxidase in modulation of antioxidant potential and cancer cell survival mechanisms in glioblastoma U-87 MG cells. Metab Brain Dis. 2017 Oct;32(5):1705-1716. doi: 10.1007/s11011-017-0057-6. Epub 2017 Jul 5.
156. Birben E, Sahiner UM, Sackesen C, Erzurum S, Kalayci O. Oxidative stress and antioxidant defense. World Allergy Organ J. 2012 Jan;5(1):9-19. doi: 10.1097/WOX.0b013e3182439613. Epub 2012 Jan 13.
157. Fionda C, Abruzzese MP, Santoni A, Cippitelli M. Immunoregulatory and Effector Activities of Nitric Oxide and Reactive Nitrogen Species in Cancer. Curr Med Chem. 2016;23(24):2618-2636.
158. Fahey JM, Emmer JV, Korytowski W, Hogg N, Girotti AW. Antagonistic Effects of Endogenous Nitric Oxide in a Glioblastoma Photodynamic Therapy Model. Photochem Photobiol. 2016 Nov;92(6):842-853. doi: 10.1111/php.12636. Epub 2016 Oct 17.
159. Pazhouhi M, Sariri R, Rabzia A, Khazaei M. Thymoquinone synergistically potentiates temozolomide cytotoxicity through the inhibition of autophagy in U87MG cell line. Iran J Basic Med Sci. 2016 Aug;19(8):890-898.
160. Khazaei M, Pazhouhi M. Temozolomide-Mediated Apoptotic Death Is Improved by Thymoquinone in U87MG Cell Line. Cancer Invest. 2017 Apr 21;35(4):225-236. doi: 10.1080/07357907.2017.1289383. Epub 2017 Mar 29.
161. Dávila-González D, Choi D, Rosato RR, Granados-Principal SM Kuhn JG, Li WF, Qian W, Chen W, Kozielski AJ, Wong H, Dave B, Chang JC. Pharmacological Inhibition of NOS Activates ASK1/JNK Pathway Augmenting Docetaxel-Mediated Apoptosis in Triple-Negative Breast Cancer. Clin Cancer Res. 2018 Mar 1;24(5):1152-1162. doi: 10.1158/1078-0432.CCR-17-1437. Epub 2018 Jan 4.
162. Sarkar S, Korolchuk VI, Renna M, Imarisio S, Fleming A, Williams A, Garcia-Arencibia M, Rose C, Luo S, Underwood BR, Kroemer G, O'Kane CJ, Rubinsztein DC. Complex inhibitory effects of nitric oxide on autophagy. Mol Cell. 2011 Jul 8;43(1):19-32. doi: 10.1016/j.molcel.2011.04.029.
163. Dávila-González D, Chang JC, Billiar TR. NO and COX2: Dual targeting for aggressive cancers. Proc Natl Acad Sci U S A. 2017 Dec 26;114(52):13591-13593. doi: 10.1073/pnas.1717440114. Epub 2017 Dec 13.

164. Miconi G, Palumbo P, Dehcordi SR, La Torre C, Lombardi F, Evtoski Z, Cimini AM, Galzio R, Cifone MG, Cinque B. Immunophenotypic characterization of human glioblastoma stem cells: correlation with clinical outcome. J Cell Biochem. 2015 May;116(5):864-76. doi: 10.1002/jcb.25043.
165, Liang XH, Jackson S, Seaman M, Brown K, Kempkes B, Hibshoosh H, Levine B. Induction of autophagy and inhibition of tumorigenesis by beclin 1. Nature. 1999 Dec 9;402(6762):672-6.
166. Verderio C, Gabrielli M, Giussani P. Role of sphingolipids in the biogenesis and biological activity of extracellular vesicles. J Lipid Res. 2018 Aug;59(8):1325-1340. doi: 10.1194/jlr.R083915. Epub 2018 May 31.
167. Kim YC, Guan KL. mTOR: a pharmacologic target for autophagy regulation. J Clin Invest. 2015 Jan;125(1):25-32. doi: 10.1172/JCI73939. Epub 2015 Jan 2.
168. Paquette M, El-Houjeiri L, Pause A. mTOR Pathways in Cancer and Autophagy. Cancers (Basel). 2018 Jan 12;10(1). pii: E18. doi: 10.3390/cancers10010018.